PEOPLE'S DEMOCRATIC REPUBLIC OF ALGERIA
MINISTRY OF HIGHER EDUCATION AND SCIENTIFIC RESEARCH
UNIVERSITY YAHIA FARES OF MEDEA



FACULTY OF TECHNOLOGY

THESIS

To obtain the degree of

DOCTOR in: Automatic

Specialty: Automatic and Industrial Informatics

Presented by: Sadok Bouziane Yazid

Thesis title

Contribution to the Optimization of Energy Management in a Microgrid Integrating Conversion and Hybrid Storage Elements

---

Defended in front of a jury composed of:

Last and first Name	Grade	Institution of affiliation	Designation
HOUASSINE Hamza	Professor	University of Bouira	President
HENINI Noureddine	Professor	University of Medea	Supervisor
TLEMCANI Abdelhalim	Professor	University of Medea	Co-supervisor
MEDJBER Ahmed	MCA	University of Medea	Examiner 1
BENTOUATI Smain	MCA	University of Medea	Examiner 2

Academic year: 2025/2026

REPUBLIQUE ALGERIENNE DEMOCRATIQUE ET POPULAIRE
MINISTERE DE L'ENSEIGNEMENT SUPERIEUR ET DE LA RECHERCHE SCIENTIFIQUE
UNIVERSITE DE MEDEA



FACULTE DE TECHNOLOGIE

THESE DE DOCTORAT

Présentée en vue de l'obtention du diplôme de

Docteur en : Automatique

Spécialité : Automatique et Informatique Industrielle

Présentée par : Sadok Bouziane Yazid

Thème

Contribution à l'optimisation de la gestion d'énergie dans un micro-réseau intégrant des éléments de conversion et de stockage hybride

---

Présentée devant le jury composé de :

Nom & Prénom	Grade	Institution d'affiliation	Désignation
HOUASSINE Hamza	Professeur	Université de Médéa	Président
HENINI Noureddine	Professeur	Université de Médéa	Directeur de thèse
TLEMCANI Abdelhalim	Professeur	Université de Médéa	Co- Directeur de thèse
MEDJBER Ahmed	MCA	Université de Médéa	Examinateur 1
BENTOUATI Smain	MCA	Université de Médéa	Examinateur 2

Année académique : 2025/2026

Dedication

To my parents, whose unwavering faith has been my anchor throughout this doctoral journey. Your steadfast support and belief in me never faltered, even in moments of self-doubt. From the day I shared this ambition, you embraced it with conviction, offering reassurance that became my lifeline. The resilience and perseverance I have witnessed in you have shaped my own determination, inspiring me to face every challenge with courage and resolve. Your guidance, strength, and unconditional love have been the foundation of my scholarly path.

This achievement is as much yours as it is mine. With profound gratitude, I dedicate this milestone to you my mentors, my champions, and my greatest inspiration. ***Thank you, Mom****.*

Finally, I extend my heartfelt appreciation to everyone I have had the privilege of knowing and working with throughout my PhD journey. The collective support, wisdom, and encouragement I received have been instrumental in shaping my growth as a researcher and scholar.

Acknowledgements

***Alhamdulillah**, all praise and thanks are due to Allah, who has granted me intellect, willpower, and perseverance. Praise be to Allah for turning yesterday's dreams into today's reality, for guiding me through obstacles and challenges, and for leading me toward success and achievement. Thank you, Allah, for blessing me with strength, patience, determination, and the joy of accomplishment. Through this journey, I have learned never to despair of Allah's generosity, for He bestows His blessings at the perfect time. Alhamdulillah, always and forever.*

*I would like to express my deepest gratitude to my primary supervisor, **Prof. HENINI Noureddine**, for his unwavering support, profound expertise, and invaluable guidance throughout this research journey. His encouragement, patience, and dedication have been instrumental in shaping both this thesis and my academic development.*

*My sincere appreciation also goes to my co-supervisor, **Prof. TLEMÇANI Abdelhalim**, for his insightful feedback, critical observations, and constructive suggestions, which have greatly enriched the quality and depth of this work.*

*Finally, **Alhamdulillah**, I am grateful for every opportunity, every challenge overcome, and every success achieved along the way. May this work stand as a humble testament to faith, perseverance, and the power of community support.*

الملخص

أدى تزايد الطلب العالمي على الطاقة المستدامة أدى إلى تسريع الانتقال نحو مصادر الطاقة المتجددة، وخاصة الأنظمة الكهروضوئية طاقة الرياح والطاقة الشمسية، اللتين تُعدان من أبرز التقنيات لتوليد طاقة نظيفة وصديقة للبيئة. ومع ذلك، تواجه هذه الأنظمة تحديات كبيرة ناتجة عن التقطع والتغيرات في الإشعاع الشمسي وسرعة الرياح، مما يؤدي إلى انخفاض في الكفاءة والاستقرار. وللتغلب على هذه التحديات، يجب اعتماد استراتيجيات متقدمة للتحكم وإدارة الطاقة تضمن التشغيل الموثوق والاستخدام الأمثل للطاقة المتاحة.

تركز هذه الأطروحة على تحسين أداء أنظمة الطاقة المتجددة من خلال تطوير تقنيات ذكية لإدارة الطاقة وتحسينها. في البداية، تم تحليل ومقارنة مختلف الخوارزميات لتتبع نقطة القدرة القصوى بهدف تحديد الطرق الأكثر كفاءة في زيادة استخلاص الطاقة من الأنظمة الكهروضوئية. بعد ذلك، تم تصميم نظام طاقة متجددة هجين يدمج الألواح الشمسية وتوربينات الرياح والبطاريات والمكثفات الفائقة لتحسين موثوقية الطاقة وكفاءة التخزين. كما تم اقتراح استراتيجية ذكية لإدارة الطاقة تعتمد على المنطق الضبابي لتنظيم تدفق الطاقة بين مصادر التوليد ووحدات التخزين، بما يضمن استقرار النظام تحت ظروف بيئية وأحمال مختلفة.

أظهرت نتائج المحاكاة فعالية الاستراتيجيات المقترحة، حيث حسّنت خوارزميات تتبع نقطة القدرة القصوى كفاءة تحويل الطاقة، في حين أثبتت استراتيجية إدارة الطاقة القائمة على المنطق الضبابي قدرتها على تحقيق توازن في تدفق الطاقة وتقليل تقلبات الجهد الكهربائي وإطالة عمر البطاريات. بشكل عام، تقدم هذه الدراسة إطاراً متكاملاً لتحسين استقرار وكفاءة وموثوقية أنظمة الطاقة المتجددة الهجينة، مما يعزز من دمجها في شبكات الطاقة الذكية المستقبلية.

الكلمات المفتاحية: أنظمة الطاقة المتجددة، الطاقة الكهروضوئية، تتبع نقطة القدرة القصوى، تقنيات التحسين، أنظمة الطاقة المتجددة الهجينة، استراتيجيات إدارة الطاقة.

Abstract

The growing global demand for sustainable energy has accelerated the shift toward renewable sources, with photovoltaic (PV) and wind systems emerging as leading technologies for clean power generation. Despite their potential, these systems suffer from intermittency and variability caused by changing weather conditions, which often compromise their efficiency and stability. To address these challenges, advanced control and optimization approaches are required to ensure reliable operation and optimal energy utilization.

This thesis focuses on the performance of renewable energy system performance through intelligent power management and optimization strategies. First, various Maximum Power Point Tracking (MPPT) algorithms are investigated and compared to identify the most effective methods for improving PV energy extraction. Building on this, a hybrid renewable energy system (HRES) combining photovoltaic panels, wind turbines, batteries, and supercapacitors is developed to increase overall reliability and energy storage efficiency. A novel Fuzzy Logic–based Energy Management Strategy (FL-EMS) is then proposed to coordinate power distribution among the different sources and storage elements, ensuring smooth operation under varying environmental and load conditions.

Simulation results validate the effectiveness of the proposed approaches. The optimized MPPT algorithms achieve higher conversion efficiency, while the FL-EMS demonstrates superior performance in maintaining power balance, minimizing voltage fluctuations, and extending battery lifespan. Overall, this research presents a comprehensive framework for improving the stability, efficiency, and reliability of hybrid renewable energy systems, advancing their integration into future smart microgrids.

Keywords: Renewable Energy Systems, Photovoltaic, Maximum Power Point Tracking, Optimization Techniques, Hybrid Renewable Energy Systems, Energy Management Strategies.

Résumé

La demande mondiale croissante en énergie durable a accéléré la transition vers les sources renouvelables, notamment les systèmes photovoltaïques (PV) et éoliens, qui représentent des technologies clés pour une production d'énergie propre. Malgré leur potentiel, ces systèmes souffrent de l'intermittence et de la variabilité des conditions météorologiques, ce qui compromet souvent leur efficacité et leur stabilité. Pour surmonter ces limitations, il est nécessaire de recourir à des approches de commande et d'optimisation avancées afin d'assurer un fonctionnement fiable et une utilisation optimale de l'énergie.

Cette thèse vise à améliorer les performances des systèmes d'énergie renouvelable grâce à des stratégies intelligentes de gestion et d'optimisation de l'énergie. Dans un premier temps, différents algorithmes de suivi du point de puissance maximale (MPPT) sont étudiés et comparés afin d'identifier les méthodes les plus efficaces pour optimiser l'extraction d'énergie photovoltaïque. Ensuite, un système hybride d'énergie renouvelable (HRES) combinant des panneaux photovoltaïques, des éoliennes, des batteries et des supercondensateurs est conçu pour accroître la fiabilité et l'efficacité du stockage énergétique. Une stratégie innovante de gestion de l'énergie, basée sur la logique floue (FL-EMS), est proposée afin de coordonner la distribution de la puissance entre les différentes sources et unités de stockage, garantissant ainsi une exploitation stable sous diverses conditions environnementales et de charge.

Les résultats de simulation valident l'efficacité des approches proposées. Les algorithmes MPPT optimisés améliorent le rendement de conversion énergétique, tandis que la stratégie FL-EMS démontre une performance supérieure en maintenant l'équilibre de puissance, en réduisant les fluctuations de tension et en prolongeant la durée de vie des batteries. Dans l'ensemble, cette recherche propose un cadre complet pour améliorer la stabilité, l'efficacité et la fiabilité des systèmes hybrides d'énergie renouvelable, facilitant leur intégration dans les microréseaux intelligents de demain.

Mots-clés : Systèmes d'énergie renouvelable, Photovoltaïque, Suivi du Point de Puissance Maximum, Techniques d'optimisation, Systèmes hybrides d'énergie renouvelable, Stratégies de gestion de l'énergie.

Table of Contents

Dedication ..... **i**

Acknowledgements ..... **ii**

Abstract ..... **iv**

Table of Contents ..... **vi**

List of Figures ..... **xi**

List of Tables ..... **xiv**

List of Symbols ..... **xv**

Chapter I: General Introduction **16**

I.1 Background 16

I.2 Motivation of the Study 18

I.3 Research Objectives 19

I.3.1 Development and Evaluation of Innovative Metaheuristic and AI MPPT Algorithms 20

I.3.2 Modelling and Management of a Hybrid Energy System 20

I.4 Problem Statement 21

I.5 Significance of the Study 22

I.6 Thesis Structure 22

I.7 Conclusion 24

Chapter II: Comprehensive Literature Review on Control and Integration of Photovoltaic and Wind Electrical Power Hybrid Systems with Energy Storage.....25

II.1 Introduction.....25

II.2 Photovoltaic (PV) Solar Systems.....27

II.2.1 PV Cell Operating Principle 28

II.2.2 From Solar Cells to PV Arrays: Configuration and Protection.....29

II.2.3 Equivalent Circuit and Mathematical Model of PV Cells 30

II.2.4 Critical Points in PV Module I-V and P-V Characteristic Curves.....32

II.2.5 Temperature and Irradiance Effects on the Characteristics of the PV 34

II.2.6 Overview of PV Panel Technologies 36

II.3 Wind Generators 38

II.3.1 Mathematical Model of Wind Turbines 39

II.3.2 Wind Generator Technologies.....41

II.4 The Need for Hybridization 42

II.4.1 HRES with/without Grid Setup 43

II.4.1.1 On-Grid Systems.....43

II.4.1.2 Off-Grid Systems 44

II.4.1.3 Microgrid Systems 44

II.5 Energy Storage Technologies use in HRES 45

II.5.1 Batteries 46

II.5.2 Supercapacitors 47

II.6 Energy Management Strategies 47

II.7 Conclusion 49

Chapter III: Performance Evaluation of Metaheuristic-AI MPPT Algorithms for Photovoltaic Systems with DC-DC Converters 52

III.1 Introduction 52

III.2 Concept of MPPT: 53

III.3 DC-DC Topologies: 54

III.3.1 Buck Converter 56

III.3.2 Boost Converter 58

III.3.3 Buck-boost Converter 60

III.4 MPPT Algorithms 63

III.4.1 Classifications 64

III.4.1.1 Conventional Methods 64

III.4.1.2 Advanced (soft computing) Methods 66

III.4.1.2.1 Artificial Intelligence Methods 67

III.4.1.2.2 Metaheuristic Optimization Methods: 68

III.4.1.2.2.1 Particle Swarm Optimization (PSO): 69

III.4.1.2.2.2 Grey Wolf Optimization (GWO): 71

III.4.1.2.2.3 Ant Colony Optimization (ACO) 75

III.4.1.2.2.4 Cuckoo Search (CS) 77

III.4.1.2.2.5 The Harris Hawk Optimization (HHO) 80

III.4.1.2.2.6 Horse Herd Optimization Algorithm (HOA) 85

III.5 Performance Evaluation of MPPT Algorithms 89

III.5.1 Tracking Accuracy 89

III.5.2 Efficiency 89
III.5.3 Robustness 90
III.5.4 Tracking Speed 90
III.6 PV System Configuration 91
III.6.1 Simulation Results and Discussion 92
III.6.1.1 Algorithms Under Uniform Solar Illumination 93
III.6.1.2 Non-Uniform Irradiance Condition 103
III.7 Conclusion 113
Chapter IV: Modeling, Control, and Integration of a PV/Wind/HESS Microgrid with Energy Management Strategy 115
IV.1 Introduction 115
IV.2 Proposed System Description 116
IV.3 Modelling of System Components 117
IV.3.1 Wind Energy Model 117
IV.3.1.1 PMSG Modelling 119
IV.3.1.2 Torque Calculation 119
IV.3.2 Photovoltaic (PV) Model 121
IV.3.3 Maximum Power Point Tracking (MPPT) 122
IV.4 Energy Storage System ESS 123
IV.4.1 Battery Modelling 123
IV.4.2 Supercapacitor (SC): 125

IV.4.3 Role of Bidirectional Converters: 127

IV.4.3.1 Charging Mode (Buck Converter): 128

IV.4.3.2 Discharging Mode (Boost Converter): 128

IV.5 Sizing of the ESS Components 128

IV.5.1 The Supercapacitor Sizing: 128

IV.5.2 Battery Sizing: 129

IV.6 HESS Control 129

IV.7 Fuzzy Logic Energy Management 131

IV.8 Simulation Results 136

IV.8.1 Case 1: Variations in Irradiance and Wind Velocity. 136

IV.8.2 Case 2: Variations in Irradiance and Wind Velocity and Load Demands 144

IV.8.3 Dynamic Load Changes Using Real-Time Data 151

IV.9 Conclusion 160

Chapter V: General Conclusion 163

Bibliography 166

List of Figures

Figure I-1 World electricity generation by source on16 May 2023 [9]. 17
Figure I-2 Trends in the capacity of installed wind and solar systems [11]..... 17
Figure I-3 Weather data by National Renewable Energy Laboratory (NREL), USA [14]. 18
Figure II-1 Solar Cell Construction. 27
Figure II-2 Operating Principles of PN Junction Solar Cells 28
Figure II-3 Solar cell, Module, Panel and Array..... 30
Figure II-4 I-V and P-V Characteristic Curves of a PV Module. 32
Figure II-5 : I-V and P-V Curves at Different Levels of Irradiance 34
Figure II-6 Temperature Effect on I-V P-V Characteristic Curves of PV 35
Figure II-7 Model of a photovoltaic cell with one diode. 37
Figure II-8 Model of a photovoltaic cell with two diodes. 37
Figure II-9 Model of a photovoltaic cell with three diodes. 38
Figure II-10 Functional block diagram of wind turbine system. 40
Figure II-11 Passive and active storage systems. 46
Figure II-12 Proposed EMS classification 48
Figure III-1 Block Diagram of a MPPT Controller. 54
Figure III-2 Basic Model of a DC-DC Converter. 55
Figure III-3 Classification of DC-DC Converters. 56
Figure III-4 Buck Converter. 57
Figure III-5 Tracking and non-Tracking Regions of the I-V Curve for Buck DC-DC Converters. 58
Figure III-6 Boost Converter. 59
Figure III-7 Tracking and non-Tracking Regions of the I-V curve for Boost DC-DC Converters. 60
Figure III-8 Buck-Boost Converter. 61
Figure III-9 Operational MPPT Regions in DC-DC Buck-Boost, SEPIC, and Cuk Converters. 63
Figure III-10 MPPT Techniques Classification. 66
Figure III-11 Flowchart of the Standard PSO-MPPT based Algorithm. 70
Figure III-12 GWO MPPT Algorithm Flowchart. 74

Figure III-13 ACO-MPPT based Algorithm. 76
Figure III-14 CS-MPPT based Algorithm..... 79
Figure III-15 Control flow chart of HHO. 84
Figure III-16 Diagram representing grazing, hierarchy, sociability, imitation, defense mechanisms, and roam of the HOA. 87
Figure III-17 Flowchart of the HOA algorithm. 88
Figure III-18 Model Block Diagram of Metaheuristic MPPT comparison connected to PV System. 91
Figure III-19 Illumination Profile of the Uniform Solar Irradiance Condition (USI). 93
Figure III-20 PV Power Waveforms 94
Figure III-21 PV Power with PSO MPPT..... 94
Figure III-22 PV Power GWO MPPT 95
Figure III-23 PV Power ACO MPPT..... 95
Figure III-24 PV Power CS MPPT 96
Figure III-25 PV Power HHO MPPT 96
Figure III-26 PV Power HOA MPPT..... 97
Figure III-27 PV Power - FLC MPPT 97
Figure III-28 PV Power - NNA MPPT 98
Figure III-29 Comparison of MPPT Algorithms 101
Figure III-30 PV Characteristic Curves of the Studied PSC Case..... 104
Figure III-31 PV Power-PSO MPPT under PSC 105
Figure III-32 PV Power-GWO MPPT under PSC 105
Figure III-33 PV Power-ACO MPPT under PSC 106
Figure III-34 PV Power-CS MPPT under PSC..... 106
Figure III-35 PV Power-HHO MPPT under PSC..... 107
Figure III-36 PV Power-HOA MPPT under PSC 107
Figure III-37 PV Power-FLC MPPT under PSC 108
Figure III-38 PV Power-NNA MPPT under PSC 108
Figure III-39 Comparison of MPPT Algorithms under PSC 111
Figure IV-1 System Proposed 117
Figure IV-2 Wind Turbine model and PMSG scheme. 120
Figure IV-3 block schematic of the MPPT-using PI control. 123
Figure IV-4 Model of battery 125

Figure IV-5 Model of SC 127
Figure IV-6 Hybrid ESS control scheme. 130
Figure IV-7 Proposed fuzzy logic energy management system 133
Figure IV-8 Wind Velocity 136
Figure IV-9 Wind system power 137
Figure IV-10 irradiance variation 137
Figure IV-11 PV Power Output 138
Figure IV-12 Battery/SC Chargin Discharging Modes 138
Figure IV-13 Load Power Demand 139
Figure IV-14 Dc voltage 139
Figure IV-15 Power waveforms case1 140
Figure IV-16 Irradiance Variation 144
Figure IV-17 PV Power 144
Figure IV-18 wind Velocity 145
Figure IV-19 Wind system power 145
Figure IV-20 ESS Charging/Discharging 146
Figure IV-21 Variable Load 146
Figure IV-22 DC Bus Voltage 147
Figure IV-23 Power Waveforms case2 147
Figure IV-24 city of MEDEA, Algeria 151
Figure IV-25 Wind velocity for 24h 152
Figure IV-26 wind turbine system power output for 24h 153
Figure IV-27 irradiance variation for 24 h 153
Figure IV-28 PV system Power output for 24h 154
Figure IV-29 Battery/SC Charging-Discharge 154
Figure IV-30 battery state of charge SOC% 155
Figure IV-31 Variable Load for 24h 155
Figure IV-32 DC Voltage 156
Figure IV-33 power waveforms under Real data 156
Figure IV-34 FL EMS Zoomed Part 1 157
Figure IV-35 FL-EMS Zoomed Part2 157

List of Tables

Table III-1 PV Module Specifications. 92
Table III-2 comprehensive analysis of the algorithm's 102
Table III-3 Comparative Performance of MPPT Techniques under Uniform and Partial Shading Conditions 112
Table IV-1 Wind electrical system parameters 120
Table IV-2 PV electrical system Parameters 121
Table IV-3 Battery electrical system Parameters 125
Table IV-4 SC electrical system Parameters 127
Table IV-5 Converter electrical system Parameters 128
Table IV-6 Fuzzy logic 133
Table IV-7 Summary of control modes in FL-EMS 135
Table IV-8 The results analysis description case 1 141
Table IV-9 The results analysis description case 2 148
Table IV-10 Real data analysis description 152

List of Symbols

ACO	Ant Colony Optimization
AI	Artificial Intelligence
ANN	Artificial Neural Network
BDC	Bidirectional Converters
BESS	Battery Energy Storage System
CS	Cuckoo Search
DDM	Double-Diode Model
EAs	Evolutionary Algorithms
EES	Electrical Energy Storage
EMS	Energy Management Strategies
ESSs	Energy Storage Systems
FBC	Filter-Based Control
FLCs	Fuzzy Logic Controllers
GA	Genetic Algorithm
GM	Global Maximum
GMPP	Global Maximum Power Point
HES	Hybrid Energy System
HESS	Hybrid Energy Storage Systems
HHO	Harris Hawks Optimization
HOA	Horse Herd Optimization Algorithm
HRES	Hybrid Renewable Energy Systems
MPC	Model Predictive Control
MPP	Maximum Power Point
MPPT	Maximum Power Point Tracking
MG	Microgrids
MS	Management System
ML	Machine Learning
OCV	Open Circuit Voltage
PMSG	Permanent magnet synchronous generator
PS	Partial Shading
P&O	perturb and observe
PSO	particle swarm optimization
PV	Photovoltaic
PWM	Pulse width modulation
RB	Rule Based
RC	Robust Control
SC	Supercapacitors
STC	Standard Test Condition
SDM	Single-Diode Model
SMC	State Machine Control
SOC	State of Charge
SPVS	Solar Photovoltaic System
UIC	Uniform Irradiance Condition
USI	Uniform Solar Irradiance
WT	Wind Turbine

Chapter I: General Introduction

I.1 Background

Energy has been a fundamental driver of human development, from early civilizations exploiting wind and solar resources to modern industrial societies characterized by rapidly increasing energy consumption. Over the last century, this growth has been largely supported by fossil fuels, which still dominate the global energy mix. However, rising energy demand driven by population growth and economic expansion, particularly in emerging economies combined with environmental concerns, resource depletion, and fossil fuel price volatility, has accelerated the global transition toward sustainable energy alternatives.

Among renewable sources, solar and wind energy have emerged as the most promising due to their abundance, scalability, and environmental compatibility. Wind energy originates from solar-induced atmospheric pressure gradients, while solar energy has been exploited for millennia through passive and active applications. Historically, wind energy was utilized for transportation and irrigation as early as 3100 BC and later evolved into mechanical windmills across Mesopotamia, China, and Europe [1]. Similarly, solar energy played a central role in ancient architecture and daily life, with early applications documented in China, Egypt, Greece, and Rome [2], [7]. Despite this long-standing reliance on renewables, the Industrial Revolution marked a shift toward fossil fuels, resulting in severe environmental impacts and record global temperature increases.

In response, global energy strategies increasingly prioritize renewable energy deployment. Projections indicate that by 2050, global energy demand will reach approximately 55 PWh annually, with electricity consumption increasing by about 140%. Solar photovoltaic (PV) and wind technologies are expected to dominate future renewable capacity due to their declining costs and technological maturity Figure I-1. According to the European Commission, renewable sources primarily PV, wind, and hydropower could supply up to 85% of global electricity by 2050. Recent trends confirm this trajectory, with global renewable capacity reaching approximately 3146 GW in 2021, nearly 90% of which was contributed by wind and solar energy Figure I-2 [9], [12].

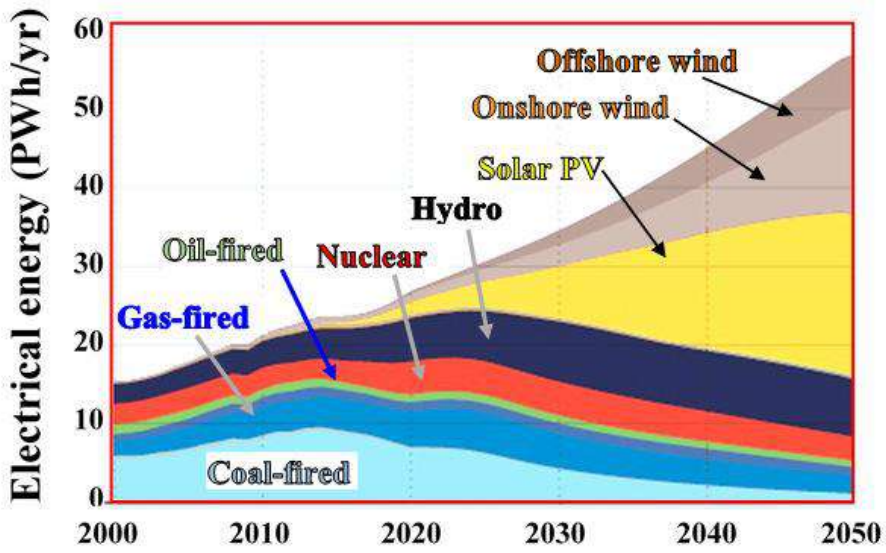


Figure I-1 World electricity generation by source on16 May 2023 [9].

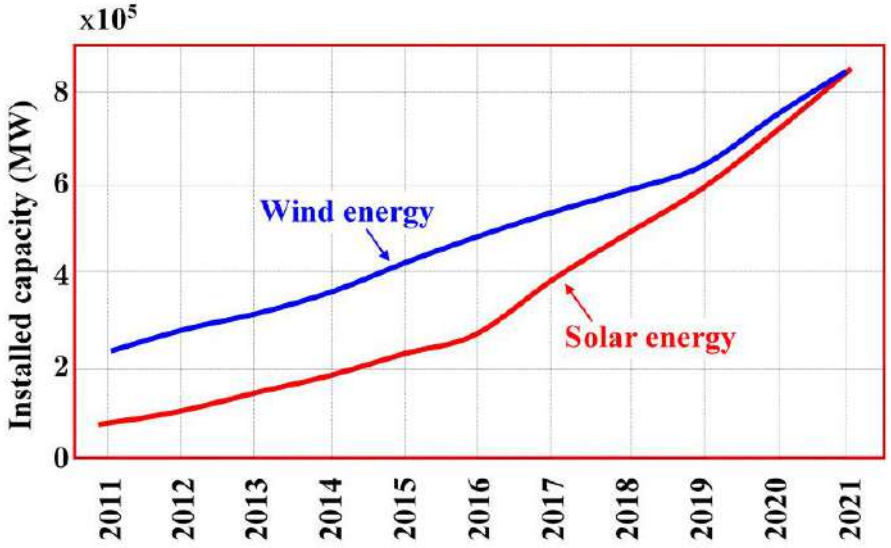


Figure I-2 Trends in the capacity of installed wind and solar systems [11].

Despite their advantages, the performance of solar photovoltaic systems (SPVSs) and wind energy conversion systems (WECSs) is inherently dependent on stochastic environmental conditions such as solar irradiance, temperature, and wind speed. This intermittency limits the reliability of standalone systems. Hybrid renewable energy systems (HRESs), which combine complementary sources such as wind and solar, offer an effective solution by smoothing power fluctuations and improving supply continuity. Meteorological data from the National

Renewable Energy Laboratory (NREL) highlight the temporal variability of these resources and underscore the benefits of hybrid configurations Figure I-3 [14], [15].

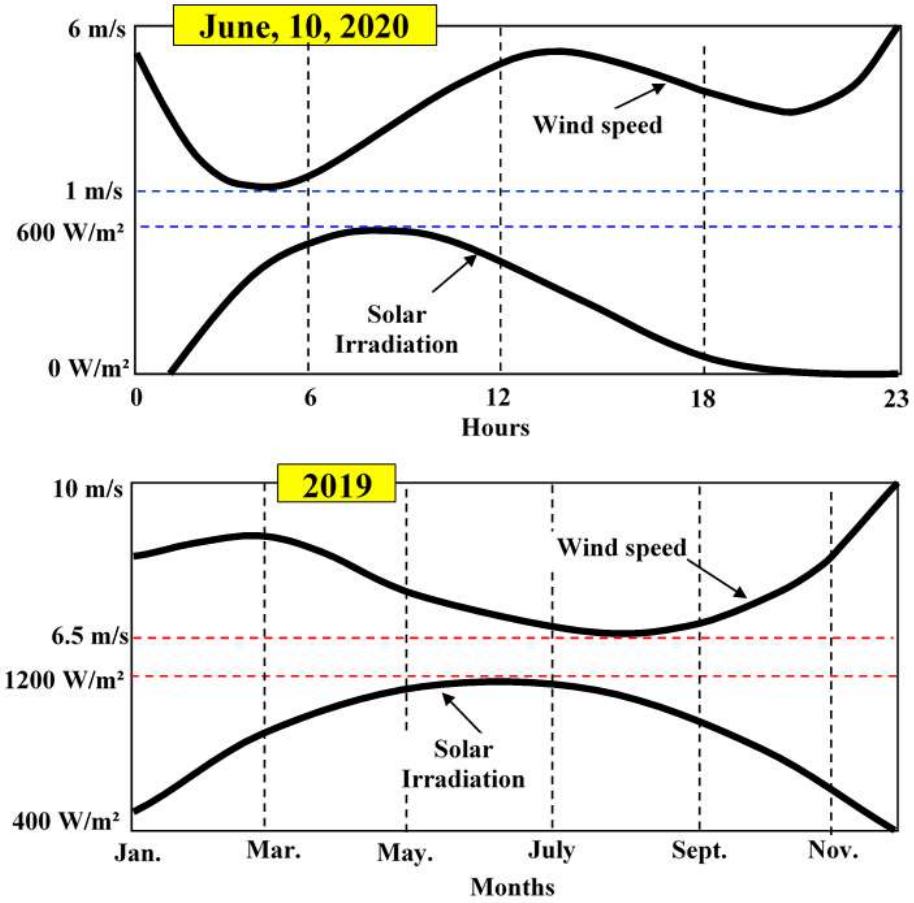


Figure I-3 Weather data by National Renewable Energy Laboratory (NREL), USA [14].

Consequently, PV–wind hybrid systems have attracted significant research and industrial interest due to their enhanced reliability, cost-effectiveness, and suitability for off-grid and remote applications [10], [16], [19]. Large-scale implementations worldwide including projects in the United States, Australia, Denmark, and Spain demonstrate the technical feasibility and scalability of hybrid renewable systems, confirming their role as a key solution for meeting future global energy demands sustainably [20], [23].

I.2 Motivation of the Study

The escalating threat of climate change underscores the urgent need to transition from conventional fossil fuel-based energy systems toward cleaner, more sustainable alternatives.

While considerable advancements have been made in deploying renewable energy technologies particularly solar and wind, these sources, when used independently, are subject to inherent limitations. Solar power is dependent on daylight and weather conditions, while wind energy is influenced by irregular and unpredictable wind patterns. This intermittency compromises the stability and reliability of energy supply, posing a major obstacle to the large-scale integration of renewables into existing power systems.

In addition, current policy frameworks and economic incentives are often insufficient to support the coordinated integration of diverse renewable sources into a single, unified, and efficient system. This study is driven by the pressing need to investigate how hybrid renewable energy systems (HRES) specifically those that combine solar and wind power can overcome the limitations associated with standalone configurations.

By addressing the technical, operational, and control challenges of such hybrid systems, this research aims to contribute to the development of more reliable and resilient energy infrastructures. Ultimately, the study seeks to support the broader global objective of reducing carbon emissions, enhancing energy security, and facilitating the transition to a sustainable, decentralized energy.

I.3 Research Objectives

The research presented in this thesis is dedicated to advancing renewable energy technologies and promoting their broader adoption across various applications. By concentrating on the development and evaluation of cutting-edge methodologies, this work aims to significantly enhance the efficiency, reliability, and cost-effectiveness of hybrid renewable energy systems. The ultimate goal is to support the global transition towards a more sustainable energy future through innovative technological solutions.

The primary aim of this thesis is to improve the performance of photovoltaic PV systems by introducing and evaluating novel MPPT algorithms. In addition, it seeks to develop advanced energy management strategy for hybrid energy system that incorporate a range of components, including PV array, Wind Turbine, battery, and supercapacitor. The thesis addresses these research objectives through two main areas of focus:

I.3.1 Development and Evaluation of Innovative Metaheuristic and AI MPPT Algorithms

The first part of this thesis introduces and critically evaluates novel metaheuristic MPPT algorithms and Artificial Intelligent based MPPT Algorithms designed to address the limitations of existing methods. This section focuses on the following objectives:

- Introduction of Novel MPPT Algorithms: Particle Swarm Optimization (PSO), Grey Wolf Optimization (GWO), Ant Colony Optimization (ACO), Cuckoo Search (CS) algorithm, Harris Hawk Optimization (HHO), Horse-Herd Optimization Algorithm (HOA), Fuzzy Logic Control (FLC) and Artificial Neural Network (ANN) These algorithms are developed to enhance the performance of MPPT in photovoltaic systems.
- Implementation and Testing: Implement and test the algorithms individually in a connected PV system. Evaluate their performance under varying irradiance and partial shading conditions.
- Performance Comparison: Perform a detailed comparison between these MPP Algorithms, the evaluation includes key performance metrics such as tracking accuracy, efficiency, and robustness, with a focus on how these novel algorithms perform relative to each other.

I.3.2 Modelling and Management of a Hybrid Energy System

The second part of the thesis focuses on the development and evaluation of a hybrid energy system that integrates multiple energy sources and storage technologies. This section aims to develop an effective EMS capable of optimizing power flow and ensuring the reliable operation of the hybrid system. The specific objectives addressed in this part are:

- Model and design a hybrid energy system that combines a PV array, a wind turbine a battery, and a supercapacitor (PV-Wind Turbine-Battery- SC). This objective involves creating a detailed system design that integrates these components into a cohesive and efficient hybrid energy system.

- Develop and implement an energy management strategy (EMS): Fuzzy Logic Controller (FLC-EMS). These strategies aim to optimize power flow among the different energy sources and storage devices, ensuring a balanced distribution of energy, stable operation, and improved overall system efficiency.
- Evaluate the performance of the hybrid energy system by testing the system under varying load conditions and irradiance, Wind velocity profiles. This includes analyzing system behavior at different battery state-of-charge (SOC) levels to assess how EMS influences efficiency, stability, and overall system performance.

This research employs **MATLAB/Simulink** for simulating the hybrid renewable energy system and testing our energy management strategy.

The simulation model includes detailed representations of PV panels, wind generators, batteries, supercapacitors, and converters.

I.4 Problem Statement

Despite the increasing deployment of renewable energy systems, the intermittent and unpredictable nature of photovoltaic (PV) and wind power generation presents significant challenges to achieving a stable and reliable energy supply especially in standalone microgrid configurations. These fluctuations in energy production often led to supply-demand imbalances, voltage instability, and reduced power quality.

Traditional energy management systems, lack the flexibility and intelligence required to adapt to real-time changes in both generation and load conditions. Furthermore, energy storage systems, particularly batteries, can suffer from degradation due to frequent cycling and sudden power surges.

Although supercapacitors can handle rapid power fluctuations effectively, coordinating their operation with batteries in a hybrid energy storage system (HESS) requires an intelligent control strategy to optimize performance and extend the lifespan of the storage components.

The current literature offers limited solutions that fully address this coordination in the context of a hybrid PV-wind microgrid. Thus, there is a clear need to develop an adaptive intelligent energy management system capable of managing the dynamics of a hybrid generation and storage system in real time, while ensuring efficient energy utilization, operational reliability, and longevity of the storage units.

I.5 Significance of the Study

This study addresses a critical gap in the integration of renewable energy technologies into standalone microgrids. By focusing on a hybrid system that combines PV panels, wind turbines, batteries, and supercapacitors, this research aims to improve the overall performance, stability, and reliability of microgrid operation.

The incorporation of intelligent control strategies, such as fuzzy logic, allows for dynamic and responsive energy management that can adapt to the nonlinear and variable behavior of both energy sources and load demands. The research provides insights into optimal control techniques that can reduce battery stress, enhance system efficiency, and improve the quality of power delivery.

Moreover, the results from this study are expected to contribute to the design of more robust energy management frameworks for future off-grid applications, especially in remote or underdeveloped regions where grid access is limited and energy reliability is crucial.

I.6 Thesis Structure

The present thesis is organized into five chapters, each addressing a specific aspect of the research.

Chapter 1 introduces the research problem and provides a comprehensive overview of the study. It outlines the background of renewable energy technologies, discusses the motivations underlying this work, and defines its main objectives. The chapter also highlights the scientific contributions and significance of the research within the broader context of sustainable energy systems.

Chapter 2 focuses on the fundamental operating principles of photovoltaic (PV) and wind energy systems. It begins by explaining the physical and electrical mechanisms through which PV cells convert solar energy into electricity. The discussion encompasses PV cell modeling, module and array configurations, mathematical representations, and characteristic performance parameters. The challenges affecting PV technology particularly those related to weather variability and load fluctuations are also addressed. The second part of the chapter is devoted to wind turbines, describing their structural design, operational principles, classifications, and mathematical modeling, while emphasizing the diversity of existing topologies. The chapter further introduces hybrid energy systems (HES), examining their configurations, constituent energy sources, and advanced storage technologies. A review of HES developments over the past decade is provided, highlighting key innovations and global applications. Finally, the chapter discusses the role of Energy Management Systems (EMS) in optimizing HES performance and presents an extensive literature review of existing EMS strategies and their classifications, establishing a foundation for understanding their contribution to system efficiency and reliability.

Chapter 3 explores the concept of Maximum Power Point Tracking (MPPT) and its critical role in enhancing the energy yield of PV arrays. It then analyzes various DC–DC converter topologies utilized in MPPT systems, detailing their circuit structures and operational principles to identify the most efficient design for the proposed system. The chapter continues with a comprehensive review of MPPT algorithms, examining their categories, operational mechanisms, and distinguishing characteristics, with particular emphasis on metaheuristic approaches and artificial intelligent methods. A detailed analysis of widely adopted metaheuristic and AI techniques is provided, along with performance evaluation criteria used to assess algorithm suitability for different photovoltaic applications. Subsequently, the theoretical framework of the proposed algorithms is presented and independently analyzed, followed by their implementation in MATLAB/Simulink. The simulation results under diverse operating conditions are discussed and evaluated.

Chapter 4 presents the design and configuration of the proposed hybrid energy system, which integrates a photovoltaic array, a wind turbine, a battery bank, and a supercapacitor. The chapter elaborates on the control strategies governing system operation, particularly the Energy

Management Strategy (EMS) based on Fuzzy Logic Control (FLC-EMS). The MATLAB/Simulink model of the hybrid system is developed and simulated to validate the effectiveness of the proposed control approach. The simulation results obtained under varying irradiance levels, load profiles, and battery state-of-charge conditions demonstrate the robustness and efficiency of the FLC-EMS in ensuring optimal power management and demand satisfaction.

Chapter 5 concludes the thesis by summarizing the major findings, highlighting the research contributions, and outlining potential directions for future work.

I.7 Conclusion

This chapter established the overall context and motivation of the research by emphasizing the importance of renewable energy systems in advancing global sustainability objectives, while acknowledging the challenges arising from their intermittent and variable nature. It defined the research problem, underscored the relevance of hybrid energy storage systems, and clarified the main objectives and scope of the present study.

The next chapter provides a comprehensive review of the existing literature on renewable energy generation technologies, energy storage solutions, and energy management strategies. This review serves as the theoretical foundation for the development of the hybrid energy system proposed in this thesis.

Chapter II: Comprehensive Literature Review on Control and Integration of Photovoltaic and Wind Electrical Power Hybrid Systems with Energy Storage

II.1 Introduction

The increasing penetration of renewable energy sources into modern power systems has become a strategic response to growing energy demand, environmental concerns, and the depletion of fossil fuel resources. Among the various renewable technologies, photovoltaic (PV) and wind energy systems have gained significant attention due to their abundance, technological maturity, and decreasing installation costs. Nevertheless, the large-scale and standalone deployment of these sources is inherently constrained by their intermittent and stochastic nature, which can lead to power fluctuations, voltage instability, and reduced system reliability.

In standalone and microgrid applications, these challenges are further amplified, as the absence of grid support requires the system to maintain power balance autonomously under continuously varying environmental and load conditions. As a result, hybrid renewable energy systems (HRES), which combine multiple renewable sources most commonly PV and wind have emerged as an effective solution to enhance supply reliability and improve energy availability. By exploiting the complementary characteristics of solar irradiance and wind speed profiles, PV–wind hybrid systems can significantly mitigate power variability and ensure more stable energy production.

However, hybridization alone is insufficient to guarantee reliable operation. The integration of energy storage systems (ESS) plays a crucial role in compensating for generation intermittency, managing surplus energy, and maintaining system stability. Batteries are widely employed for long-term energy storage due to their high energy density, but their performance and lifespan are adversely affected by frequent charge–discharge cycles and high-power transients. Conversely, supercapacitors exhibit high power density, rapid response, and exceptional cycle life, making them well-suited for handling short-term power fluctuations.

Consequently, hybrid energy storage systems (HESS), combining batteries and supercapacitors, have gained increasing research interest as a means to improve storage efficiency, enhance dynamic performance, and extend battery lifetime.

The effective coordination of multiple energy sources and storage devices within a hybrid system necessitates the implementation of an advanced energy management strategy (EMS). An EMS is responsible for regulating power flows, ensuring supply–demand balance, preserving storage health, and maintaining voltage and power quality. Traditional rule-based and control-oriented EMS approaches, although simple, often lack the flexibility required to address nonlinear system dynamics and uncertainties associated with renewable energy generation. In response, intelligent control techniques such as fuzzy logic–based energy management have been widely investigated due to their ability to handle system nonlinearities, incorporate heuristic knowledge, and operate effectively under uncertain and time-varying conditions.

In parallel, the performance of photovoltaic systems strongly depends on the effectiveness of Maximum Power Point Tracking (MPPT) algorithms, which aim to extract the maximum available power under changing irradiance and temperature conditions. Conventional MPPT methods exhibit limitations in dynamic environments, particularly under partial shading conditions, motivating the development of advanced and intelligent MPPT techniques.

In this context, this chapter presents a comprehensive literature review on the modeling, control, and integration of PV–wind hybrid energy systems with energy storage. It critically examines the operating principles and mathematical models of photovoltaic and wind energy systems, reviews energy storage technologies with particular emphasis on hybrid battery-supercapacitor configurations, and surveys existing energy management strategies used in hybrid renewable systems. The objective of this review is to identify current limitations, highlight research gaps, and establish a solid theoretical foundation for the advanced MPPT algorithms and intelligent energy management strategy developed in the subsequent chapters.

II.2 Photovoltaic (PV) Solar Systems

Photovoltaic (PV) power systems are a foundational technology in the renewable energy sector, converting solar radiation directly into electrical energy through the photovoltaic effect. This phenomenon occurs within solar cells, typically fabricated from silicon, which are interconnected to form solar panels [24]. Due to the semiconductor materials used in solar cell, their electrical characteristics including current, voltage, and resistance varies when subjected to sunlight.

The structure of Photovoltaic (PV) cells is demonstrated in Figure II-1. Mainly the PV cell is formed of two layers of semiconductors materials. The upper layer is the n-type semiconductor layer, which is known as the emitter layer. The base layer is a p-type semiconductor layer. In the n-type semiconductor layer, the dominant charge carriers are negatively charged electrons that have been provided by donor impurity atoms. Conversely, the p-type semiconductor layer is characterized by positively charged holes as the primary charge carriers, which are created by acceptor impurity atoms. The two semiconductor types are sandwiched, resulting in the generation of the p-n junction between the layers [25].

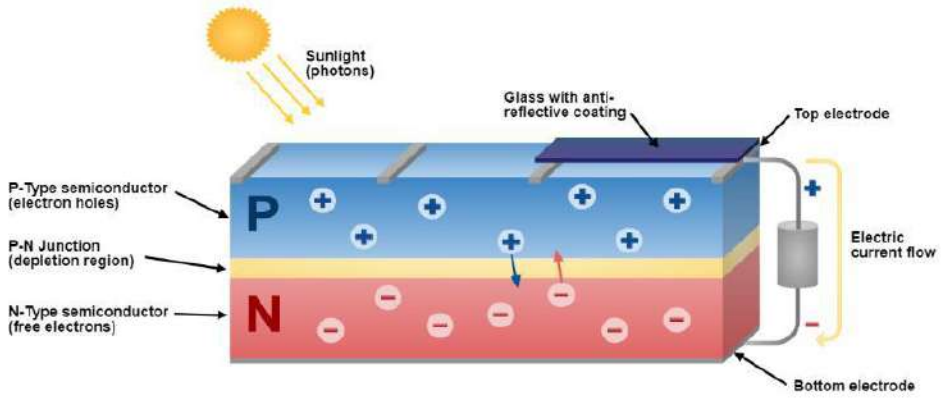


Figure II-1 Solar Cell Construction.

Electrodes are added to the top of the P-type layer and the bottom of the n-type layer for collecting electric current flow. Finally, the entire assembly is encapsulated in a thin glass with an anti-reflective coating to prevent incident light energy losses caused by reflections and to secure PV cells from any type of mechanical shocks.

II.2.1 PV Cell Operating Principle

Near the p-n junction, electrons from the n-region migrate into the p-region resulting in a layer of positively charged ions on the n-layer. Similarly, a layer of positively charged ions on the p-side is resulted from the diffusion of the p-side's holes into the n-side. Repositioning of negatively and positively charged ions creates a potential barrier [25].

When the solar cell is exposed to sunlight Figure II-2, photons with a wavelength of 1.2 micrometers or higher are absorbed by the semiconductor. Consequently, the energy supplied by the photons excites the electrons in the p-type layer, liberating them to travel randomly. As a result, a number of electron-hole pairs are produced. The freed electrons are swept across the junction into the n-type layer, while the holes are extracted by the p-type semiconductor layer. Due to the high electron mobility across the boundary, reverse movement against the field gradient is restricted, resulting in a charge imbalance between the two semiconductor regions [26]. As a result of the localized effects of the fixed field, electrons are drawn into the n-layer, creating a natural tendency for them to leave the layer and restore the charge equilibrium. To accomplish this, electrons will follow an alternative path if one is available. By establishing an external circuit that allows the electrons to return to the other layer to amalgamate with the holes, a continuous flow of current is generated, sustained by the presence of light striking the solar cell [26], [27].

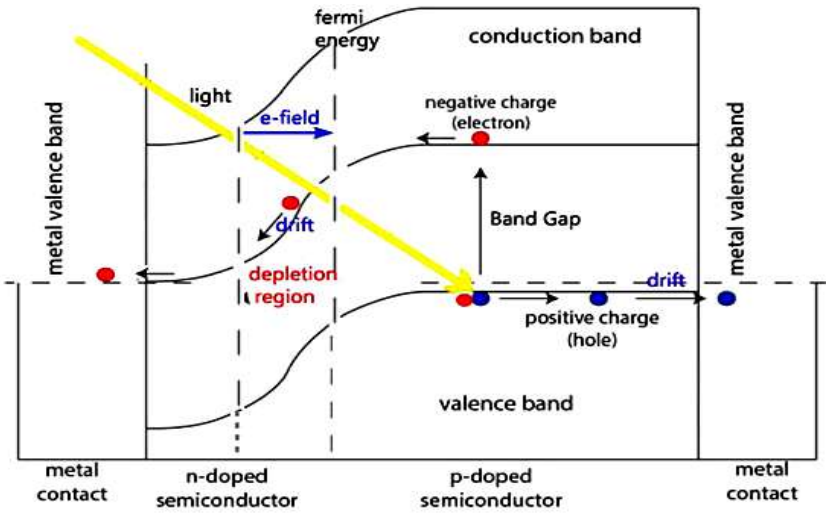


Figure II-2 Operating Principles of PN Junction Solar Cells

The thickness of the n-type layer needs to be narrower compared to the p-type layer. This construction facilitates faster electron movement through the circuit, enabling current generation before the electrons have a chance to recombine with the holes. Furthermore, an anti-reflective coating is applied on top of the n-layer. The primary function of this coating is to reduce surface reflections, which in turn boosts the amount of light that reaches and is absorbed by the semiconductor material [25].

II.2.2 From Solar Cells to PV Arrays: Configuration and Protection

A single solar cell typically produces an output voltage of less than 1V (up to 0.58V), which may not be adequate for many high-power applications. To overcome this limitation, solar cells are interconnected in series and/or parallel configurations to form PV modules [28], [29]. Connecting cells in series increases the output voltage, while connecting them in parallel increases the output current. These modules are then connected in series to form PV strings or panels, which are further interconnected in parallel to create a complete PV array. This arrangement ensures that the combined output current and voltage of the PV array are sufficient to meet the necessary requirements.

To safeguard the panel's surface from potential damage, it is covered with a flat glass surface. This glass enclosure serves as a protective barrier against dust and other environmental hazards while also enhancing the panel's performance by concentrating more sunlight into the cells. The PV panels within an array are usually mounted on a support structure, such as a mounting rack or frame, to optimize their orientation and angle towards the sun for maximum energy production. Figure II-3 illustrates the PV cell, module, string, and array.

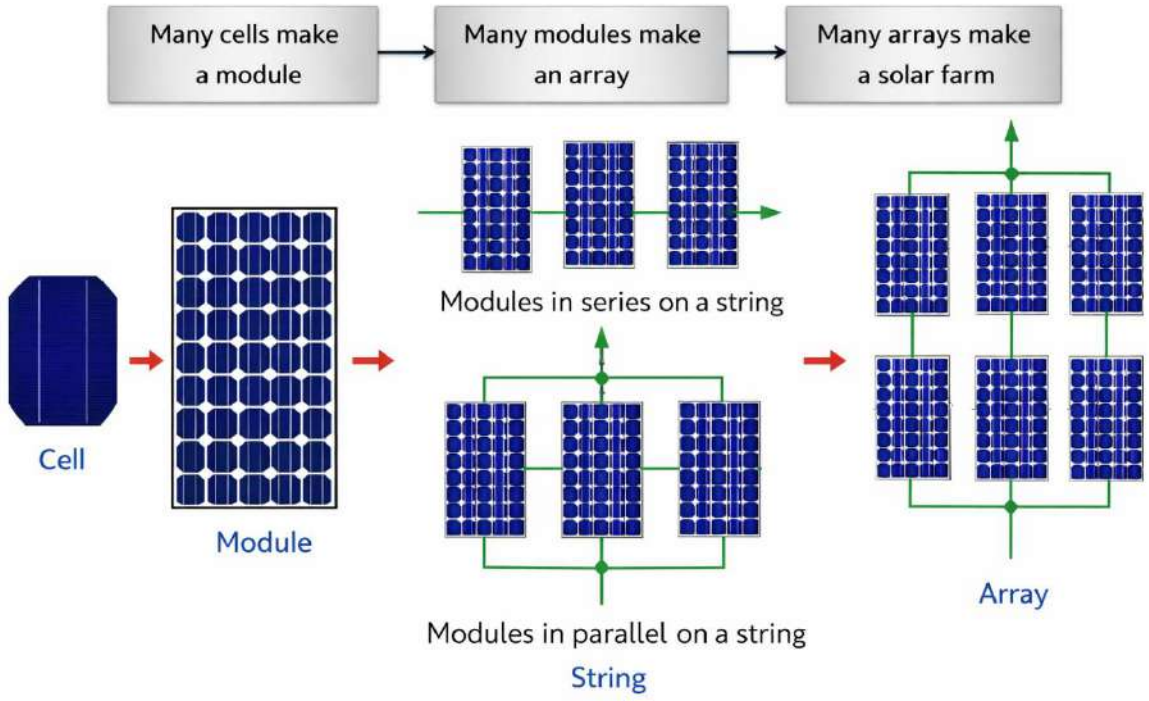


Figure II-3 Solar cell, Module, Panel and Array

The basic configurations for PV systems consist of series and parallel arrangements, from which other configurations are derived. Other topologies utilized in PV systems include series-parallel (SP), total-cross-tied (TCT), and bridge-linked (BL). These additional configurations are implemented to enhance the efficiency and dependability of PV systems and are commonly employed in various applications based on specific needs [31].

II.2.3 Equivalent Circuit and Mathematical Model of PV Cells

Different theoretical models of photovoltaic cells based on basic electrical components with known behavior have been proposed in the literature. All of these equivalent models are used to closely approximate and determine the electronic behavior of a solar cell and to predict its energy production. Real solar cells experience power dissipation through series resistance caused by the ohmic contact on the front surface, as well as shunt resistance resulting from leakage current. Hence, in practical applications, a basic solar cell is typically characterized by an ideal diode (*Di*) connected in parallel with a current source. The current source represents

the generated photocurrent when sunlight hits the solar panel, symbolizing the flow of electrons. The diode, on the other hand, represents the p-n transition area of the solar cell, where the conversion of light energy into electrical energy takes place [32]. Additionally, the solar cell model incorporates a shunt resistance (R_{Sh}) and a series resistance (R_S) in connection with the load.

The electrical behavior of a PV cell can be described by the following expression:

$$I = I_{ph} + I_d \tag{II.1}$$

where I represents the total current generated by the solar cell, I_{ph} is the photocurrent produced by incident sunlight, and I_d denotes the diode (dark) current. The generated current I is directly proportional to the intensity of incident solar radiation.

The output power of a PV cell is calculated using the standard power formula:

$$P = I.V \tag{II.2}$$

where P is the output power, I is the current, and V is the voltage at the terminals of the solar cell. The terminal voltage can be estimated using the Shockley diode equation [33]:

$$V = V_{oc} - I.R_S \tag{II.3}$$

where V_{oc} is the open-circuit voltage, and R_S represents the series resistance of the cell.

The overall efficiency nPV of a solar PV system, defined as the ratio of electrical power output to the total incident solar energy, is given by:

$$n_{PV} = P_{max}/P_{inc} \tag{II.4}$$

where P_{max} is the maximum electrical power output and P_{inc} is the incoming solar energy. PV system efficiency is affected by several factors, including temperature variations, irradiance levels, and the physical and electrical properties of the cell materials.

The instantaneous power output of a PV system, expressed in kilowatts (kW), can be modeled as follows [24,28]:

$$P_{PV,t} = C_{PV} n_{PV} . \left(\frac{G_{T,t}}{G_{T,STC}}\right) . [1 - \alpha_p (T_{C,t} - T_{C,STC})] \quad \text{(II.5)}$$

where:

C_{PV} is the rated capacity of the PV array (kW), n_{PV} is the PV derating factor (%), $G_{T,t}$ is the incident solar irradiance (kW/m²), $G_{T,STC}$ is the solar irradiance at Standard Test Conditions (kW/m²), α_p is the temperature coefficient of power (%/°C), $T_{C,t}$ is the PV cell temperature (°C), $T_{C,STC}$ is the cell temperature at STC (°C).

Figure II-4 depicts the characteristic curve of the PV cell.

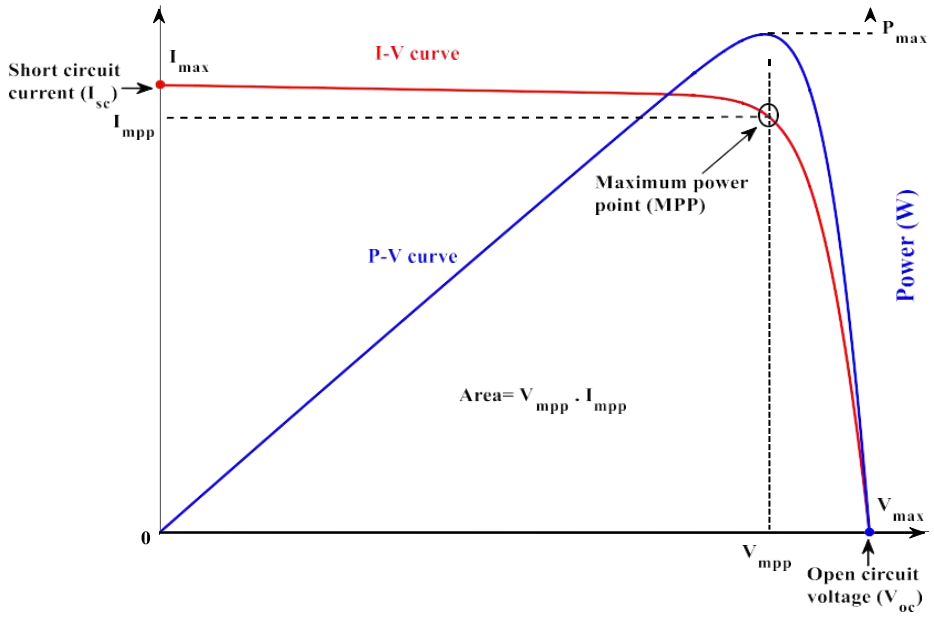


Figure II-4 I-V and P-V Characteristic Curves of a PV Module.

II.2.4 Critical Points in PV Module I-V and P-V Characteristic Curves

a. **Short-Circuit Current (I_{sc}):** It represents the maximum current output of a PV system under open-circuit conditions, where the voltage is zero and the system is short-circuited. This current is crucial for designing PV systems, as it sets the

upper limit for current capacity and helps in sizing components like wires, fuses, and inverters. I_{sc} is affected by factors such as the panel's cross-sectional area, light intensity, light spectrum, and optical properties, including absorption and reflection. Understanding I_{sc} is essential for system performance and safety calculations [37].

b. **The open-circuit voltage (*Voc*):** is the maximum voltage a PV system can produce when no current is flowing, indicating that the system is open-circuited. *Voc* is a critical parameter in PV system design, defining the maximum voltage and helping in sizing components like charge controllers, inverters, and batteries. It is influenced by factors such as photocurrent, saturation current, and cell temperature, all of which affect the system's performance and efficiency [37].

c. **Maximum Power Point (*MPP*):** This is the point on the I-V characteristic curve where the product of current and voltage is maximum, indicating the maximum power of the PV system. The MPP is the operating point at which the PV system can deliver the most power to an external load.

d. **Current at Maximum Power Point (I_{mpp}):** This is the current output of the PV system at the MPP, and represents the maximum current that the system can deliver to an external load. Imp is an important parameter for PV system design, as it sets the upper limit for the current that the system can deliver.

e. **Voltage at Maximum Power Point (V_{mpp}):** This is the voltage output of the PV system at the MPP, and represents the maximum voltage that the system can deliver to an external load. V_{mpp} is an important parameter for PV system design, as it sets the upper limit for the voltage that the system can deliver.

Overall, these five points are provided by the manufacturer datasheet and provide important information about the performance and efficiency of a PV system, and are commonly used in PV system design and analysis. Location of these specific points is influenced by a combination of factors, including the level of illumination, temperature, and load resistance. By understanding these points, designers can optimize the performance of their PV systems and ensure that they are delivering the optimal amount of power to their load.

II.2.5 Temperature and Irradiance Effects on the Characteristics of the PV

The performance of a solar panel is influenced by a range of environmental factors, with solar irradiance being the most dominant one due to its significant impact on the electrical characteristics of solar panels. Equation (II.6) highlights the relationship between solar irradiance and the electrical output of the solar panel, indicating that as the intensity of solar irradiance increases, the electrical output of the solar panel also increases [25]. Consequently, the efficiency of a solar panel is directly dependent on the amount of sunlight it receives. Figure II-5 illustrates the impact of irradiance on the I-V and P-V characteristics of a solar panel across different levels of irradiance. It shows that the output current I_{pv} of a PV module is greatly influenced by the variation in solar irradiance (G), whereas the output voltage V_{pv} remains almost constant [37].

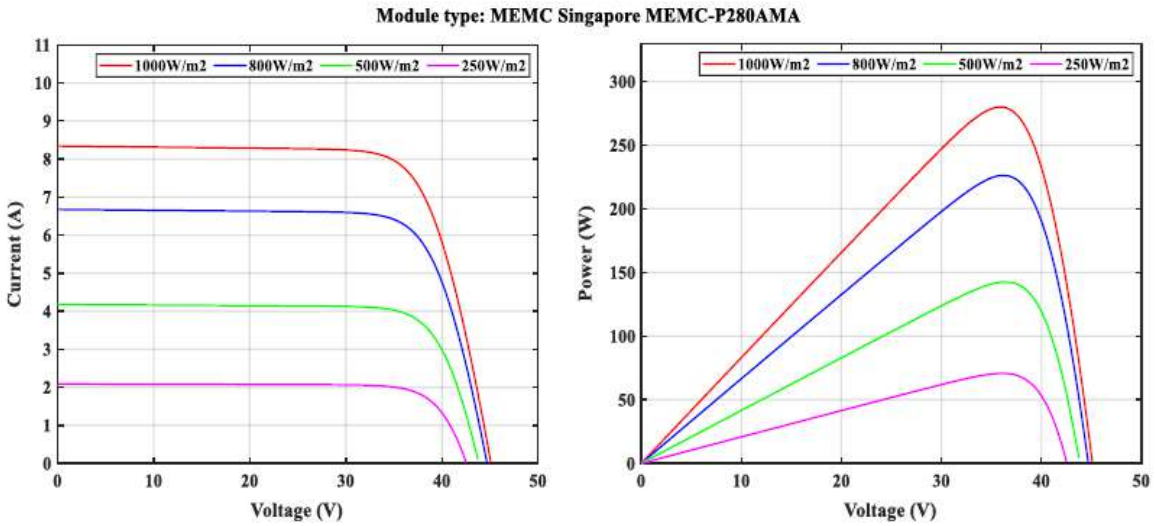


Figure II-5 : I-V and P-V Curves at Different Levels of Irradiance

$$I_{sc} = (I_{sc,STC} + K_1(T - T_{STC}))\frac{G}{G_m} \quad \text{(II.6)}$$

Where: $I_{sc,STC}$ is the short-circuit current at STC, K_1 is the temperature coefficient of the short- circuit current, T_{STC} is the standard test condition temperature (usually 25°C), G_m is the standard irradiance, usually 1000 W/m², G and T are the actual irradiance and temperature, respectively.

Apart from the effect of irradiance, the temperature of a PV panel is another crucial parameter that significantly influences its output power. According to Figure II-6, as the temperature increases, the short circuit current $I_{sc}$of the panel tends to slightly increase, while the *Voc* decreases. Additionally, for changing temperatures, the voltage varies widely while the current remains almost unchanged. Overall, the effect of temperature on the panel's performance is detrimental to its output power. At higher temperatures, the panel operates at a lower voltage, resulting in a reduced power output compared to its rated MPP [37]. This can be explained by the dependency of the open circuit voltage *Voc* on the cell temperature as follows where K_V is the temperature coefficient of the open-circuit voltage (typically negative) and $V_{oc,STC}$ is the open-circuit voltage at STC [38].

$$V_{oc} = V_{oc,STC} + K_V(T - T_{STC}) \tag{II.7}$$

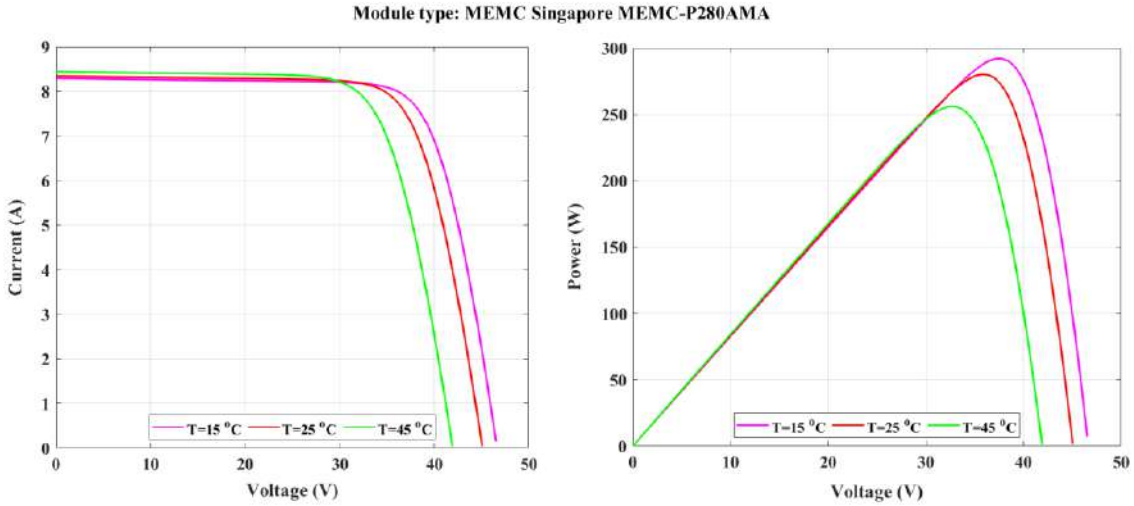


Figure II-6 Temperature Effect on I-V P-V Characteristic Curves of PV

In conclusion, it can be inferred that the MPP varies with changing environmental conditions. Specifically, the MPP is directly proportional to the solar irradiance level and inversely proportional to the ambient temperature. Consequently, the operating point of the PV panel fluctuates accordingly, leading to a reduction in power output. To address these fluctuations, careful consideration of the operating conditions and optimization of the PV

system design are essential. Equations (II.8) (II.9) outline the mathematical relationship between the MPP and weather conditions, such as temperature and irradiance [37], [38], [39].

$$I_{\text{mpp}} = K_i I_{sc} \tag{II.8}$$

$$V_{\text{mpp}} = K_V V_{oc} \tag{II.9}$$

K_i and K_V are current and voltage proportional factors, respectively.

Overall, the temperature and irradiance effects on PV system characteristics interact with each other. Higher irradiance levels can partially compensate for the negative impact of temperature on the PV system's performance. Therefore, understanding the complex relationship between temperature, irradiance, and PV system characteristics is essential for designing and operating efficient PV systems that can adapt to varying environmental conditions and maximize energy generation.

II.2.6 Overview of PV Panel Technologies

Individual solar cells are typically connected in series and/or parallel configurations to form a module, and multiple modules combined create a solar panel. In large-scale applications, several panels are interconnected again in series and/or parallel to form a photovoltaic array or station.

The manufacturing of solar cells utilizes a variety of technologies, each with distinct characteristics and performance profiles [42]:

- **Monocrystalline silicon:** Offers high efficiency (up to ~26%) and low maintenance requirements; however, it is associated with a relatively high manufacturing cost [43].
- **Polycrystalline silicon:** Provides moderate efficiency (~22%) but, similar to monocrystalline cells, involves significant production expenses [44].

- **Thin-film technology:** Achieves efficiencies around 23% and benefits from lower production costs; however, it suffers from mechanical fragility and durability limitations [45].
- **High-Concentration Photovoltaics (HCPV):** Capable of reaching efficiencies close to 28% with relatively low production costs. Nonetheless, these systems demand intensive maintenance and precise solar tracking [46].

Numerous studies have been conducted to model the electrical behavior of solar cells. The most widely recognized modeling approaches include the single-diode model (SDM), double-diode model (DDM), and triple-diode model (TDM), as illustrated in Figures II-7–II-9 [23].

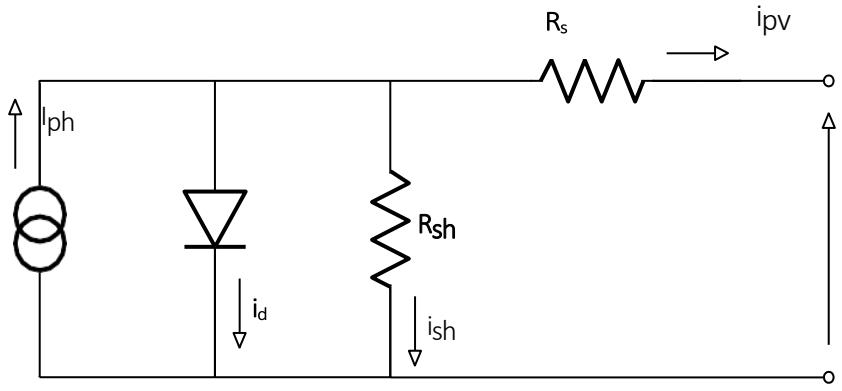


Figure II-7 Model of a photovoltaic cell with one diode.

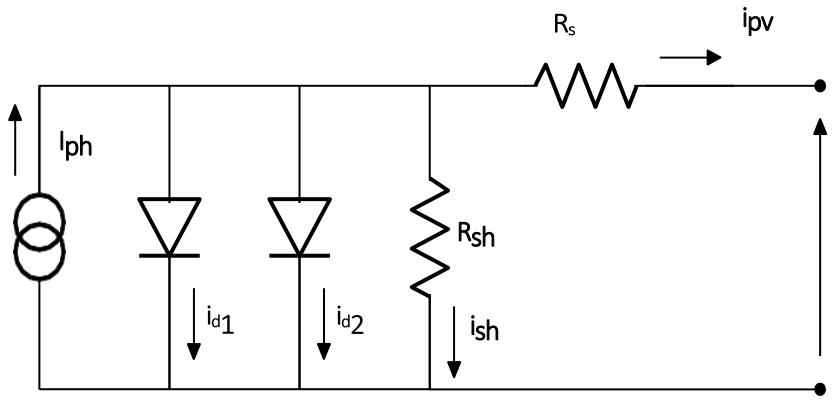


Figure II-8 Model of a photovoltaic cell with two diodes.

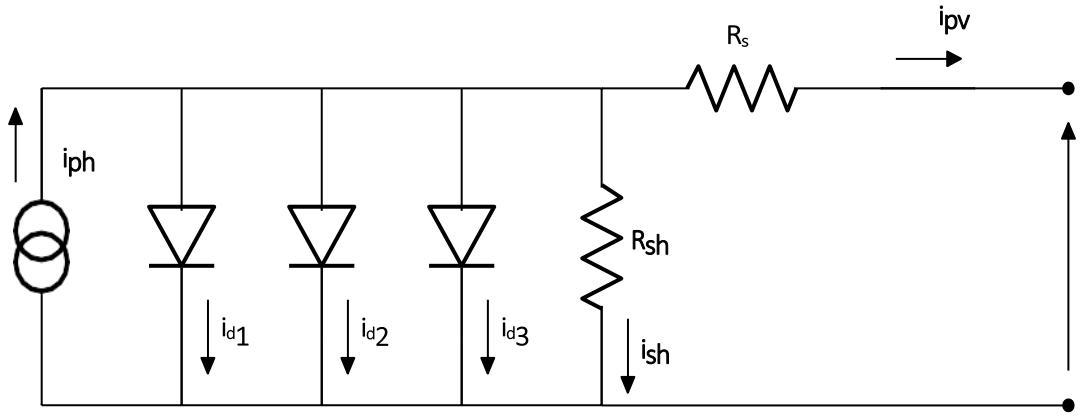


Figure II-9 Model of a photovoltaic cell with three diodes.

The three photovoltaic models illustrated in Figures II-7–II-9 namely, the single-diode model (SDM), double-diode model (DDM), and triple-diode model (TDM) differ in terms of their accuracy, computational complexity, and suitability for specific applications. The SDM is commonly employed in control-oriented simulations due to its simplicity and lower computational requirements. However, it is not well-suited for detailed analysis of material behavior or intrinsic cell performance. In contrast, the TDM provides a more comprehensive and accurate representation of photovoltaic cell dynamics, as it accounts for a broader range of internal physical phenomena, including recombination losses and leakage currents [47].

A comparative overview of solar cell technologies and modeling approaches is provided in [42], where the authors evaluate each model's strengths and limitations. The study also outlines several parameter estimation techniques used to calibrate these models to real-world performance data, offering guidance for researchers and system designers.

II.3 Wind Generators

Wind energy systems convert the kinetic energy of atmospheric air movement into electrical power, providing a clean, renewable, and sustainable energy source. The key components of these systems are wind turbines (WTs), which operate by capturing wind energy through rotor blades that rotate in response to airflow. The mechanical rotation is transmitted to a generator, where electricity is produced via the principle of electromagnetic induction.

II.3.1 Mathematical Model of Wind Turbines

Wind turbines are broadly classified into two main configurations based on their axis of rotation: Horizontal-Axis Wind Turbines (HAWTs) and Vertical-Axis Wind Turbines (VAWTs). HAWTs, which feature an axle parallel to the ground, are generally characterized by superior aerodynamic efficiency compared to their vertical counterparts [47–50]. This higher performance is often attributed to their airfoil-shaped blades, which resemble airplane wings and are capable of operating effectively in high wind conditions. However, HAWTs require substantial support structures to bear the considerable weight of the nacelle, resulting in a high total cost. Conversely, VAWTs offer advantages in terms of lower installation cost and reduced acoustic emissions [51].

Aerodynamic models are based on fluid mechanics and Newton's second law. The kinetic energy from wind that can be recovered by a turbine is expressed as the aerodynamic power:

$$P_{WT,t} = \frac{1}{2}.\rho.A.V_w^3.C_p(\lambda,\beta) \tag{II.10}$$

where: $\lambda = \frac{Rw}{v}$

where $P_{WT,t}$ is the power output (W), A is the swept area of the turbine rotor (m²), R is the length of the blade (m), ρ is the air density (kg/m³), V_w is the wind speed (m/s) C_p is the power coefficient, which reflects the aerodynamic efficiency of the turbine and is influenced by blade design, tip-speed ratio, and control systems.

The parameters λ and β are, respectively, the tip speed ratio and the pitch angle of the turbine [52].

The theoretical maximum power coefficient (Cp) for any wind energy converter is 0.59, a value established by the Betz limit. For electricity generation, the turbine is mechanically linked to a generator shaft. Given that turbine rotational speeds are typically low, a speed-increasing gearbox is commonly integrated between the turbine and the generator Figure II-10.

Nevertheless, this gearbox can be eliminated in certain specific cases by employing generators with a high number of poles, which consequently yields the advantage of reducing the overall mass of the wind turbine system.

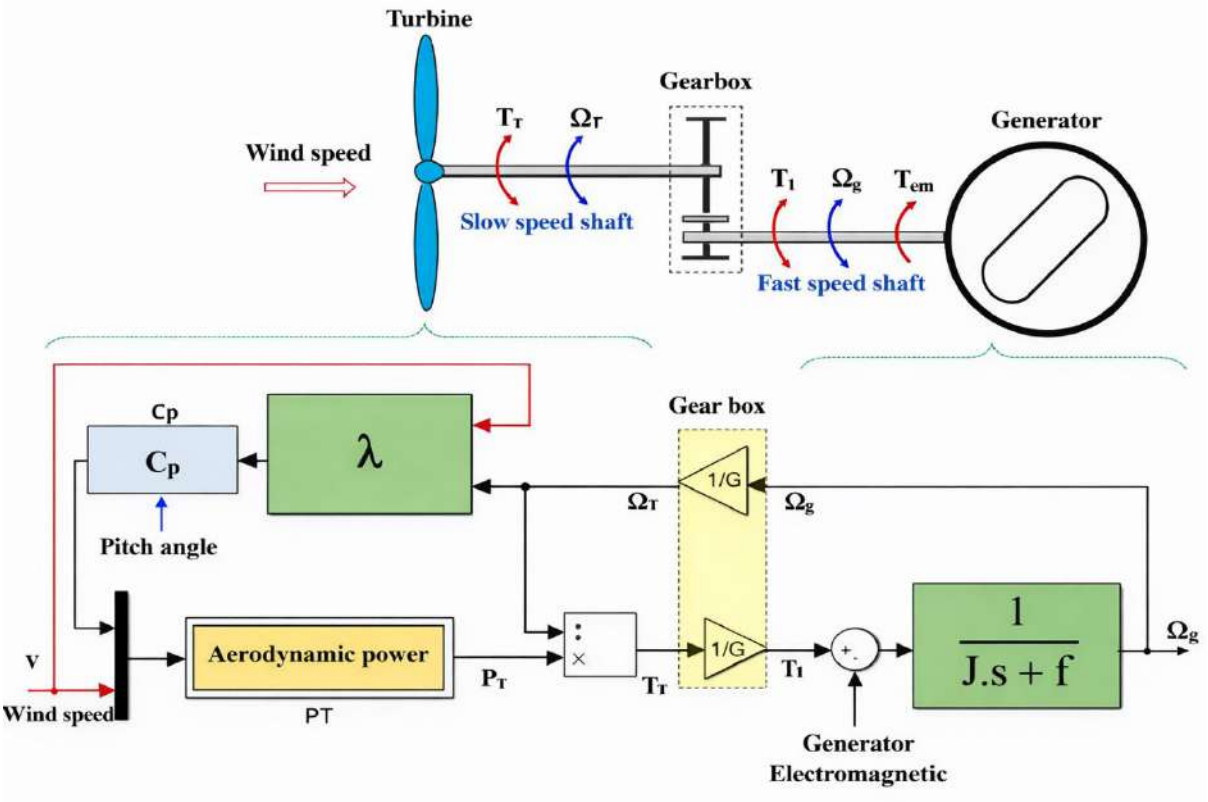


Figure II-10 Functional block diagram of wind turbine system.

Wind turbine systems offer several notable advantages, such as the generation of emission-free energy, the reduction of dependence on fossil fuels, and low operating and maintenance costs once installed [53]. Moreover, wind energy contributes to energy diversification and resilience, especially in regions with favorable wind conditions.

However, wind energy systems also face significant challenges. Chief among them is the intermittency and unpredictability of wind speeds, which can affect power generation stability. Additionally, the visual and acoustic impacts of wind turbines may raise concerns in residential or ecologically sensitive areas. Issues related to land use, turbine siting, and maintenance in remote locations further complicate widespread deployment.

II.3.2 Wind Generator Technologies

In wind energy systems, the selection of an appropriate generator is a critical design decision, influenced by multiple criteria such as the type of output power (AC or DC), power-to-weight ratio, capability for variable-speed operation, pole count, cost, and system integration requirements. A variety of generator types are available for such applications, including DC machines, induction generators, and synchronous generators. While traditional DC generators are largely obsolete in modern wind systems, their functionality has been replaced by brushless DC machines, which offer improved reliability and efficiency.

The principal generator types employed in wind energy conversion systems are outlined below [56–59]:

- **Synchronous Generator:** Characterized by its simple and robust construction, this generator is relatively inexpensive to manufacture. However, the absence of an excitation winding poses operational challenges, particularly in generator mode, as external reactive power typically sourced from the electrical grid is required for magnetization. This dependency negatively affects the power factor. Moreover, the cost of power electronic converters is elevated, as they must be rated for the system's full power capacity.
- **Doubly Fed Induction Generator (DFIG):** This configuration offers direct access to the rotor, enabling independent control of stator power. Approximately 25% of the total system power flows through the rotor, allowing the use of a lower-rated converter, which results in reduced losses and enhanced efficiency. The system also facilitates straightforward power factor control. Nevertheless, DFIGs suffer from certain drawbacks, including the mechanical complexity of the brush–slip ring assembly, the relatively heavy structure, higher maintenance requirements, and the sophisticated nature of the converter control systems.
- **Wound-Field Synchronous Generator:** This generator type can be directly coupled to the wind turbine shaft, significantly reducing the overall weight of the turbine assembly. Additionally, reactive power control is achievable via the

excitation winding. However, synchronization with the electrical grid is required before connection, adding a layer of operational complexity.

- **Permanent Magnet Synchronous Generator (PMSG):** PMSGs eliminate the need for a gearbox, thereby reducing mechanical complexity and overall turbine weight. Their absence of rotor excitation windings results in no rotor copper losses, and they offer high torque density and an excellent power-to-mass ratio. However, these advantages are offset by higher manufacturing costs and the potential risk of permanent magnet demagnetization due to thermal stresses.

II.4 The Need for Hybridization

The hybridization of renewable energy systems is primarily driven by the inherent limitations and operational challenges associated with individual renewable sources. While technologies such as solar and wind power offer significant environmental and economic advantages, their intermittent and variable nature often compromises the reliability of power generation. Hybrid renewable energy systems (HRES) aim to overcome these limitations by integrating multiple energy sources commonly solar, wind, hydro, and in some cases, low-emission fossil fuel-based backup systems to capitalize on their complementary characteristics.

- **Enhanced Reliability and Supply Stability**: By combining renewable sources that operate optimally under different conditions such as solar energy during daylight hours and wind energy during nighttime or overcast periods HRES can deliver a more stable and continuous power output. This mitigates the risk of energy shortages during resource-deficient periods and improves overall supply reliability [60].
- **Improved Year-Round Availability**: Seasonal and geographic variations in renewable energy availability can limit the effectiveness of single-source systems. Hybrid configurations address this issue by diversifying energy inputs, thereby ensuring a more consistent and resilient energy supply throughout the year [61].
- **Increased Efficiency Through Storage Integration**: Many renewable sources, such as photovoltaic systems, tend to produce surplus energy during peak conditions. Hybrid systems that incorporate energy storage technologies, such as batteries or

supercapacitors, can store excess energy and deploy it during periods of low generation. This improves system efficiency and reduces energy wastage.

- **Support for Grid Stability**: The fluctuating nature of standalone renewable sources can pose challenges for grid operators. Hybrid systems equipped with energy storage components can function as distributed stabilizers, providing supplemental power during peak demand periods. This reduces grid congestion and enhances the overall stability and resilience of power networks [62].
- **Viability in Remote and Off-Grid Regions**: In areas with limited access to centralized power infrastructure or where a single renewable source is insufficient, hybrid systems offer a practical and cost-effective solution. By integrating multiple generation sources, these systems can reduce or eliminate reliance on diesel generators, making them especially suitable for rural or island communities [63,64].
- **Pathway Toward a Cleaner Energy Transition**: HRES can also facilitate the gradual decarbonization of the energy sector. By incorporating clean backup systems such as battery storage or high-efficiency, low-emission generators hybrid systems ensure continuity of supply while reducing dependence on traditional fossil fuels [65].

II.4.1 HRES with/without Grid Setup

Hybrid Renewable Energy Systems (HRES) can be broadly categorized according to their connection to the centralized grid infrastructure. The three main classifications include on-grid, off-grid, and microgrid systems. Each configuration has distinct technical, operational, and regulatory implications.

II.4.1.1 On-Grid Systems

In on-grid configurations, the HRES is directly connected to the main utility grid. One of the key advantages of this setup is the ability to inject excess electricity into the grid, often supported by incentive mechanisms such as feed-in tariffs or net metering policies [66]. On-grid systems benefit from existing grid infrastructure and are typically easier to implement in terms of regulatory compliance. However, their performance and reliability are contingent on the stability of the utility grid; power outages or grid disturbances can impact their

functionality. These systems are particularly well-suited to urban and suburban regions where grid access is robust and reliable [67].

II.4.1.2 Off-Grid Systems

Off-grid HRES operate entirely independently from the centralized electricity grid and are predominantly deployed in remote or rural locations where grid connectivity is absent or unreliable. These systems rely heavily on energy storage solutions, such as battery banks, to store surplus energy for use during periods of low or no renewable generation [68]. Although off-grid systems offer complete energy autonomy and can significantly reduce reliance on fossil fuels, they typically involve higher capital expenditures due to the required storage infrastructure and the complexity of energy management and control systems [69].

II.4.1.3 Microgrid Systems

Microgrids represent a hybrid configuration that combines aspects of both grid-connected and off-grid systems. These localized energy networks are capable of operating in grid-connected mode or in islanded mode during grid disruptions [70,71]. A typical microgrid incorporates a diverse mix of energy sources including PV panels, wind turbines, and possibly conventional generators along with energy storage components such as batteries or supercapacitors. This dual-mode functionality enhances system resilience, particularly in critical infrastructure settings like universities, military installations, and industrial campuses.

In the present work, our modeling and simulation efforts focus primarily on a microgrid system in isolated mode, representing a standalone environment independent from any central grid. This approach allows for an in-depth evaluation of energy management strategies under self-sustained operating conditions.

Modern hybrid microgrids often employ both AC and DC power converters to efficiently integrate various renewable sources and storage technologies. These configurations not only improve the flexibility and reliability of energy delivery but also contribute to broader goals of energy resilience, environmental sustainability, and distributed energy resource (DER)

integration. By optimizing the balance between energy supply and demand, hybrid microgrids support stable operation and play a vital role in advancing global clean energy initiatives.

II.5 Energy Storage Technologies use in HRES

A wide range of energy storage technologies can be integrated into Hybrid Renewable Energy Systems (HRES) to ensure reliable and continuous power supply. The incorporation of storage systems within hybrid architectures plays a crucial role in mitigating the intermittent nature of renewable energy sources. In addition to energy buffering, storage systems contribute to several operational objectives, including voltage and current peak regulation, mitigation of voltage fluctuations, harmonic reduction, frequency stabilization, load shedding, and enhancement of transient system stability.

Among the available storage technologies, batteries and supercapacitors are the most widely adopted solutions. The design and selection of battery storage systems depend on multiple constraints, such as operating voltage and current levels, charge–discharge ratios and durations, thermal operating conditions, cycle life, as well as economic and physical considerations including cost, size, and weight. Currently, commercially available batteries are primarily based on lead–acid, nickel–cadmium, lithium-ion, and lithium-ion polymer technologies [23].

To achieve improved performance and reduced installation costs, hybrid energy storage systems (HESS) combining batteries and supercapacitors are increasingly employed. Such hybrid configurations effectively attenuate high-frequency power fluctuations while extending battery lifetime. Depending on system requirements, the hybrid storage system can be connected either directly to the DC bus or through bidirectional DC–DC converters, as illustrated in Figure II-11.

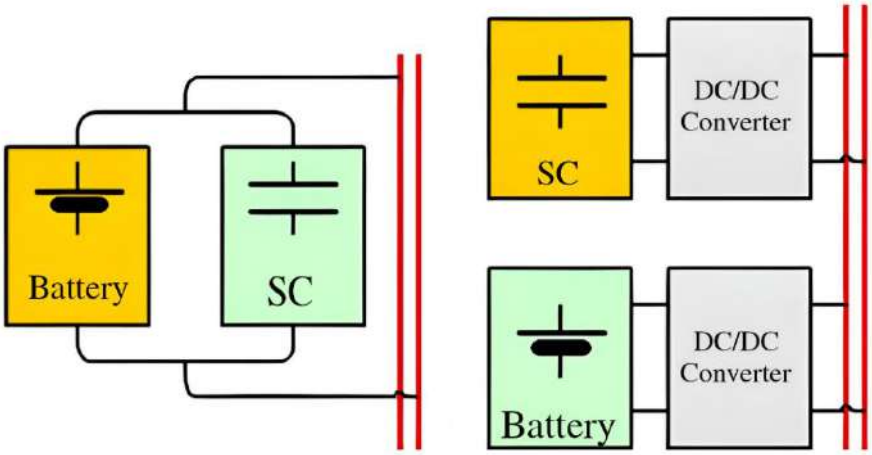


Figure II-11 Passive and active storage systems.

Several results can be found in the specialized literature dealing with hybrid systems combining PV and wind turbines. These results can be divided in two categories: those dealing with systems without storage [70–81] and those dealing with systems integrating a storage system [82].

II.5.1 Batteries

Batteries store electrical energy through controlled electrochemical reactions that produce a flow of electrons, enabling the supply of power to connected electrical loads. They represent the most widely used energy storage technology in Hybrid Renewable Energy Systems (HRES), particularly for compensating for the variable and intermittent power output of renewable energy sources such as photovoltaic and wind systems. During periods of excess generation, batteries store surplus energy and subsequently release it during intervals of low generation or peak load demand, thereby enhancing system reliability and continuity of power supply. A variety of battery technologies are currently employed in renewable energy applications, each characterized by distinct operational and performance attributes. Common battery types include lead–acid, lithium-ion, each offering specific advantages and limitations with respect to cost, cycle life, energy density, charging efficiency, and maintenance requirements [83]. The selection of an appropriate battery technology therefore depends on the specific technical and economic requirements of the hybrid energy system.

II.5.2 Supercapacitors

Supercapacitors, also referred to as ultracapacitors, are advanced energy storage devices capable of storing substantially more energy than conventional capacitors while maintaining superior charge–discharge characteristics. They exhibit a significantly higher energy density compared to traditional capacitors, enabling increased energy storage per unit mass or volume [84].

In the context of Hybrid Renewable Energy Systems (HRES), supercapacitors are commonly employed as a complementary technology or in certain cases, as an alternative to conventional battery storage. Although their energy density remains lower than that of batteries, supercapacitors offer exceptionally high-power density, rapid response, and very fast charging and discharging capabilities, making them particularly suitable for short-duration, high-power applications.

Within HRES architectures, supercapacitors are primarily utilized to regulate power balance and manage transient operating conditions. They are highly effective in mitigating rapid power fluctuations resulting from sudden variations in generation or load demand, such as abrupt load increases or momentary surges in wind or solar power output [85]. By rapidly absorbing or delivering energy, supercapacitors significantly enhance system stability and improve the overall dynamic performance of the energy management strategy.

II.6 Energy Management Strategies

Hybrid Power Systems (HPS) based on Renewable Energy Sources (RES) have emerged as promising and sustainable solutions for clean energy generation, particularly in isolated or remote areas where grid connection is not feasible. To enhance their performance and reliability, diverse renewable conversion systems have been integrated, and the implementation of intelligent energy distribution strategies has become increasingly important.

Effective energy management is therefore essential for achieving smart grid functionality, improving reliability, and enhancing overall efficiency. The primary goal of EMS is to ensure that energy generation and consumption are optimized in a manner that minimizes

operational costs and environmental impact. According to one widely accepted definition, an energy management strategy refers to [86]. This definition emphasizes the dual objectives of economic optimization and environmental sustainability.

Given the intermittent nature of renewable energy sources and the stochastic nature of load demand, numerous supervisory and control strategies for HPS have been proposed in recent years [87]. The main challenge lies in developing appropriate control approaches for the converters associated with each energy source in order to meet specific performance objectives. These converters play a key role in maximizing the extracted power and adapting energy production according to system demand.

In general, management strategies for HPS can be classified into two main categories: Rule-Based (RB) and Optimization-Based (OB) strategies, as illustrated in Figure II-15.

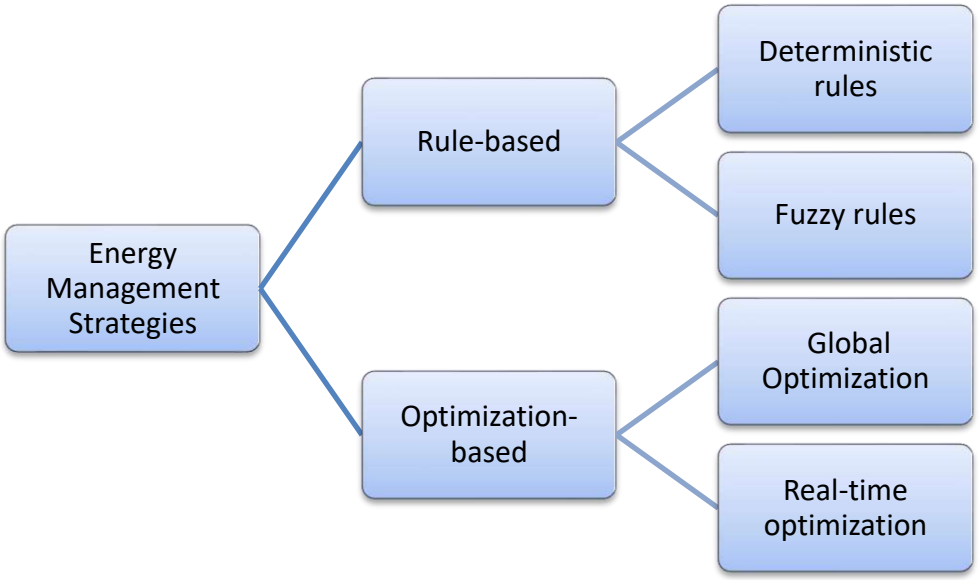


Figure II-12 Proposed EMS classification

Rule-Based Energy Management Systems (RB-EMS) operate according to a predefined set of rules established through expert knowledge and systematic analysis of system behavior. These strategies are generally straightforward to implement and exhibit reliable performance

in real-time applications; however, they do not always guarantee an optimal operational solution under dynamic conditions.

RB-EMS can be categorized into two main types: deterministic and fuzzy systems. Deterministic strategies rely on explicit, experience-based rules derived from specific operational objectives. In contrast, fuzzy rule-based approaches employ fuzzy logic principles to manage uncertainties and nonlinearities inherent in renewable systems. Fuzzy logic provides greater robustness against measurement inaccuracies and allows smoother adaptation to variable operating conditions, thereby improving control flexibility compared to deterministic methods.

On the other hand, Optimization-Based EMS (OB-EMS) employ mathematical optimization techniques to minimize a defined cost function while satisfying system constraints. The principal aim of these strategies is to determine the optimal power allocation among generation sources, storage elements, and loads to meet demand in the most efficient and economical manner. Optimization-based control is typically divided into two categories:

Global optimization, which minimizes cost functions by considering both historical data and predicted system dynamics;

Real-time optimization, which continuously updates control decisions based on current operating conditions to achieve near-optimal economic performance.

Both RB and OB strategies encompass a variety of algorithms that may incorporate classical control principles or artificial intelligence (AI)-based methods to enhance the overall performance of hybrid power systems. The existing literature presents numerous EMS architectures developed to address the inherent challenges of hybrid renewable systems, including both conventional and intelligent control techniques.

II.7 Conclusion

This chapter has presented a comprehensive and critical review of the literature related to the modeling, control, and integration of photovoltaic and wind energy systems within

hybrid renewable energy frameworks. The fundamental operating principles of photovoltaic cells and wind turbines were examined in detail, highlighting their electrical characteristics, modeling approaches, and performance dependence on environmental conditions such as solar irradiance, temperature, and wind speed. The analysis confirms that although PV and wind technologies are mature and widely deployed, their inherent intermittency and stochastic behavior remain major challenges for reliable power generation, particularly in standalone and microgrid applications.

To mitigate these limitations, the concept of hybrid renewable energy systems (HRES) was explored, emphasizing the complementary nature of solar and wind resources. The literature demonstrates that hybridization significantly improves supply continuity and system reliability compared to single-source configurations. Furthermore, the integration of energy storage systems was identified as a critical component for smoothing power fluctuations and ensuring energy balance. Conventional battery-based storage solutions provide effective long-term energy buffering but suffer from degradation issues when subjected to frequent charge–discharge cycles and high-power transients. In contrast, supercapacitors exhibit fast dynamic response and high cycle life, making them suitable for short-term power support. Consequently, hybrid energy storage systems (HESS), combining batteries and supercapacitors, have emerged as an effective solution to enhance storage performance and extend battery lifespan.

In addition, this chapter reviewed existing energy management strategies (EMS) employed in hybrid renewable systems. Classical rule-based and control-oriented approaches, while simple to implement, often lack the adaptability required to handle nonlinear system dynamics and rapidly changing operating conditions. More advanced strategies based on intelligent control techniques, particularly fuzzy logic–based EMS, have demonstrated superior robustness, flexibility, and decision-making capability under uncertainty. However, the literature also reveals that many existing EMS implementations are system-specific and do not fully exploit the coordinated operation of hybrid storage elements in standalone PV–wind microgrids.

Despite the extensive research conducted in this field, several gaps remain evident. First, there is a need for more efficient and robust Maximum Power Point Tracking (MPPT)

techniques capable of maintaining optimal performance under fast irradiance variations and partial shading conditions. Second, the coordinated control of hybrid energy storage systems using intelligent EMS requires further investigation, particularly in terms of reducing battery stress while ensuring DC bus stability and power quality. Finally, a unified framework that combines advanced MPPT algorithms with an intelligent energy management strategy for PV–wind–battery–supercapacitor systems is still lacking in the literature.

These identified gaps provide the motivation for the research contributions presented in the subsequent chapters. Chapter 3 focuses on the development and comparative evaluation of advanced metaheuristic and artificial intelligence–based MPPT algorithms for photovoltaic systems under uniform and partial shading conditions. Chapter 4 builds upon this foundation by proposing and validating an intelligent fuzzy logic–based energy management strategy for a standalone PV–wind microgrid equipped with a hybrid energy storage system. Together, these contributions aim to enhance the efficiency, stability, and reliability of hybrid renewable energy systems operating under realistic and dynamic conditions.

Chapter III: Performance Evaluation of Metaheuristic-AI MPPT Algorithms for Photovoltaic Systems with DC-DC Converters

III.1 Introduction

The Maximum Power Point (MPP) is crucial for maximizing the energy yield of a Photovoltaic (PV) system. The relationship between a PV array's voltage, current, and power is highly nonlinear and dynamically sensitive to environmental changes, particularly solar irradiance and cell temperature. Consequently, PV system performance relies heavily on Maximum Power Point Tracking (MPPT) the continuous adjustment of the array's operating point to extract the highest available power under prevailing conditions. The MPPT algorithm is an essential control component that interfaces between the PV array and the power conversion stage to optimize energy harvesting.

The DC-DC converter topology is equally pivotal in this process. Its design must effectively condition the variable PV output and interface it with the load or grid requirements, directly impacting the overall system efficiency and energy extraction capability.

This chapter provides a comprehensive overview of the technologies essential for maximizing PV system efficiency. It begins by establishing the fundamental concept of MPPT and introducing the relevant DC-DC converter topologies that form the power conversion backbone. The main focus, however, is a detailed exploration of MPPT algorithms, classifying them into conventional methods and advanced metaheuristic (nature-inspired) approaches. We discuss the operating principles, strengths, and weaknesses of these diverse techniques. Critically, the chapter presents an in-depth comparative performance analysis of different leading metaheuristic algorithms Particle Swarm Optimization (PSO), Grey Wolf Optimizer (GWO), Ant Colony Optimization (ACO), Cuckoo Search (CS), Harris Hawks Optimization (HHO), Horse Herd Optimization Algorithm (HOA), And Artificial Intelligent methods AI, Fuzzy Logic Control (FLC) and Artificial Neural Network (NNA) conducted under varying irradiance and partial shading conditions. This analysis, simulated in MATLAB, provides

critical insights into the algorithms' tracking accuracy, speed, and suitability for ensuring stable voltage regulation, minimizing power fluctuations, and enhancing overall system reliability.

III.2 Concept of MPPT:

The primary challenges faced by PV systems are their dependence on climatic changes and the high upfront cost of installation. PV cells, being based on semiconductor materials, exhibit non- linear power-voltage characteristics. To maximize power extraction under diverse conditions, the implementation of MPPT technology is necessary. The MPP identifies a distinct point on the I-V or P-V plot, specific to solar irradiance and temperature, at which the PV system operates with optimal efficiency and achieves its maximum power output. However, the continuous variation of climatic conditions and load profile throughout the day poses a significant challenge in accurately tracking the PV system's maximum power point.

Two primary approaches are commonly employed to maximize power extraction from PV sources. The first approach entails the mechanical tracking of solar panels, whereby the panels are positioned to maintain a fixed angle of 90 degrees with respect to the incoming solar rays, regardless of the terrain. This strategy aims to optimize solar irradiation exposure throughout the day, thereby enhancing power output. However, while the mechanical tracking technique is relevant to the discussion, it falls beyond the current scope of this research [88].

In the second approach, the electrical MPPT method is employed. It involves the integration of an electronic device between the PV array and the load. This device works as an impedance matching circuit and it consists of two essential components, as illustrated in Figure III.1: a switching power interface and an MPPT control algorithm [25]. The power interface can utilize different types of DC-DC converters, including boost, buck, buck-boost, along with other configurations. These converters are employed with the primary goal of transferring the maximum power from the PV module to the load. This is achieved by adjusting the duty cycle of the converter, which effectively varies to maintain the system operating point near the MPP. At the MPP, the input impedance of the converter seen by the PV is adjusted to match the impedance of the PV source, ensuring the transfer of the highest available power [89], [90].

Therefore, the use of a suitable MPPT algorithm or calculation mode is required to dynamically track and locate the MPP point and adjust the duty cycle accordingly.

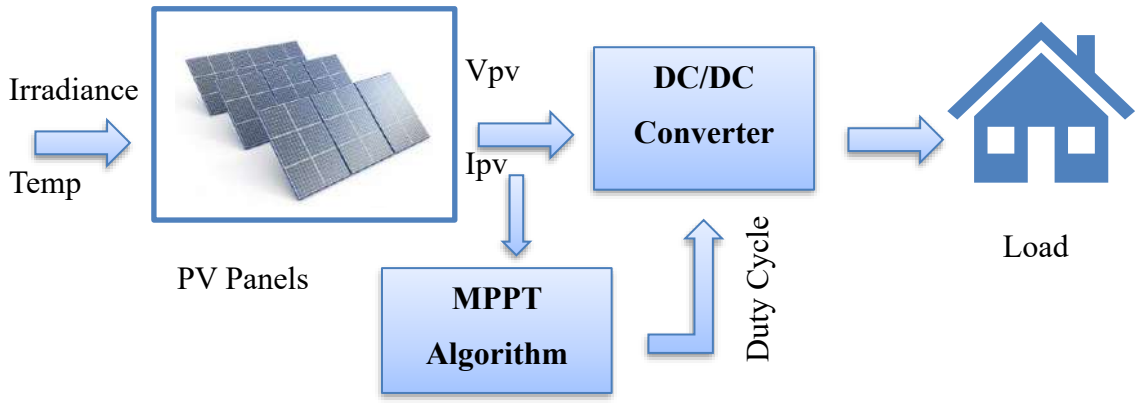


Figure III-1 Block Diagram of a MPPT Controller.

III.3 DC-DC Topologies:

DC/DC converters play a pivotal role in the field of power electronics, serving as essential components in a wide range of applications. Power electronics, based on solid-state electronics, encompasses the fundamental principles and advanced techniques employed for the regulation and conversion of electrical energy. Within this context, DC/DC converters assume critical significance, as they enable precise control and reliable conversion, making them indispensable for achieving optimal performance in diverse systems [91]. These converters are instrumental in converting unregulated DC inputs into controlled DC outputs, effectively meeting specific voltage and current requirements. Whether the objective is to step up or step down the voltage, DC/DC converters offer the necessary switching capability. Their extensive utilization in domains such as DC power supply and DC motor drives enables efficient management and transformation of electrical energy [90].

DC-DC converters have become an integral part of modern solar photovoltaic (SPV) systems due to the prevalence of renewable energy resources that generate DC voltage. These converters serve as impedance matching units and have two primary tasks: facilitating the

connection between PV panels, renewable energy sources, load, or the grid, and driving the PV panel to operate at its MPP. According to the maximum power transfer theorem, to extract the maximum power from the PV source, it is important to match the load resistance to the Thevenin equivalent resistance of the PV module [92].

DC-DC converters play a crucial role in achieving this impedance matching by adjusting the terminal voltages of the PV array to align with the load impedance. They have the ability to increase or decrease the internal impedance of the PV array, ensuring efficient power transfer [89]. Power semiconductor switches such as MOSFET or IGBT are commonly used in these converters. These switches operate by receiving an appropriate pulse with a suitable duty cycle at the gate terminal, allowing for precise switching according to the desired output voltage.

Figure III.2 illustrates the fundamental architecture of a DC-DC converter, which comprises various components such as inductors, diodes, capacitors, and switches with control. These components collectively control the conversion process. By modifying the connections or arrangements within the "switching network" and "low-pass filter" sections, different types of DC-DC converters can be implemented [93]. This flexibility allows for customization and adaptation of the converter's functionality to suit specific requirements.

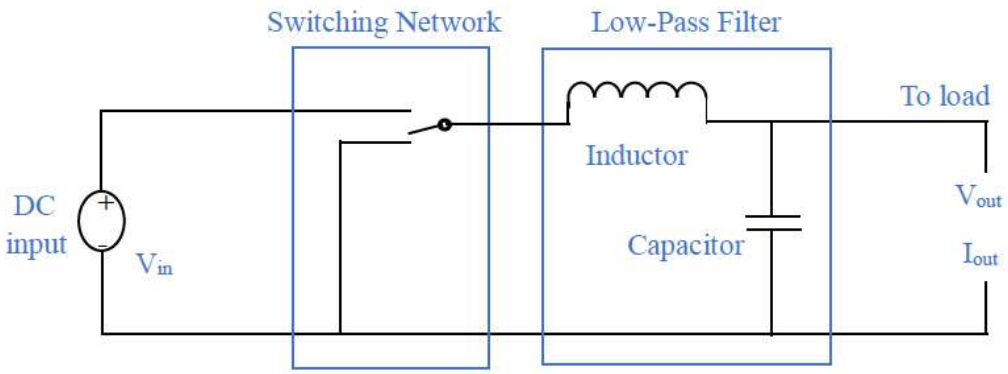


Figure III-2 Basic Model of a DC-DC Converter.

The types of DC-DC converters are categorized based on their applications, switching methods, current modes, and more. One commonly used classification is based on whether the

converter is isolated or non-isolated as illustrated in Figure III.3. In an isolated converter, there is an electrical barrier between the input and output, providing protection for sensitive loads. The output polarity can be configured as positive or negative, and these converters have high noise interference capability. On the other hand, non-isolated converters do not have an electrical barrier, resulting in a simpler design and lower cost [94].

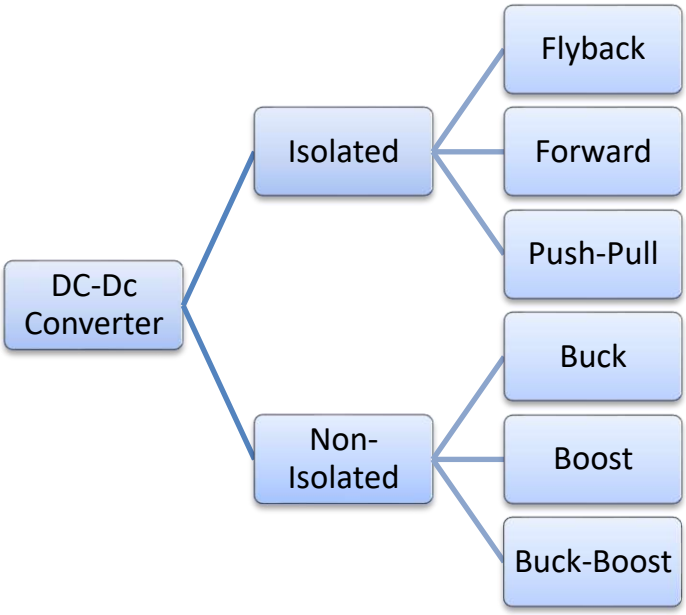


Figure III-3 Classification of DC-DC Converters.

Both isolated and non-isolated converter topologies have their own advantages and disadvantages. However, non-isolated DC-DC converter topologies are often more advantageous. Although they may have some drawbacks such as high duty cycle ratios, poor voltage gain, and additional circuitry, these topologies are still more beneficial and feasible option for integrating with renewable energy applications, and they are commonly used along with MPPT controller for peak power tracking. Among the non-isolated converter types, three main ones are widely used: buck, boost, and buck-boost converters [95].

III.3.1 Buck Converter

The DC-DC buck converter, also known as a step-down converter, is commonly used to convert higher input voltage magnitudes to lower output voltage magnitudes. This makes it

suitable for integrating higher module voltages to lower loads or battery voltages [92]. The circuit topology of a buck converter is illustrated in Figure III.4.

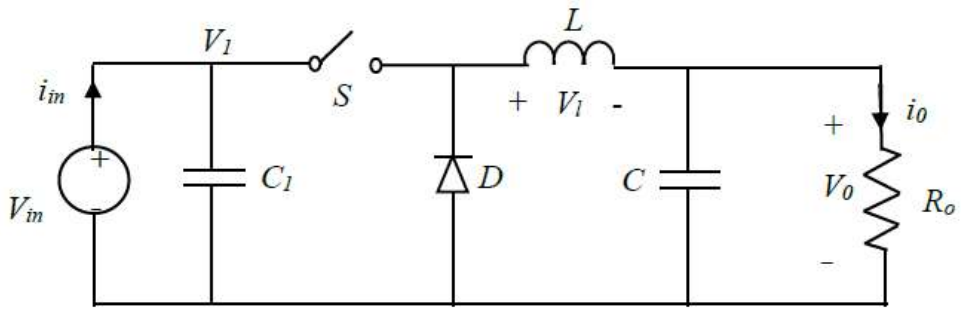


Figure III-4 Buck Converter.

According to the operation of the circuit, the buck converter can also be referred to as a current-voltage converter. When the converter switch is activated, the diode is reverse biased and ceases to conduct current, causing the inductor to store energy. As a result, the inductor current increases gradually from its lowest to highest value. Conversely, when the switch is deactivated, the energy stored in the inductor is delivered to the capacitor and the load via a freewheeling diode. This leads to the inductor current decreasing from its highest to lowest value [92]. Equation III.1, III.2 and III.3 outlines the mathematical relationships for the transformation ratio of the output voltage Vo, output current Io, and output resistance Ro [89].

$$\frac{V_0}{V_{in}} = D \tag{III.1}$$

$$\frac{I_0}{I_{in}} = \frac{1}{D} \tag{III.2}$$

$$R_{in} = \frac{R_0}{D^2} \tag{III.3}$$

PV apparent impedance denoted as R_{in} is the converter input impedance. By adjusting the duty cycle of the converter "D", the input impedance can be varied, potentially matching the optimum panel resistance, R_{MPP}, for maximum power transfer. However, due to the limited duty cycle range (between zero and one) in a buck converter, it can only reflect R_{in} between the load resistance R_0 and infinity. As a result, it cannot achieve values above the I_{MPP} of the

PV module and is unable to track I-V curve points that are close to I_{SC}. Therefore, the buck converter is restricted to tracking the MPP within a specific operating region where $R_0 \geq R_{MPP}$, this limitation is illustrated in Figure III.5 [25].

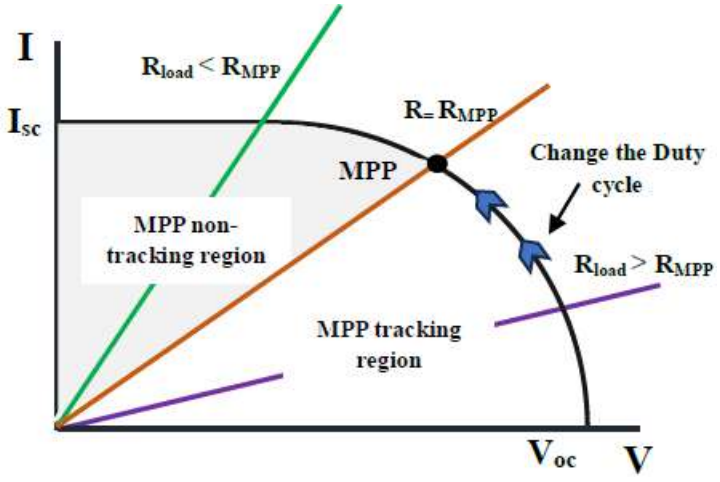


Figure III-5 Tracking and non-Tracking Regions of the I-V Curve for Buck DC-DC Converters.

III.3.2 Boost Converter

The boost converter, also known as a step-up converter, is used in PV applications where a higher load-side voltage is required. By the law of conservation of energy, the input power equals the output power. Consequently, in a boost converter, the output voltage is higher than the input voltage, resulting in a lower output current compared to the input current [92]. Figure III.6 displays the circuit configuration of a conventional boost converter. When the input-side switch is activated (ON period), the inductor connected to the source stores energy, causing the current through it to rise from its minimum to maximum level. During this time, the output voltage is present at the cathode of the diode, while the anode is at zero voltage and reverse biased, keeping the diode in the OFF state. As a result, the load is isolated from the source during the ON period, and the output capacitor maintains a continuous load current [92].

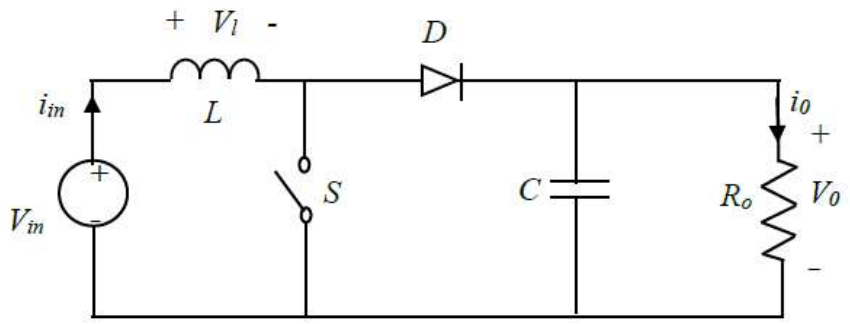


Figure III-6 Boost Converter.

When the switch is turned off, the inductor voltage reverses polarity, and the sum of the inductor voltage and source voltage appears across the switch and diode. Since this voltage exceeds the output voltage, the diode becomes forward-biased, allowing current to flow through it. The inductor discharges, and its current decreases from its peak value to a minimum, transferring stored energy to the load. Equations of the output voltage, current and resistance are shown below [92], [96]:

$$\frac{V_0}{V_{in}} = \frac{1}{1-D} \tag{III.4}$$

$$\frac{I_0}{I_{in}} = 1 - D \tag{III.5}$$

$$R_{in} = R_0(1 - \mathrm{D})^2 \tag{III.6}$$

In a boost converter, the source voltage is supplied to both the load and the output capacitor. The output current remains continuous, ensuring a steady flow of power to the load. However, the input current in a boost converter can be either continuous or discontinuous, depending on the operating conditions. To maintain a continuous load current, a high-value output capacitor is employed [92].

Regarding the resistance conversion ratio in a boost converter, the duty cycle value is limited to the range of [0,1]. Consequently, a boost converter is unable to reflect impedances greater than the load impedance R_0, and thus cannot reach values close to a module's open-circuit voltage V_{oc}. The boost converter tracks the MPP within a restricted operational region

where the panel resistance is below or equal to the load resistance which means boost operates only when $R_0 \leq R_{MPP}$, as depicted in Figure III.7. It is important to note that under low irradiation conditions, the boost converter cannot track the MPP because the point lies outside the operating region [25], [96].

The boost converter finds practical use in different scenarios, including the implementation of regenerative braking circuits for DC motors and the provision of regulated DC power supplies. An intermediate boost converter is generally required to connect low-voltage DC sources, such as photovoltaic systems and fuel cells, to the grid [33]. It plays a critical role in maintaining a high output voltage, ensuring that even if the PV array voltage falls to low values, the system can still deliver the required voltage for seamless grid integration.

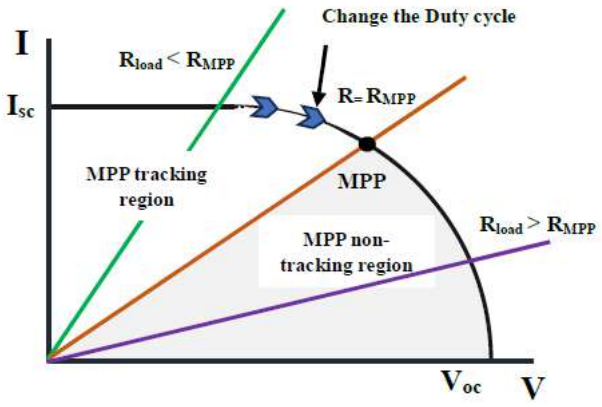


Figure III-7 Tracking and non-Tracking Regions of the I-V curve for Boost DC-DC Converters.

III.3.3 Buck-boost Converter

A buck-boost converter, also known as a bi-directional converter or a step-up/down converter, is a type of DC-DC converter that has the capability to provide an output voltage that can be either higher or lower than the input voltage. It is characterized by having an output voltage of negative polarity relative to the common terminal of the input voltage [25]. This converter topology is often referred to as a voltage to current to voltage converter. It is particularly useful in scenarios where there is a need to connect battery or load voltages that are closely matched with module voltages [25]. The buck-boost topology is achieved by

cascading a buck converter and a boost converter, combining their functionalities to enable bidirectional power flow and voltage conversion [97]. The circuit topology of a buck-boost converter is illustrated in Figure III.8, It demonstrates the arrangement and interconnection of the components involved in this type of DC-DC converter.

In a buck-boost converter, the switching operation governs energy transfer between the input source, inductor, and output. When the switch is turned ON, the diode is reverse biased, preventing current flow to the output, while the inductor accumulates energy from the input source. During this phase, the inductor current increases from its minimum to maximum value. The output capacitor maintains load continuity by supplying current. When the switch turns OFF, the inductor releases stored energy, causing its voltage to reverse. This results in the lower terminal of the inductor becoming positive and the upper terminal negative, forward-biasing the diode and enabling conduction [92]. The inductor then transfers energy to both the load and the output capacitor. By adjusting the duty cycle of the switching signal, the converter effectively regulates the output voltage, either increasing or decreasing it relative to the input.

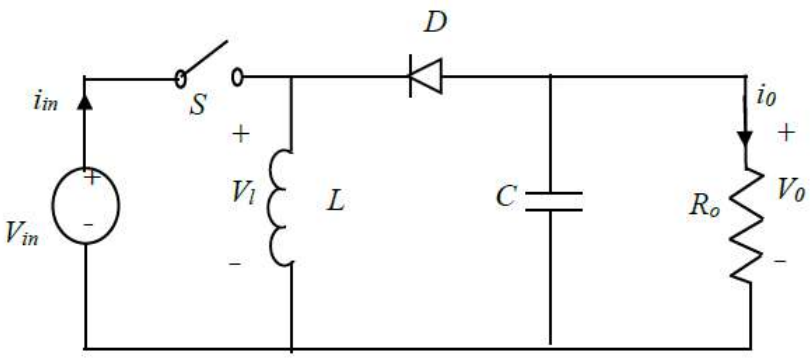


Figure III-8 Buck-Boost Converter.

The resistance and voltage conversion ratios of the buck-boost converter are derived by multiplying the corresponding conversion ratios of the buck and boost topologies. The equations for these conversion ratios are provided below [96]:

$$\frac{V_0}{V_{in}} = \frac{1}{1-D} \tag{III.7}$$

$$\frac{I_0}{I_{in}} = \frac{1-D}{D} \quad \text{(III.8)}$$

$$R_{in} = R_0\{\frac{(1-\mathrm{D})^2}{D}\} \quad \text{(III.9)}$$

The resistance conversion characteristics of the buck-boost converter indicate that an increase in the duty cycle D results in a decrease in the input impedance R_{in} . This shift modifies the operating point of the photovoltaic system, moving it towards the lower voltage region of the I-V curve. Conversely, a reduction in the duty cycle increases R_{in} , shifting the operating voltage towards the higher voltage region of the I-V curve. A key advantage of the buck-boost converter is its ability to operate across the entire voltage range without a non-operational region. By adjusting the duty cycle, the converter enables continuous operation from the short-circuit current I_{sc} to the open-circuit voltage V_{oc} , ensuring efficient power transfer under varying load conditions [25].

The equivalent load resistance reflected at the input of the buck-boost converter varies from zero to infinity, enabling operation across the entire I-V characteristic curve, as shown in Figure III.9. This adaptability allows the converter to regulate the operating point dynamically. When maximum power point tracking (MPPT) is required, the buck-boost topology offers a distinct advantage, as it remains the only configuration capable of continuously and precisely tracking the maximum power point (MPP) under varying irradiance, temperature, and load conditions. This ensures optimal power extraction from the photovoltaic module regardless of environmental fluctuations or variations in load resistance [25], [92].

The hybrid converter topology, finds widespread use in various applications including drive systems, stand-alone setups, and grid-connected photovoltaic energy generation systems [94]. In general, this topology offers higher efficiency compared to individual buck or boost converters. However, one drawback of the buck-boost topology is its inherent discontinuous input current due to the series connection between the switch and the generator. This discontinuity introduces multiple harmonic components, resulting in high input ripple and considerable noise issues [98].

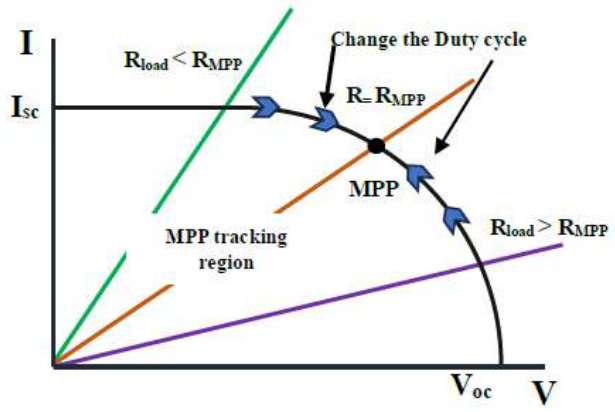


Figure III-9 Operational MPPT Regions in DC-DC Buck-Boost, SEPIC, and Cuk Converters.

III.4 MPPT Algorithms

Over the past few decades, extensive research and development have been conducted on various methods and algorithms for automatically identifying and achieving operation at the maximum power point of photovoltaic systems. These approaches have undergone thorough study, practical implementation, and publication, with ongoing advancements in the field. The majority of MPPT algorithms commonly assume that the DC-DC converter acts as a simplistic resistance transformer with a constant efficiency across all voltage levels. However, in reality, the DC-DC converter is a non-ideal device that incurs various losses. It is important to consider this fact when designing MPPT systems. The efficiency of the DC-DC converter actually varies depending on the duty cycle. Furthermore, the settling time of the converter is another crucial consideration for the effective operation of the MPPT system.

When selecting an MPPT technique for a specific PV system application, the implementation strategy becomes a crucial factor to consider. This strategy depends on the end-users' familiarity with analogue or digital circuitry and the number of sensors required for MPPT implementation [99]. Additionally, parameters such as the atmospheric conditions of the installation region, sunshine duration, and the allocated budget should be taken into consideration. By carefully considering these factors, the most appropriate MPPT method can be chosen for each system, ensuring optimal performance and energy extraction [100].

MPPT techniques typically employ current sensors, voltage sensors, or a combination of both to facilitate their implementation. One common implementation scheme involves using two sensors connected between the PV module and the power converter. These sensors enable the calculation of power at each step based on the sampled current and voltage values. This power measurement is then utilized to determine the tracking direction, such as in the Perturb and Observe (P&O) method, or to define the Global Maximum Power Point in advanced methods for PSC [25].

III.4.1 Classifications

There is no specific evaluation study that classifies MPPT comprehensively, as their suitability varies depending on the application. While some methods may be highly efficient, others may not yield the same level of performance. Consequently, a unique and universally accepted classification for MPPT algorithms does not exist. However, these methods can be categorized based on various criteria, including aspects such as modernity, tracking technique, sensing implementation, processor requirements, cost, and hardware implementation [101]. Furthermore, within each classification, numerous sub-categories exist, which consider factors such as algorithm characteristics and mathematical formulation. MPPT algorithm within these categories possesses its own set of advantages and limitations. The tracking performance of these algorithms is influenced by multiple factors, including tracking speed, tracking efficiency, accuracy, stability, complexity, and other relevant considerations.

After conducting a comprehensive review of research articles from reputable databases such as IEEE Explore, Springer, Scopus, and Google Scholar, it has been found that the classification of MPPT methods into conventional and Advanced (soft computing)-based approaches is widely used and referenced in the literature [102] Figure III.10.

III.4.1.1 Conventional Methods

Conventional MPPT methods have a long history and have been in use since the early days of PV systems, making them highly popular. Over the past few decades, several conditional MPPT techniques, including the Incremental Conductance (INC) method, Perturb

and Observe (P&O), and Hill-Climbing (HC) method [103], have been proposed. These traditional methods are known for their simplicity and cost-effectiveness, relying on straightforward algorithms or fractional calculations that facilitate their implementation.

Conventional MPPT methods perform well under uniform irradiation conditions, where the PV system generates a single GMPP. However, these algorithms exhibit limitations in their dynamic response and tend to oscillate around the MPP, particularly when faced with rapidly changing weather conditions. Consequently, they lead to significant power losses during steady-state operation and result in suboptimal performance. Moreover, these classical strategies prove to be inefficient in managing the challenges posed by Partial Shading Conditions They often converge to local maxima and struggle to accurately track the genuine GMPP due to the presence of multiple peaks in the P-V characteristics [25]. Despite extensive prior modifications and ongoing efforts to improve their performance, conventional MPPT methods continue to experience limitations in efficiently extracting power from partially shaded photovoltaic systems.

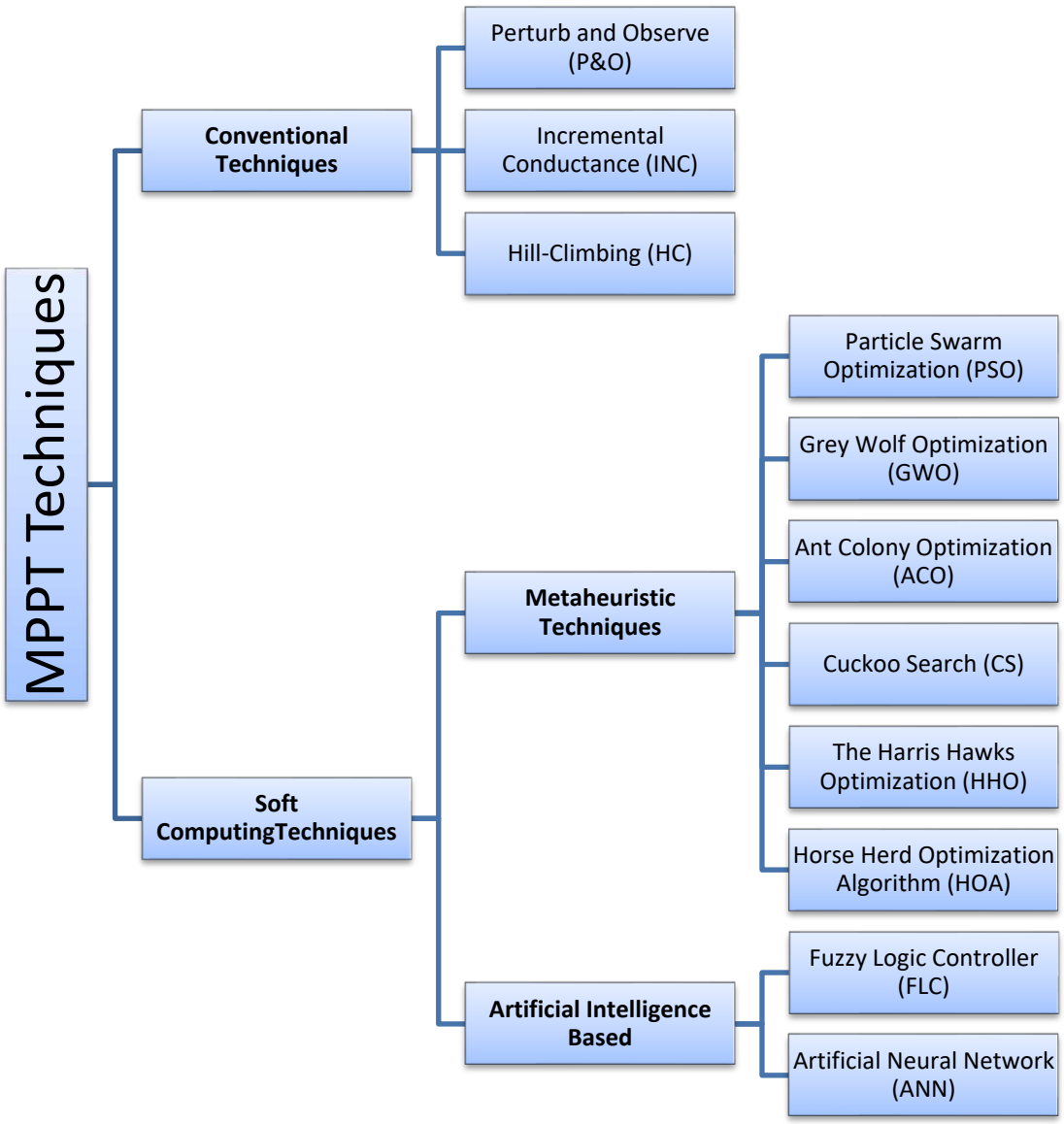


Figure III-10 MPPT Techniques Classification.

III.4.1.2 Advanced (soft computing) Methods

Advanced MPPT methods, also known as soft computing techniques, have been developed to address the limitations of traditional MPPT methods. These advanced methods aim to mitigate the drawbacks associated with conventional approaches by reducing perturbations near the MPP. Unlike conventional methods, advanced MPPT techniques are characterized by their complexity, requiring more intricate computations. However, they offer

superior tracking performance compared to conventional methods. One alternative approach is the utilization of Artificial Intelligence (AI) and Evolutionary Algorithms (EA) [25]. These strategies are capable of handling nonlinear objective functions and have been effectively applied in various implementations. Advanced MPPT methods have demonstrated excellent performance under both uniform and partial shading solar irradiance conditions. They can be further classified into two subcategories: AI-based methods and metaheuristic optimization methods. These categories encompass a diverse range of techniques that operate based on optimization principles to accurately track the MPP of PV systems.

III.4.1.2.1 Artificial Intelligence Methods

AI-Based Methods have gained prominence in MPPT due to their ability to address the non- linear characteristics of solar PV modules. These methods are considered highly efficient in solving real-life non-linear problems, surpassing the limitations of simple mathematical approaches [25]. By eliminating the need for a complete mathematical model of the system, AI methods rely on prior knowledge to design effective solutions. They offer fast, flexible, and computationally intensive approaches to the MPPT problem [104]. AI-based MPP tracking algorithms are employed to optimize the localization of the GMPP. Artificial Neural Networks (ANNs) and Fuzzy Logic Controllers (FLCs) are the main AI methods utilized for MPPT.

ANNs, known as universal approximators, provide a systematic technique for modelling complex processes where conventional mathematical methods struggle [100]. Their rapid adoption in MPPT applications is attributed to their ability to handle challenging operation equations. On the other hand, FLCs exhibit solid performance, even in the presence of system parameter changes and disturbances, owing to their nonlinear and adaptive nature. FLCs have gained increasing attention as effective artificial techniques in MPPT applications [105]. They offer improved performance compared to traditional methods while having simpler requirements compared to sophisticated neural or prediction algorithms. FLCs can be seamlessly integrated into the overall system by combining them with existing MPPT controllers, ensuring maximum power extraction for the loads. A notable drawback of FLC-based MPPT strategies is their reliance on the system. Furthermore, their design necessitates prior understanding of the behavior and characteristics of the PV array.

AI MPPT algorithms also have their drawbacks. Firstly, they can be expensive. Moreover, these algorithms require a significant amount of training data, which places a heavy burden on processor memory during the training process [99]. Another limitation of AI MPPT algorithms is their high computational complexity, requiring powerful computing resources and longer processing times, which can limit their practicality in real-time and resource-constrained applications. Additionally, the computational overhead can lead to increased energy consumption, counteracting the efficiency gains achieved through optimal power tracking [106].

III.4.1.2.2Metaheuristic Optimization Methods:

In the last three decades, metaheuristics have emerged as powerful tools for solving complex optimization problems in various domains, including photovoltaic systems. Their ability to handle multiple objectives, multiple solutions, and nonlinear formulations makes them particularly well-suited for addressing the challenges of finding the MPP in PV systems. Under uniform insolation, MPP identification is a unimodal problem with a single optimum. However, under partial shading conditions, the problem becomes multimodal with multiple local optimal [100]. Metaheuristics, with their inherent exploration capabilities, excel in navigating these complex landscapes and locating the global MPP, unlike traditional MPPT techniques. Furthermore, the effectiveness of metaheuristics extends beyond their ability to find the global MPP. They exhibit superior performance in terms of stability, reduced oscillations around the MPP, improved efficiency, faster settling times, and robustness to varying module configurations, sensitivity to different simple and complex shading scenarios and dynamic insolation conditions [106], [107].

The methods presented and studied below have been carefully chosen as they represent the most widely utilized and validated MPPT approaches among the articles reviewed. Their selection is based on their extensive application and recognition in the field.

III.4.1.2.2.1 Particle Swarm Optimization (PSO):

The Particle Swarm Optimization (PSO) represents a swarm intelligence–based metaheuristic optimization framework. Its conceptual simplicity and computational efficiency have contributed to its widespread use in engineering and scientific research. The method is derived from the collective dynamics of social animals, particularly birds and fish, and functions as a stochastic optimization algorithm that explores the search space using a population of interacting agents.

In PSO, a large number of particles (agents) traverse the search space to find the best solution by optimizing the objective function. Each particle represents a potential solution and moves in a multi-dimensional path with a certain velocity. At each iteration, particles update their velocity based on their current velocity, the previous best position P_{best} and the information obtained from the best-performing particle in their neighborhood G_{best}. Subsequently, the updated position is obtained by using the previous position with the newly calculated velocity value [108]. This collaborative knowledge sharing among particles facilitates the exploration of the search space. By leveraging the cooperative behavior of particles, PSO can effectively guide the search towards the optimal operating point, mimicking the behavior of social animals seeking the best feeding spot. The mathematical representation of the PSO algorithm's velocity v_i and position x_i is given in the following equations [109]:

$$x_i^{k+1} = x_i^k + v_i^{k+1} \tag{III.10}$$

$$v_i^{k+1} = \omega v_i^k + c_1 r_1 \left(P_{best} - x_i^k\right) + c_2 r_2 (G_{best} - x_i^k) \tag{III.11}$$

Furthermore, PSO generally exhibits superior convergence speed when compared with other evolutionary-based optimization methods. PSO-driven tracking frameworks are gradient-free, require only a few adjustable parameters, and are not tailored to a specific system structure. As a result, they provide an efficient computational solution with a strong capability to identify the global optimum [100]. In the context of MPPT for solar energy systems, PSO can be effectively utilized by considering the particle's position, x_i, as the duty cycle D_i. The velocity, in this case, serves as a perturbation to the current duty cycle. The objective of PSO

is to track the GMPP, even when faced with challenges such as partial shading or multiple peak points in the PV panel characteristic curves. To achieve this, PSO continuously updates the duty cycle until it either identifies the GMPP or satisfies the objective function, which, in this case, corresponds to the operational power of the solar panel [109]. Flowchart of the standard PSO algorithm's is presented in Figure III.11.

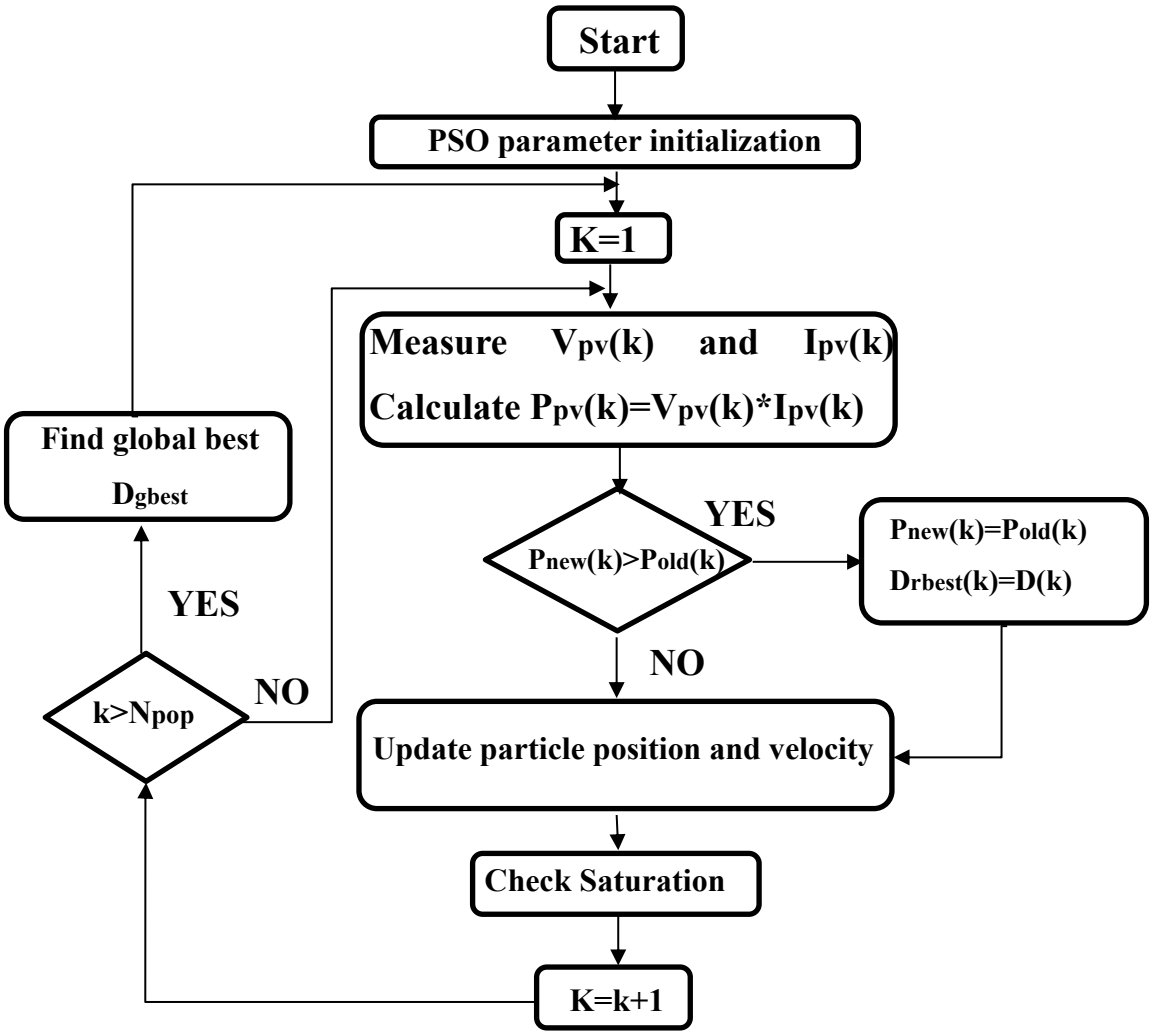


Figure III-11 Flowchart of the Standard PSO-MPPT based Algorithm.

$$D_i^{k+1} = D_i^k + v_i^{k+1} \quad \text{(III.12)}$$

The objective function can be formulated as follows:

$$P(x_i^k) > P(x_i^{k-1}) \quad \text{(III.13)}$$

The standard implementation of PSO is governed by multiple parameters selected from predefined domains, and its velocity update mechanism incorporates stochastic terms that can lead to unpredictable behavior. Although the algorithm is capable of tracking the GMPP, random particle initialization may negatively influence its convergence quality. Additionally, conventional PSO is constrained by limited exploitation capability, extensive parameter tuning, and oscillatory behavior near the MPP [109], [110]. Redundant exploration of previously visited regions by multiple particles further reduces efficiency. To address these challenges, a variety of hybridization and enhancement techniques have been introduced to improve PSO performance, with the primary objectives of increasing system efficiency and enhancing operational reliability [110].

III.4.1.2.2.2 Grey Wolf Optimization (GWO):

The Grey Wolf Optimizer (GWO) is an advanced metaheuristic optimization technique that has gained considerable attention due to its effectiveness and simplicity. The algorithm is inspired by the social hierarchy and collaborative hunting mechanisms of grey wolves. As dominant predators, grey wolves generally form packs of 5–10 members and exhibit a strictly organized leadership structure. This hierarchy is categorized into four primary roles alpha, beta, delta, and omega which collectively govern decision-making and hunting coordination within the pack [111].

The alpha wolf assumes the role of leader and is responsible for guiding the pack's hunting strategies and decisions. The beta and delta wolves assist the alpha by supporting leadership and participating in strategic planning. Conversely, the omega wolf represents the lowest hierarchical level and displays submissive behavior, typically gaining access to food after higher-ranking members. Hunting in grey wolves is a cooperative process that includes

tracking, surrounding, and attacking prey [112]. These behaviors have been idealized and translated into mathematical models that form the foundation of the GWO algorithm, as defined in equations (III.14) (III.19).

First encircling behavior of grey wolves which is mathematically modelled as indicated in the following equations [25]:

$$\vec{D} = | \vec{C}.\overrightarrow{X_p}(t) - \vec{X}(t) | \quad \text{(III.14)}$$

$$\vec{X}(t+1) = \overrightarrow{X_p}(t) - \vec{A}.\vec{D} \quad \text{(III.15)}$$

$\vec{D}$, $\vec{A}$ and $\vec{C}$ are coefficient vectors while t is the current iteration. $\vec{X}(t)$ and $\overrightarrow{X_p}(t)$ denotes the position vector of the search agent and optimum solution (prey position) respectively. Vectors $\vec{A}$ and $\vec{C}$ are calculated as follow:

$$\overrightarrow{A_{\iota(\iota=1,2,3)}} = 2\vec{a}\,.\overrightarrow{r_1} - \vec{a} \quad \text{(III.16)}$$

$$\overrightarrow{C_{\iota(\iota=1,2,3)}} = 2\overrightarrow{r_2} \quad \text{(III.17)}$$

$\overrightarrow{r_1}, \overrightarrow{r_2}$ are random vectors in the range [0,1]. a Value linearly decreases from 2 to 0 over the iterations.

The search agent's position is updated using the following formulae [189]:

$$\overrightarrow{D_\alpha} = | \overrightarrow{C_1}.\overrightarrow{X_\alpha}(t) - \vec{X}(t) |, \overrightarrow{D_\beta} = | \overrightarrow{C_2}.\overrightarrow{X_\beta}(t) - \vec{X}(t) |, \overrightarrow{D_\delta} = | \overrightarrow{C_3}.\overrightarrow{X_\delta}(t) - \vec{X}(t) | \quad \text{(III.18)}$$

$$\overrightarrow{X_1} = \overrightarrow{X_\alpha}(t) - \overrightarrow{A_1 D_\alpha}\ ,\ \overrightarrow{X_2} = \overrightarrow{X_\beta}(t) - \overrightarrow{A_2 D_\beta}\ ,\ \overrightarrow{X_3} = \overrightarrow{X_\delta}(t) - \overrightarrow{A_3 D_\delta} \quad \text{(III.19)}$$

$$\vec{X}(t+1) = \frac{\overrightarrow{X_1}+\overrightarrow{X_2}+\overrightarrow{X_3}}{3} \quad \text{(III.20)}$$

In the context of MPPT, the duty cycle of the DC–DC converter is represented by the grey wolf agents, whereas the MPP is modeled as the prey to be captured. The implementation procedure of the GWO-based MPPT strategy is summarized in the flowchart shown in Figure

III.12. Although the standard GWO algorithm suffers from intrinsic limitations, including an uneven balance between exploration and exploitation and reduced population diversity, it retains several attractive features such as rapid convergence, algorithmic flexibility, scalability, reduced parameter tuning, and implementation simplicity.

Despite these advantages, the application of GWO to MPP tracking reveals notable performance constraints. While the algorithm can efficiently identify the GMPP, this process often involves a large number of iterations, leading to increased energy losses. Moreover, GWO faces two major challenges: inadequate tracking of time-varying GMPP under fluctuating partial shading conditions and oscillatory behavior around the GMPP [111]. These limitations underscore the need for further algorithmic refinements. Consequently, several studies have proposed enhanced and hybrid GWO-based MPPT methods to preserve the algorithm's strengths while addressing its inherent weaknesses [113], [114], [115], [116].

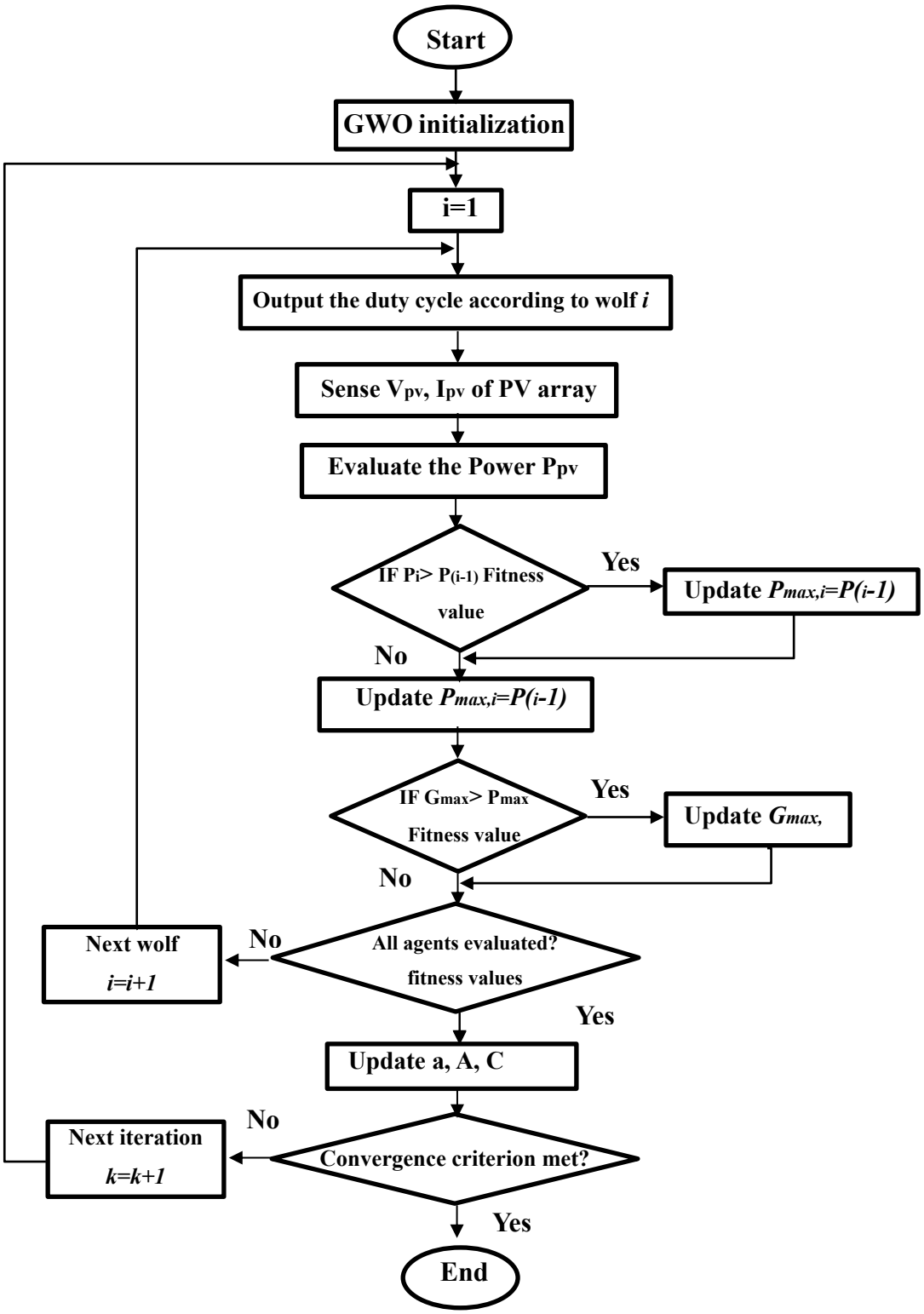


Figure III-12 GWO MPPT Algorithm Flowchart.

III.4.1.2.2.3 Ant Colony Optimization (ACO)

The Ant Colony Optimization (ACO) algorithm is a nature-inspired metaheuristic that draws on the collective foraging behavior of ant colonies to solve complex optimization problems. The algorithm abstracts the pheromone-based communication mechanism used by ants to cooperatively identify efficient paths between their nest and food sources. As ants traverse candidate paths, pheromone levels are incrementally updated, with shorter paths receiving stronger reinforcement due to higher traversal frequency, while longer paths experience pheromone evaporation. This positive feedback process promotes the emergence of optimal solutions over time by attracting an increasing number of ants toward high-quality paths [117]. The stochastic nature of path selection further enables extensive exploration of the solution space, allowing ACO to handle highly nonlinear optimization tasks.

ACO exhibits several features that are particularly advantageous for maximum power point tracking in photovoltaic systems, including parallel processing capability, adaptive learning behavior, and effective feedback control [118]. However, the algorithm may suffer from slow convergence during the initial search stage due to the absence of sufficient pheromone information. Despite this limitation, the strengths of ACO make it a suitable optimization framework for MPPT applications.

For effective implementation in PV systems, the standard ACO algorithm must be adapted to address the specific characteristics of the MPPT problem. The overall implementation strategy is illustrated in the flowchart presented in Figure III.13.

In this framework, the duty cycle of the power converter constitutes the primary control variable regulated by the ACO algorithm to achieve maximum power point tracking. The algorithm assesses the output power associated with randomly selected duty cycle candidates to steer the search process toward the global MPP. Comparative analyses have indicated that ACO-based MPPT schemes often surpass conventional and PSO-based approaches, particularly in their capacity to avoid convergence to local MPPs. Moreover, the convergence characteristics of ACO are largely independent of the initial distribution of ant agents.

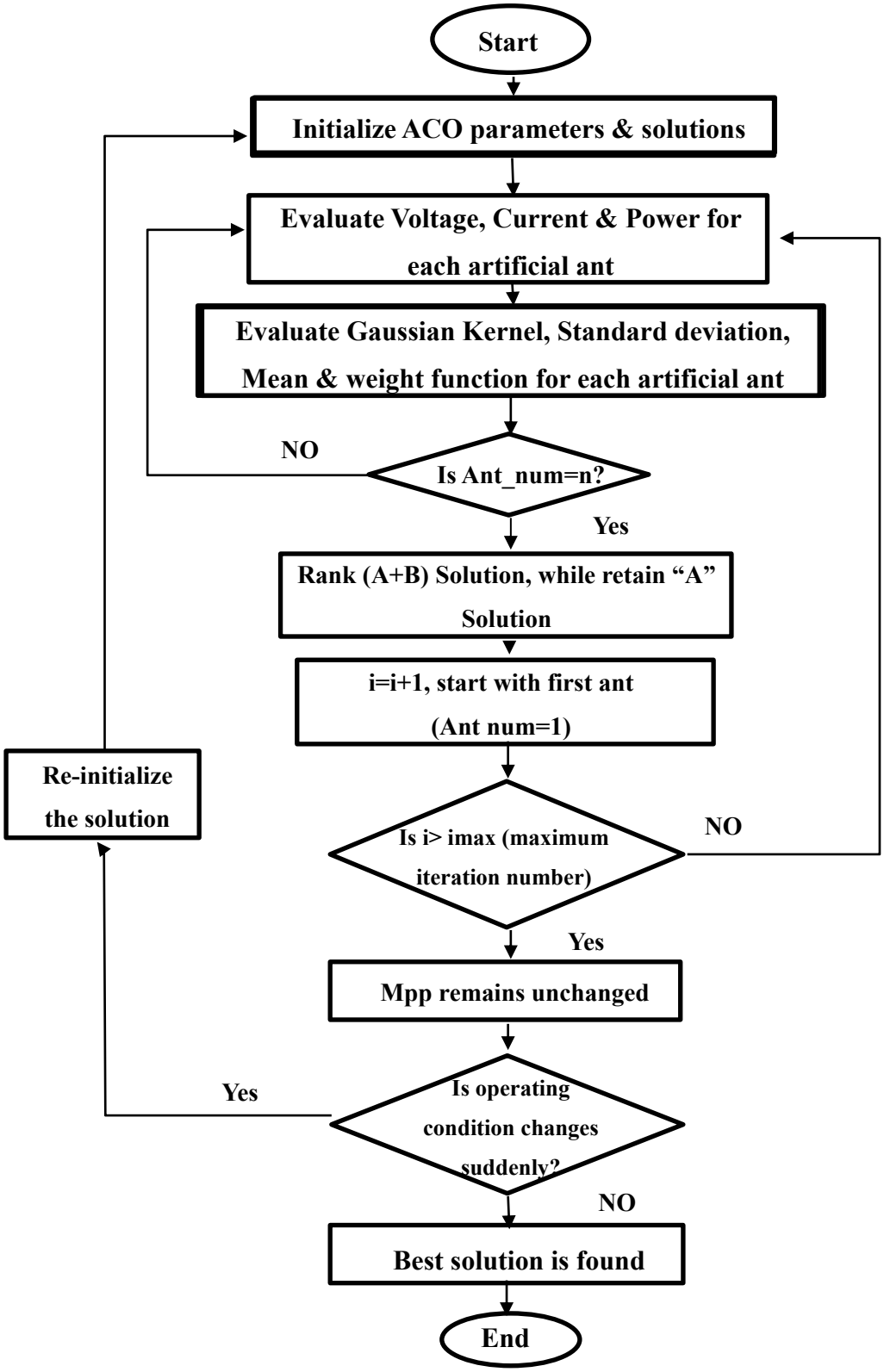


Figure III-13 ACO-MPPT based Algorithm.

However, limited attention has been given to comparisons with more recently proposed swarm-based MPPT algorithms. Consequently, ACO-based implementations may suffer from longer settling times and increased transient oscillations during startup when compared with newer optimization strategies. Additionally, initializing ants far from the global MPP can elevate the likelihood of stagnation at local optima. Although ACO is seldom adopted as a standalone MPPT method, numerous refinements and hybridizations with other soft computing techniques have been reported to enhance its performance [25].

III.4.1.2.2.4 Cuckoo Search (CS)

The Cuckoo Search (CS) algorithm is a bio-inspired optimization method based on the brood parasitism behavior exhibited by cuckoo birds. This reproductive strategy involves laying eggs in the nests of host species, often with a timing advantage that enables the cuckoo eggs to hatch earlier. In some cases, the cuckoo hatchlings remove the host eggs to gain preferential access to food. To increase acceptance by host birds, cuckoos may employ egg mimicry techniques that resemble the host's eggs [119]. Brood parasitism manifests through various mechanisms, including competitive displacement, cooperative interactions, and complete nest takeover [120].

In the CS algorithm, cuckoos are modeled as search agents and their eggs represent candidate solutions generated at each iteration. The optimization process is governed by three main assumptions: (i) each cuckoo lays one egg per iteration, (ii) only solutions with high fitness values are retained for the next generation, and (iii) the number of host nests is fixed throughout the optimization process [119], [120]. The algorithmic procedure is illustrated in the flowchart shown in Figure III.14, which accounts for host bird behaviors such as egg rejection and nest abandonment [120]. New solutions are produced using Lévy flight–based random walks, where the step size is determined by a Lévy probability distribution, as expressed in the corresponding equation [119]:

$$x_i^{t+1} = x_i^t \oplus \alpha \, Lévy(\lambda) \tag{III.21}$$

xt is the samples, t is the iteration number and $\alpha > 0$ is the step size and calculated by the following equation:

$$\alpha = \alpha_0(x_j^t - x_i^t) \quad \text{(III.22)}$$

The $Lévy(\lambda)$ is calculated using the Lévy distribution as in Equation (III.23).

$$Lévy(\lambda) \approx u = l^{-\lambda}\ , \quad (1 < \lambda < 3) \quad \text{(III.23)}$$

The brood parasitism and early hatching strategies observed in cuckoo birds form the underlying inspiration for the CS algorithm, endowing it with strong global search capability and effective convergence behavior. These properties make CS particularly attractive for MPPT applications. Compared with the Hill Climbing algorithm, which also incorporates large-scale randomization, CS employs a population-based optimization framework similar to PSO and Genetic Algorithms (GA). The inclusion of elitism and selection mechanisms, comparable to those used in Harmony Search, further enhances the robustness and exploration efficiency of CS for MPPT problems [94]. Additionally, the heavy-tailed distribution governing its randomization enables large exploratory moves, resulting in more efficient optimization than conventional Hill Climbing methods [120].

The CS algorithm is characterized by fast convergence and high accuracy, achieved with a relatively small number of adjustable parameters compared to many other metaheuristic algorithms [25]. While this simplifies practical implementation, it may constrain flexibility in MPPT scenarios requiring finer parameter control. Another limitation of CS is the complexity of its mathematical formulation [120]. Nonetheless, its adaptability and strong optimization performance have established CS as a promising technique for MPPT in renewable energy systems. As a result, numerous enhanced and hybrid CS variants have been proposed to mitigate these limitations and further improve its effectiveness in MPPT and broader optimization applications.

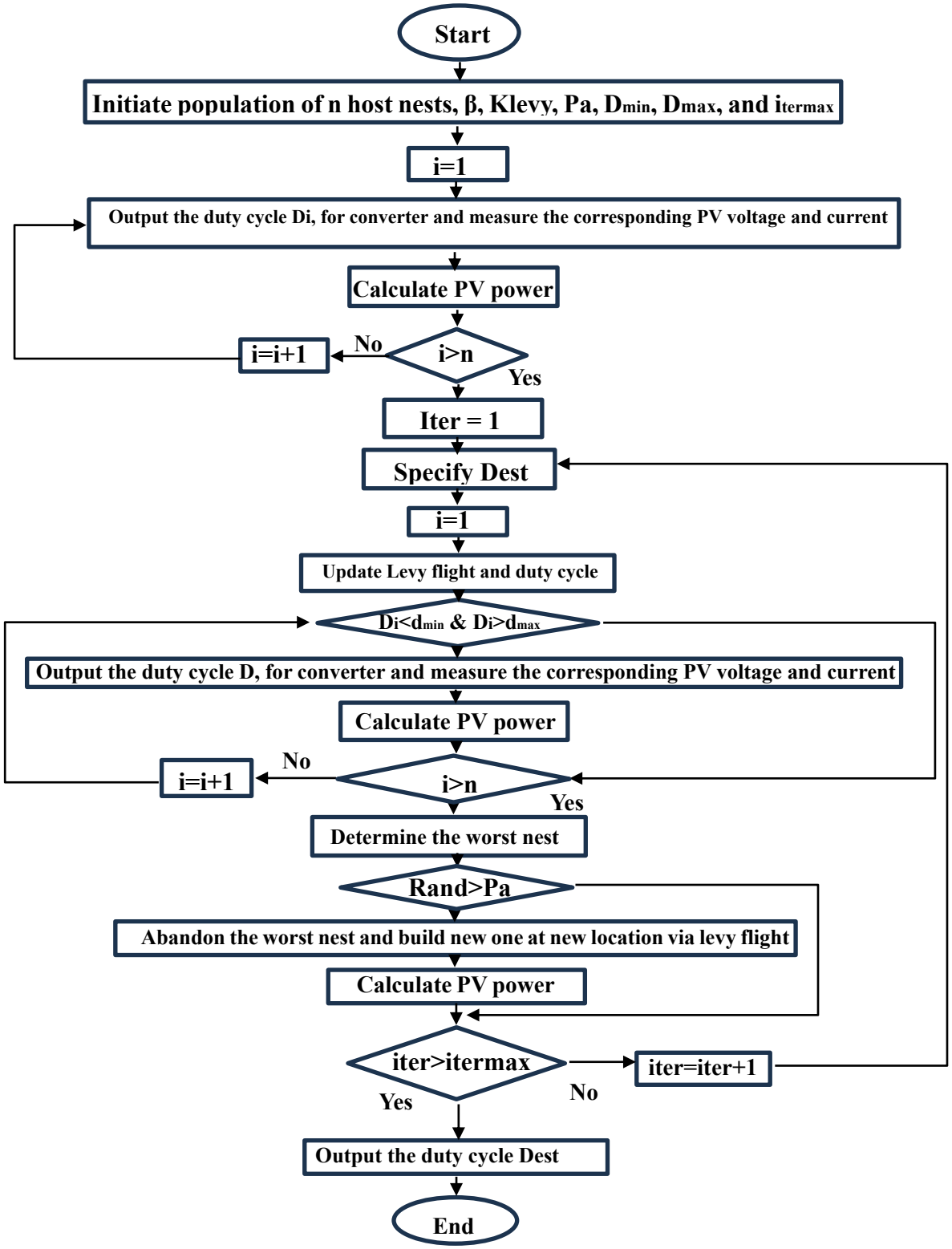


Figure III-14 CS-MPPT based Algorithm.

III.4.1.2.2.5 The Harris Hawk Optimization (HHO)

The Harris Hawks Optimization (HHO) algorithm is a recent swarm intelligence metaheuristic that draws inspiration from the cooperative hunting behavior of Harris hawks. The fundamental concept underlying this approach is derived from the natural predation strategy in which multiple hawks coordinate their movements and attacks from different directions to confuse, weaken, and ultimately capture their prey.

In this biological paradigm, Harris hawks function as a coordinated group rather than as independent agents. Typically, one hawk initiates the pursuit to distract the prey, while the remaining members alternately engage in chasing and attacking until the prey's energy is depleted. This collective and adaptive behavior is mathematically modeled in the HHO algorithm to guide its search process, enabling an effective balance between exploration of the global search space and exploitation of promising solution regions.

In comparison with other metaheuristic optimization techniques, HHO has demonstrated strong capability in solving constrained optimization problems by maintaining a flexible trade-off between global exploration and local exploitation. The algorithm operates through three principal phases. The exploration phase allows the hawks to scan the search space broadly to identify potential candidate solutions. This is followed by a transition phase, during which the algorithm dynamically regulates the shift from exploration to exploitation based on the simulated escaping energy of the prey. Finally, during the exploitation (development) phase, the hawks concentrate their search around the estimated prey location, progressively refining solutions and driving the algorithm toward convergence.

Overall, the biologically inspired cooperative hunting strategy of HHO provides high adaptability, fast convergence, and effective global optimization performance, positioning it as a competitive alternative to conventional swarm intelligence algorithms [121].

1) Exploration Phase:

Harris hawks roost somewhere randomly and search for prey through one of two strategies, with the random number q used to select the strategy to be employed.

$$\begin{cases} X(t+1) = \begin{cases} \mathrm{X}_{rand}(t) - \mathrm{r}_1 \mid \mathrm{X}_{rand}(t) - 2\mathrm{r}_2 X(t) \mid, q \geq 0.5 \\ (\mathrm{X}_{rabbit}(t) - \mathrm{X}_m(t)) - \mathrm{r}_3(LB + \mathrm{r}_4(UB - \mathrm{UL})), q \geq 0.5 \end{cases} \\ \mathrm{X}_m(t) = \frac{1}{N}\sum_i^N \mathrm{X}_i(t) \end{cases} \quad \text{(III.24)}$$

where $X(t)$ represents the current position of the Harris hawk; $\mathrm{X}_{rabbit}(t)$ represents the position of the prey rabbit; r_1, r_2, r_3, and r_4 are random numbers between 0 and 1; UB and UL indicate the position range of the hawk, which is determined by the range of the independent variable of the optimization function; $\mathrm{X}_m(t)$represents the average position of the hawk; and N is the total number of hawks.

2) Transition Phase:

HHO can switch between different exploitation behaviors according to the escape energy of the prey, and the prey energy will be greatly reduced in the process of escape. The prey energy can be expressed as:

$$E = 2E_0(1 - \frac{t}{T}) \quad \text{(III.25)}$$

Where E is the escape energy of the prey, E_0 is the initial energy of the prey, t is the current iteration, and T is the maximum iteration. In this phase, when E ≥ 0.5, a soft siege is launched; when E < 0.5, a hard siege is initiated.

3) Development Phase:

(1) Soft siege

When r ≥ 0.5 and |E| ≥ 0.5, the following model is adopted:

$$X(t+1) = \Delta X(t) - E|J\, X_{rabbit}(t) - X(t)| \quad \text{(III.26)}$$

where $\Delta X(t) = X_{rabbit}(t) - X(t)$ is the distance between the prey and the hawks, J is a random number between 0 and 2.

(2) Hard siege

When r ≥ 0.5 and |E| < 0.5, the following model is adopted:

$$X(t\ +\ 1) = X_{rabbit}(t)\ -\ E|\Delta X(t)| \tag{III.27}$$

(3) Progressive fast-dive soft siege

When r < 0.5 and |E| ≥ 0.5, the prey can still escape successfully, so the raid will still be preceded by a soft siege, which will use the following strategy to update the position:

$$\mathrm{X(t\ +\ 1)} = \begin{cases} Y, F(Y)\ <\ F(X(t)) \\ \mathrm{Z, F(Z)\ <\ F(X(t))} \end{cases} \tag{III.28}$$

$$Y\ =\ X_{rabbit}(t)\ -\ E|J\ X_{rabbit}(t)\ -\ X(t)| \tag{III.29}$$

$$Z\ =\ Y\ +\ S\ \times\ LF(D) \tag{III.30}$$

where D and S are the dimensions of the objective function and the random vector, respectively, and LF is the mathematical expression of Levy's flight.

(4) Progressive fast-dive hard siege

When r < 0.5 and |E| < 0.5, this strategy is adopted:

$$\mathrm{X(t\ +\ 1)} = \begin{cases} Y, F(Y) < F\big(X(t)\big) \\ \mathrm{Z, F(Z) < F\big(X(t)\big)} \end{cases} \tag{III.31}$$

where Y and Z are calculated as follows:

$$Y\ =\ X_{rabbit}(t)\ -\ E|J\ X_{rabbit}(t)\ -\ \mathrm{X}_m(t)| \tag{III.32}$$

$$Z\ =\ Y\ +\ S\ \times\ LF(D) \tag{III.33}$$

4) Objective Fitness Function:

For the MPPT control design, the output power of the photovoltaic array is commonly used as the fitness function, with the duty cycle D as the independent variable of the fitness function. The fitness function is defined as follows:

$$P_k(D_k) = U_k I_k \tag{III.34}$$

where k represents the iteration number, D_k indicating the duty cycle used during the k-the iteration, U_k and I_k represents the obtained output voltage and current. The MPPT control flow chart of the HHO algorithm is shown in Figure III-15 [121].

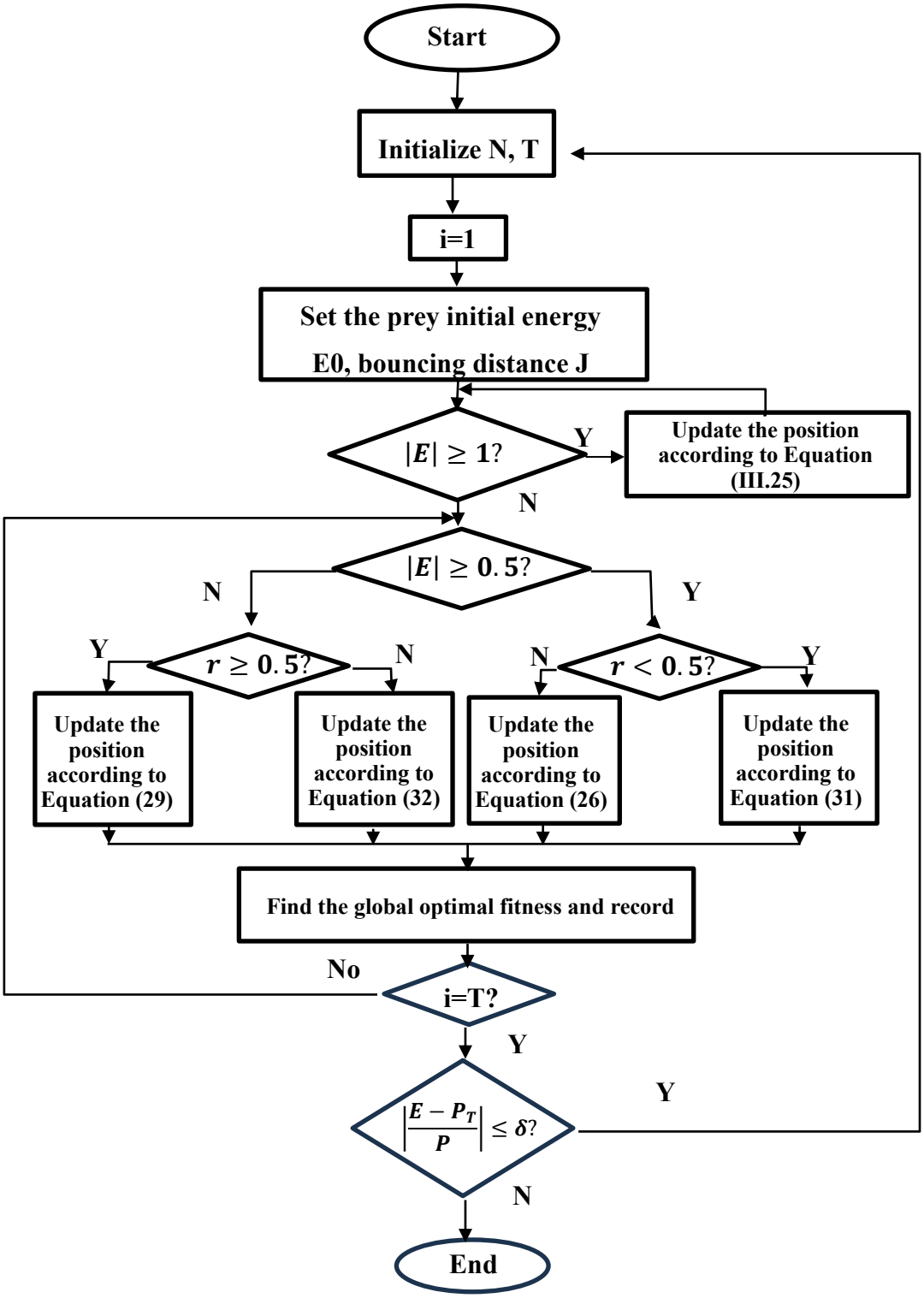


Figure III-15 Control flow chart of HHO.

III.4.1.2.2.6 Horse Herd Optimization Algorithm (HOA)

The Horse Herd Optimization Algorithm (HOA) is a bio-inspired swarm intelligence metaheuristic that models the collective and individual behavioral patterns of horses in their natural environment. The algorithm is motivated by ethological studies showing that horses exhibit complex social, hierarchical, and adaptive behaviors that vary across different stages of their lifespan [122]. By translating these behavioral characteristics into computational rules, HOA provides an effective framework for solving complex optimization problems.

Unlike many swarm-based algorithms that rely on a single or limited set of interaction mechanisms, HOA incorporates a diverse set of behaviors, allowing agents to adapt dynamically throughout the optimization process. These behaviors include grazing, hierarchy, sociability, imitation, defense mechanisms, and roaming. The integration of these components enables a balanced trade-off between exploration of the global search space and exploitation of promising regions.

A distinctive feature of HOA is its age-based population modeling. Horses are categorized into four age groups that reflect different behavioral tendencies observed in real herds. Young horses (δ, 0–5 years) represent inexperienced individuals with higher randomness in movement. Adolescent horses (γ, 5–10 years) exhibit strong curiosity and imitation behaviors. Mature horses (β, 10–15 years) demonstrate social awareness and hierarchical following, while senior horses (α, above 15 years) act as experienced leaders with stable and goal-oriented behavior.

At each iteration, the population is ranked according to fitness values, and horses are reassigned to these age groups based on their relative performance. Typically, the top-performing individuals are classified as α horses, followed by β, γ, and δ groups. This adaptive classification allows the algorithm to continuously update behavioral roles according to solution quality, enhancing convergence reliability.

The motion of each horse in the search space is governed by a combination of behavioral components, which differ depending on age group. These behaviors represent both individual intelligence and collective interaction within the herd.

1) Grazing Behavior: Grazing is a fundamental activity observed across all age groups and represents localized exploration around a horse's current position. In the optimization context, grazing allows each agent to perform a fine-grained search within a bounded neighborhood. This behavior promotes exploitation while still permitting limited exploration. The grazing influence gradually decreases over iterations, ensuring that early stages emphasize exploration, whereas later stages focus on convergence.

2) Hierarchical Behavior: Hierarchy plays a critical role in horse herds, particularly among middle-aged and mature individuals. Horses tend to follow the most experienced or dominant leader when making movement decisions. In HOA, this behavior is modeled by guiding β and γ horses toward the best-performing solution found so far. This mechanism accelerates convergence by reinforcing high-quality solutions while maintaining population coherence.

3) Sociability Behavior: Horses are inherently social animals that rely on group cohesion for survival. Sociability is represented in HOA by encouraging horses, particularly those in the β and γ age groups, to move toward the average position of the herd. This collective tendency enhances information sharing among agents and prevents excessive dispersion, contributing to algorithmic stability. Sociability also reduces the risk of premature convergence by maintaining diversity within the population.

4) Imitation Behavior: Imitation is most prominent among younger horses, which learn by observing older and more successful individuals. In HOA, this behavior enables γ and δ horses to adjust their positions based on elite solutions. Imitation strengthens exploitation by allowing weaker solutions to improve through learning, while still preserving diversity due to partial rather than complete imitation.

5) Defense Mechanism: As prey animals, horses possess strong defensive instincts. This behavior is modeled in HOA by introducing repulsion from poorly performing solutions. Horses instinctively avoid regions associated with danger or failure, which, in the optimization context, corresponds to moving away from the worst-performing individuals. This mechanism enhances robustness by preventing stagnation in low-quality regions and improves the algorithm's ability to escape local optima.

6) Roaming Behavior: Roaming reflects the natural curiosity of horses and their tendency to explore new pastures. This behavior is implemented as a controlled random movement, primarily affecting younger horses. Roaming enhances global exploration and plays a critical role in maintaining population diversity during early optimization stages. As horses mature, the influence of roaming gradually diminishes, reflecting increased behavioral stability.

A conceptual illustration of these behavioral components and their interactions is presented in Figure III-16, which summarizes the grazing, hierarchy, sociability, imitation, defense, and roaming mechanisms within the HOA framework.

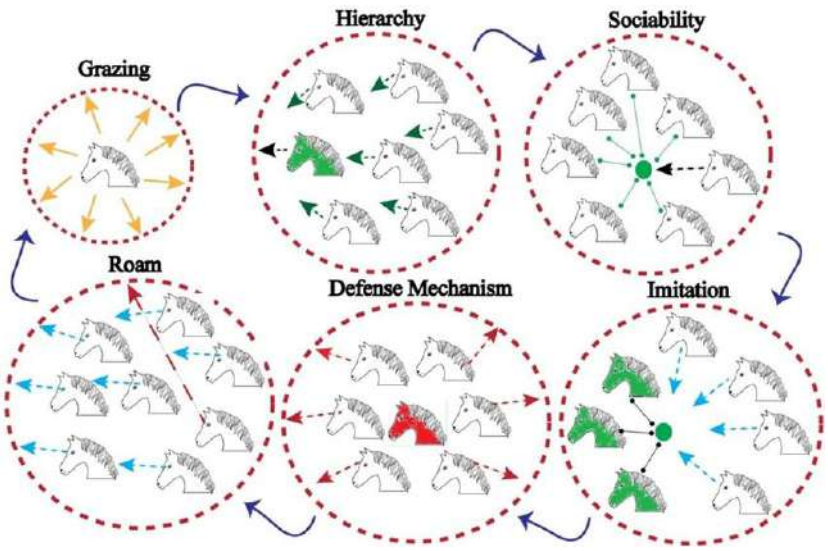


Figure III-16 Diagram representing grazing, hierarchy, sociability, imitation, defense mechanisms, and roam of the HOA.

The HOA algorithm begins with the random initialization of horse positions within the search space. During each iteration, horses are evaluated based on fitness, ranked, and

reassigned to age groups. Behavioral influences are then applied according to age-specific rules, and each horse updates its position accordingly. This process continues until a termination condition, such as a maximum number of iterations or convergence threshold, is met. The overall workflow of the HOA algorithm is illustrated in Figure III-17, which presents the sequential steps from initialization to convergence.

The multi-behavioral and age-adaptive nature of HOA provides several advantages over conventional swarm intelligence algorithms. The algorithm demonstrates strong exploration capability in early stages due to roaming and grazing behaviors, while hierarchical following and imitation enhance exploitation in later stages. The defense mechanism further improves robustness by reducing the likelihood of stagnation in poor regions of the search space [122].

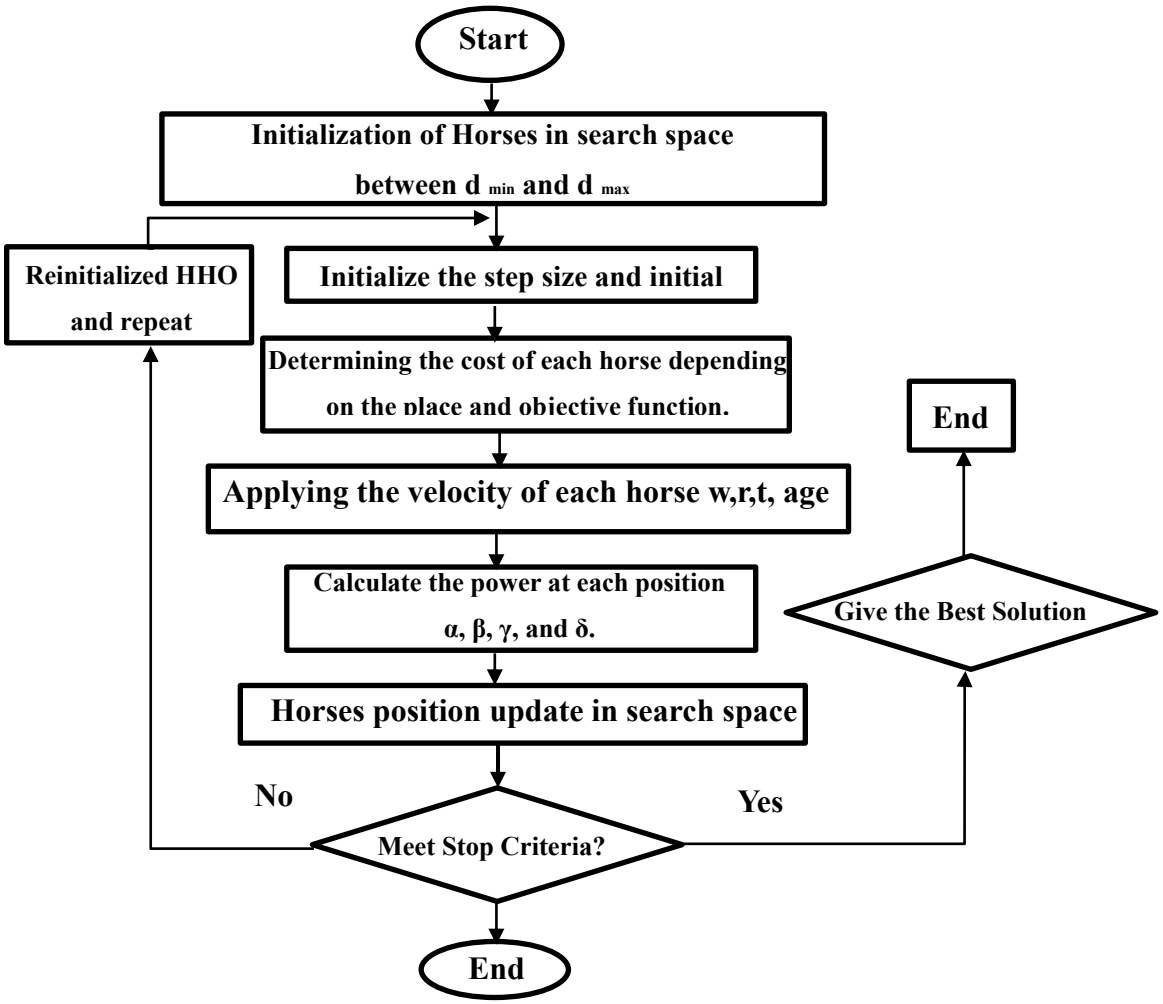


Figure III-17 Flowchart of the HOA algorithm.

III.5 Performance Evaluation of MPPT Algorithms

The literature on MPPT algorithms has identified numerous factors to evaluate their performance. Commonly, these factors are used to provide a general assessment of the algorithms' capabilities. However, it's important to note that some of these factors can be challenging to measure precisely, resulting in an approximation of the actual performance.

While there are many factors that researchers and engineers consider when evaluating MPPT algorithms, Tracking Accuracy, Efficiency, Robustness, and Tracking Speed the most critical considerations when evaluating the overall performance and effectiveness of MPPT algorithms in photovoltaic systems [25]. Since they directly impact the system's ability to maximize energy generation and maintain reliable operation under real-world conditions, [123].

III.5.1 Tracking Accuracy

Tracking accuracy is the algorithm's ability to accurately track the true maximum power point, even in the presence of rapidly changing environmental conditions, such as variations in irradiance and temperature. Accurate tracking is crucial for maximizing the energy extraction from the photovoltaic system.

III.5.2 Efficiency

Evaluating the tracking efficiency is a crucial step in quantifying how effectively an MPPT control algorithm is able to locate and maintain the MPP of a PV system. This metric directly reflects the algorithm's contribution to enhancing the overall performance of the PV system compared to other MPPT methods.

According to sources [124], the tracking efficiency is defined as the ratio between the actual power generated by the PV array and the theoretical maximum power that could be produced under the same environmental conditions during the same time period. This is an important consideration because atmospheric factors like irradiation and temperature can

fluctuate widely, necessitating that each MPPT algorithm be evaluated across a range of operating conditions to assess its comparative performance.

A well-designed MPPT control system should demonstrate robust and reliable performance across diverse atmospheric conditions. Equation (III.35) is used in a simulated PV system to quantify the tracking efficiency, as referenced in [25].

$$n_{MPPT} = \frac{1}{N}\sum_{1}^{N}\frac{P_{actual,i}}{P_{maax,i}} \quad \text{(III.35)}$$

III.5.3 Robustness

The robustness of the MPPT algorithm refers to its ability to maintain stable and reliable performance under various environmental conditions, system parameters, and disturbances. A robust algorithm can handle factors like partial shading, rapid changes in irradiance, and component variations without significant degradation in its tracking capability.

III.5.4 Tracking Speed

The tracking speed measures how quickly the algorithm can respond to changes in the operating conditions and converge to the new maximum power point. Faster tracking speed is desirable, as it allows the system to rapidly adapt to fluctuations in the environment and maintain optimal power extraction with lower power losses in the solar energy system.

In addition to these key factors, researchers and engineers may also consider other aspects, such as steady state error, Dynamic response, computational complexity, sensor requirements, adaptability, stability, and hardware compatibility, when evaluating the overall performance and effectiveness of MPPT algorithms in extracting the maximum power from photovoltaic systems [25].

After a comprehensive review, the exploration of conventional MPPT techniques and emerging metaheuristic approaches has highlighted their distinct strengths and limitations. The No Free Lunch Theorem (NFLT) states that no single optimization algorithm can consistently outperform others across all system configurations and environmental conditions [125]. This

principle applies to metaheuristic MPPT algorithms, which are often designed for specific scenarios rather than being universally applicable [126]. Their performance can be inconsistent, particularly under changing conditions. Moreover, algorithms with fewer control parameters are generally preferable, as an excessive number of control variables increases sensitivity to parameter settings, leading to suboptimal solutions and local optima [127]. Since the effectiveness of these algorithms depends on the PV system configuration and operating conditions, a universal solution is impractical. The NFLT underscores the necessity of adaptive or hybrid approaches to address the diverse requirements of photovoltaic applications.

III.6 PV System Configuration

Figure III-18 presents the schematic of the modelled system implemented in MATLAB-Simulink, representing a photovoltaic system connected with a different Metaheuristic MPPT algorithms. The system integrates the proposed MPPT algorithms to enhance energy extraction and improve overall performance, PV system includes the following main components:

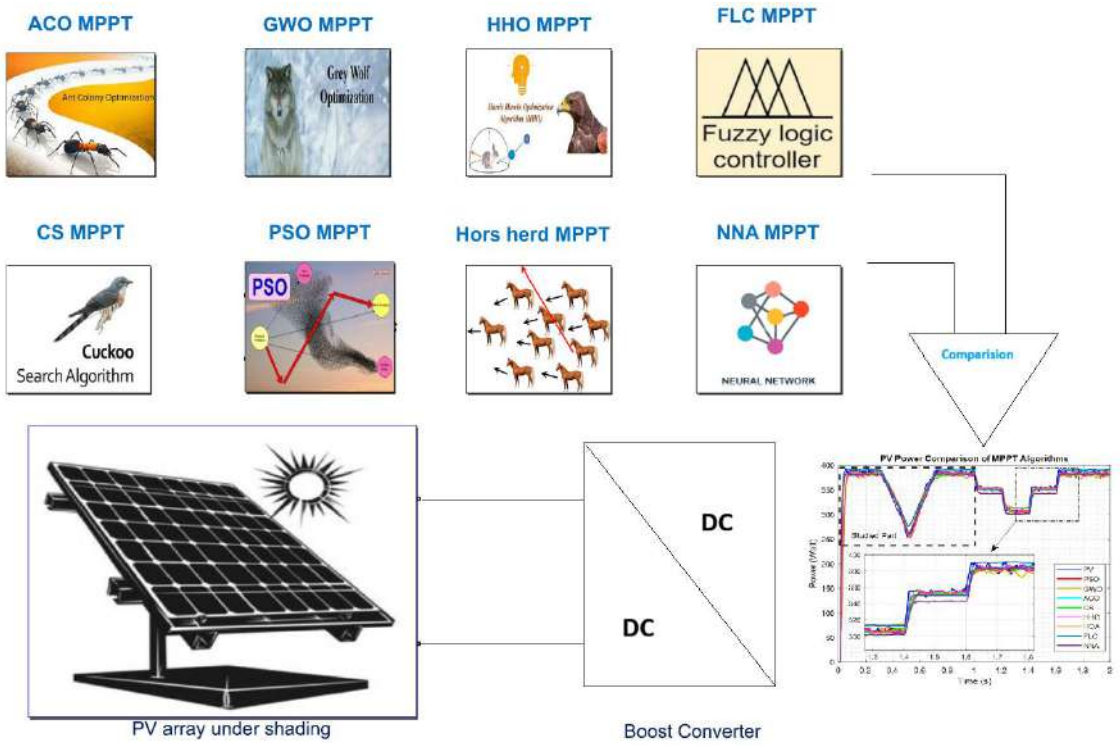


Figure III-18 Model Block Diagram of Metaheuristic MPPT comparison connected to PV System.

- The photovoltaic (PV) array generates electrical power based on the incident solar radiation and ambient temperature.

- A DC-DC converter equipped with an MPPT controller regulates the PV output voltage and ensures maximum power extraction.

- MPPT Algorithms PSO, ACO, GWO, CS, HHO, HOA, FLC and ANN.

- Measuring blocks capture electrical parameters for control and performance evaluation.

Table III-1 PV Module Specifications.

Parameters	**Value**
Cells per module (Ncell)	60
Open circuit voltage (Voc)	57.6 V
Short-circuit Current (Isc)	4.6 A
Voltage at Maximum power point (Vmp)	47 V
Current at maximum power point (Imp)	4.26 A
Maximum Power (Pmp)	200.226 W

The manufacturer's specifications and parameters for the PV array utilized in this model can be found in Table III-1.

III.6.1 Simulation Results and Discussion

This system has been modelled and simulated in MATLAB/Simulink to test the efficacy of different proposed MPPT algorithms, namely the Particle Swarm Optimization (PSO) algorithm, Grey Wolf Optimization (GWO), Ant Colony Optimization (ACO), Cuckoo Search (CS) algorithm, Harris Hawk Optimization (HHO) and Horse Herd Optimization Algorithm (HOA), also an AI Based Algorithm, Artificial Neural Network (ANN) and Fuzzy Logic Control (FLC).

The performance of these algorithms is assessed under variable irradiance conditions. Each MPPT algorithm is tested separately to thoroughly evaluate their individual performance. Subsequently, a comparative analysis is conducted to highlight the strengths and weaknesses of each algorithm, providing insights into their practical applications and effectiveness in optimizing PV system performance.

III.6.1.1 Algorithms Under Uniform Solar Illumination

The irradiance profile utilized in this simulation to test the Proposed algorithms under uniform solar illumination (USI) conditions is presented in Figure III-19. The ambient temperature is maintained at a fixed value of T = 25 C°. As shown in the figure, irradiance changes successively and rapidly between different high and low levels, for instance, there is a gradual decrease in irradiance from 1000 to 700 w/m².

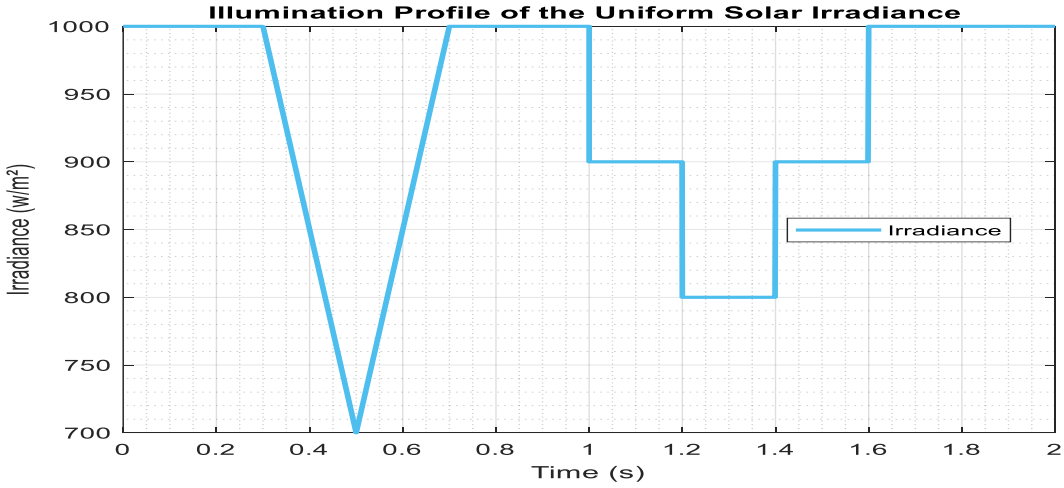


Figure III-19 Illumination Profile of the Uniform Solar Irradiance Condition (USI).

The power waveform of the PV system under Standard Test Conditions (STC) with different MPPTs Test are presented in Figure III-20.

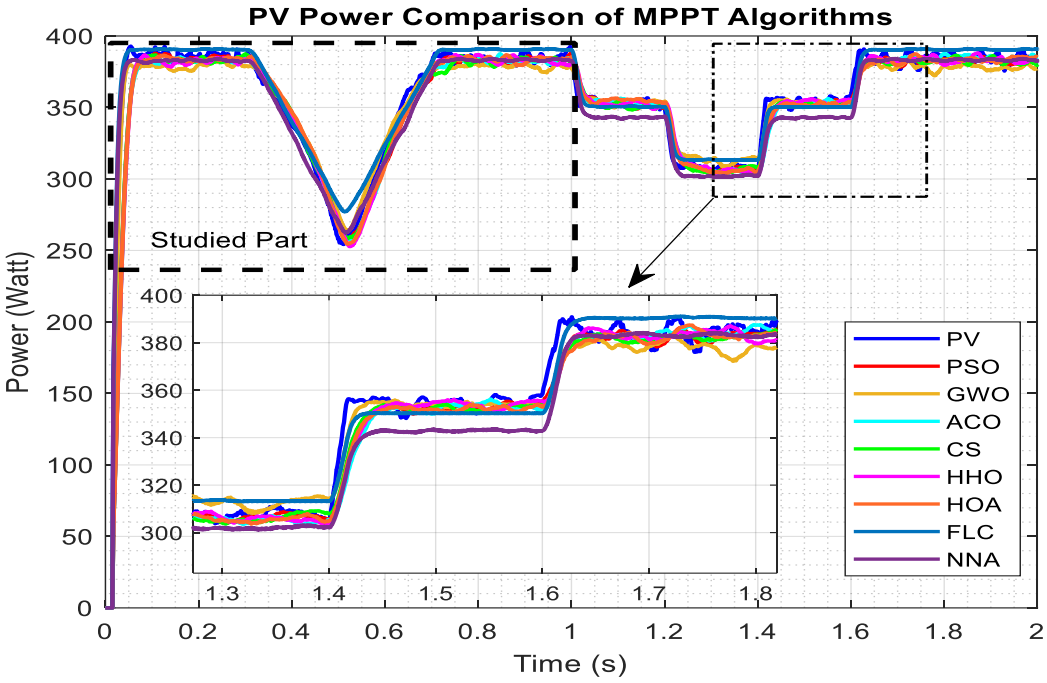


Figure III-20 PV Power Waveforms

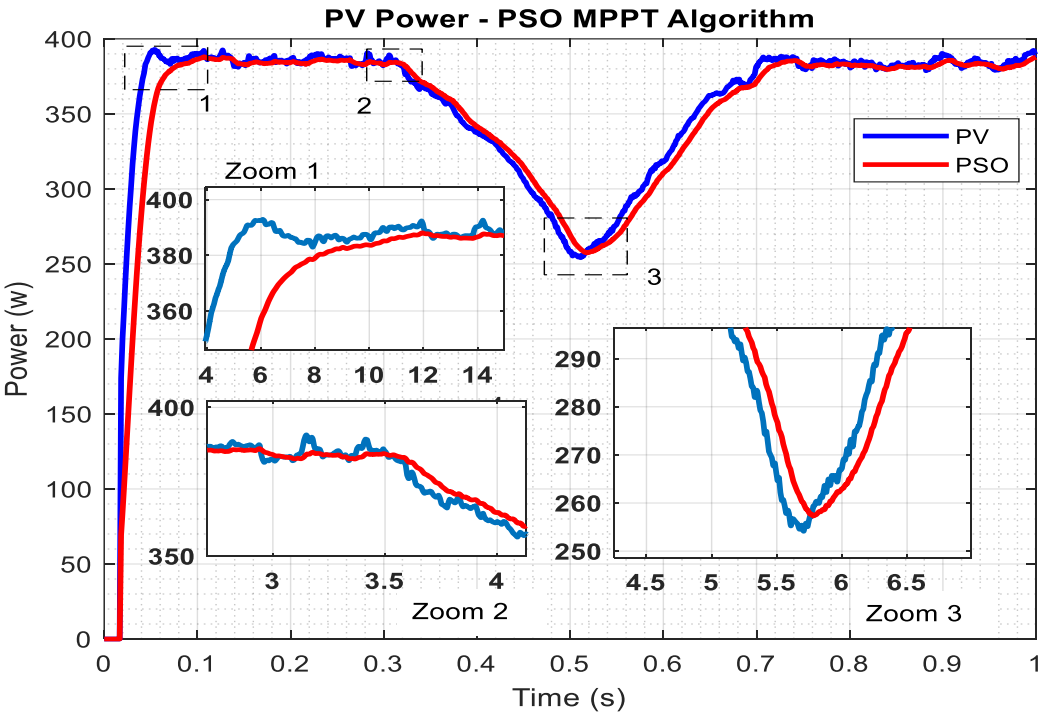


Figure III-21 PV Power with PSO MPPT

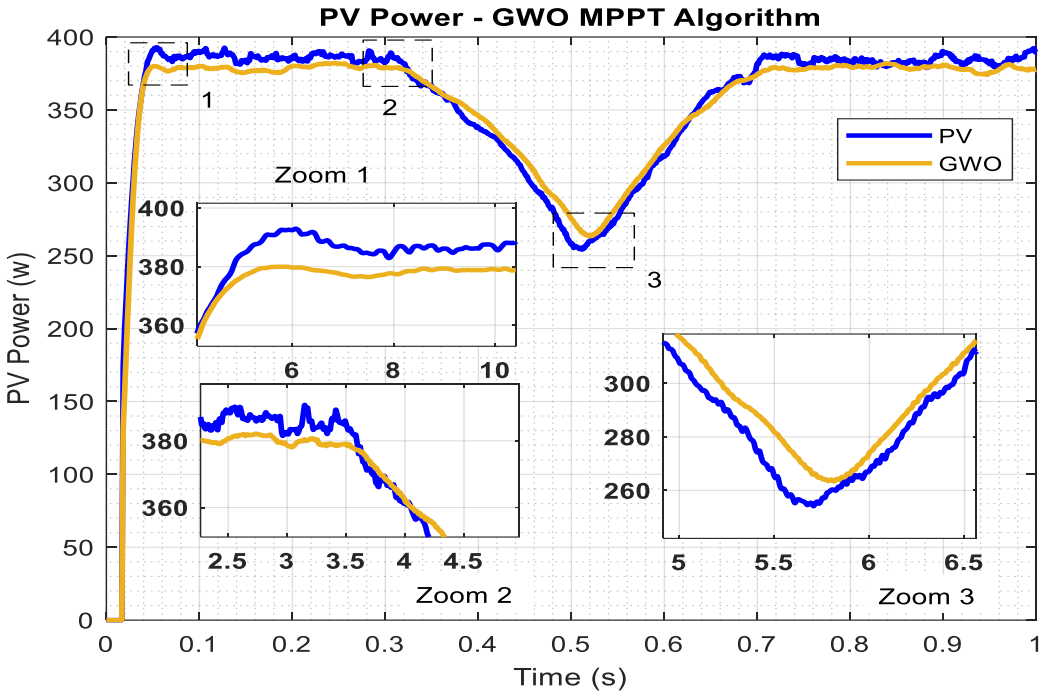


Figure III-22 PV Power GWO MPPT

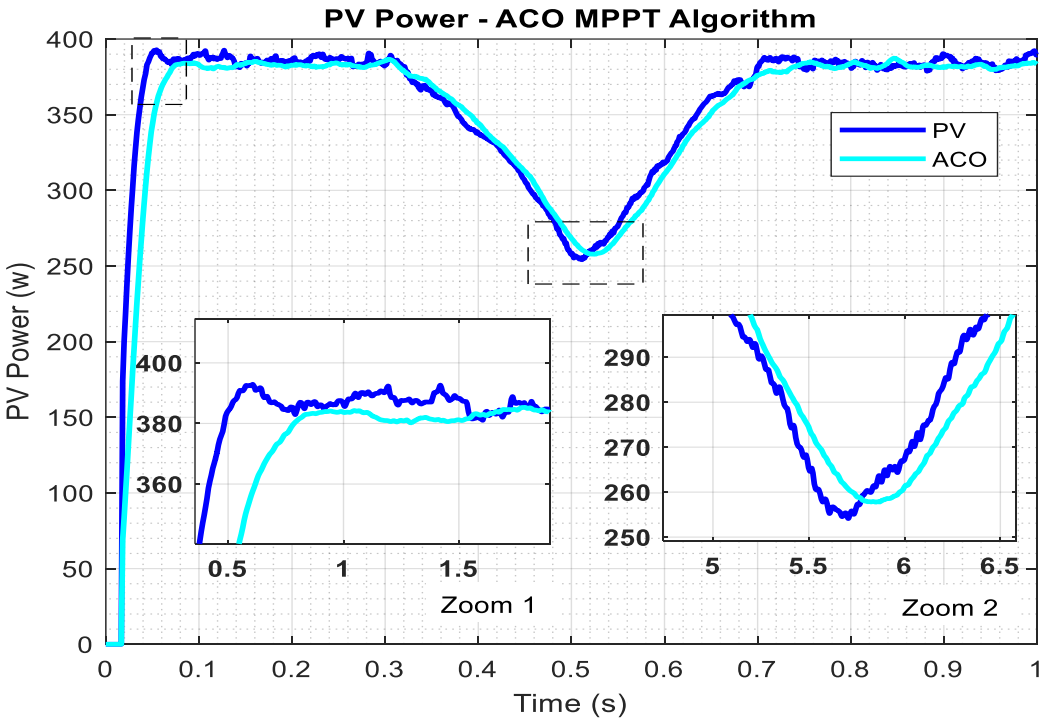


Figure III-23 PV Power ACO MPPT

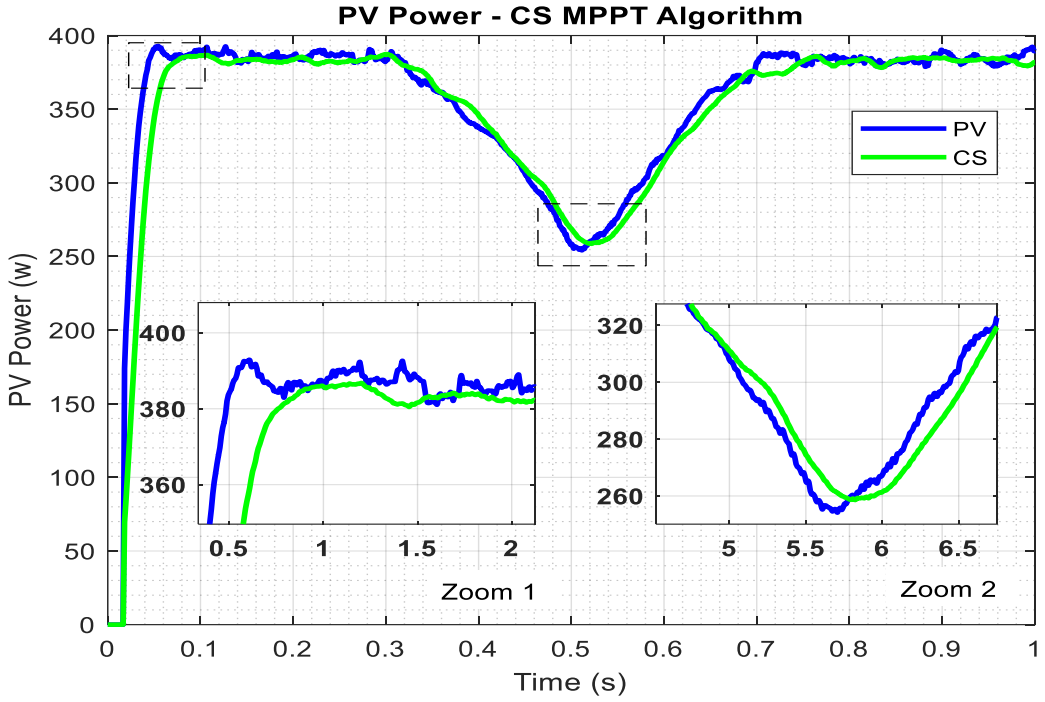


Figure III-24 PV Power CS MPPT

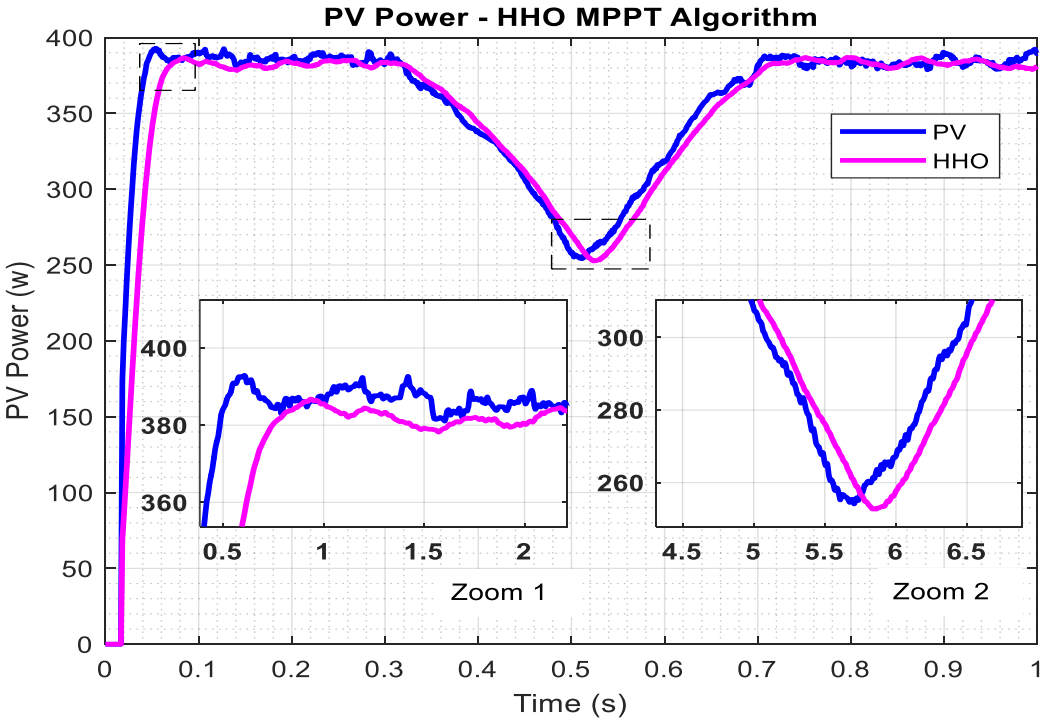


Figure III-25 PV Power HHO MPPT

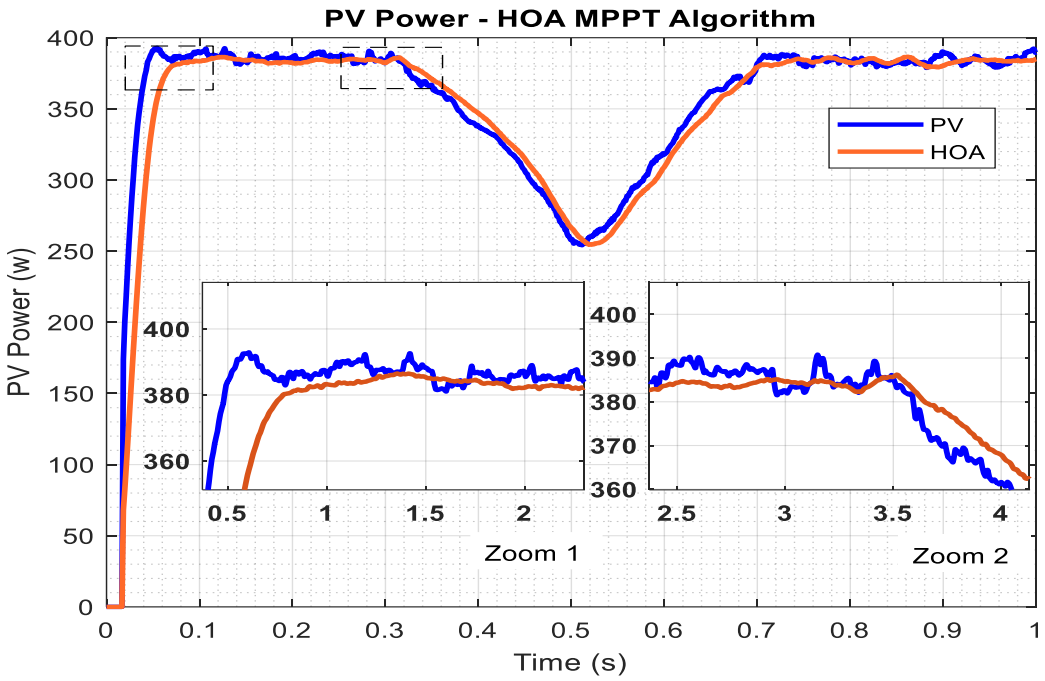


Figure III-26 PV Power HOA MPPT

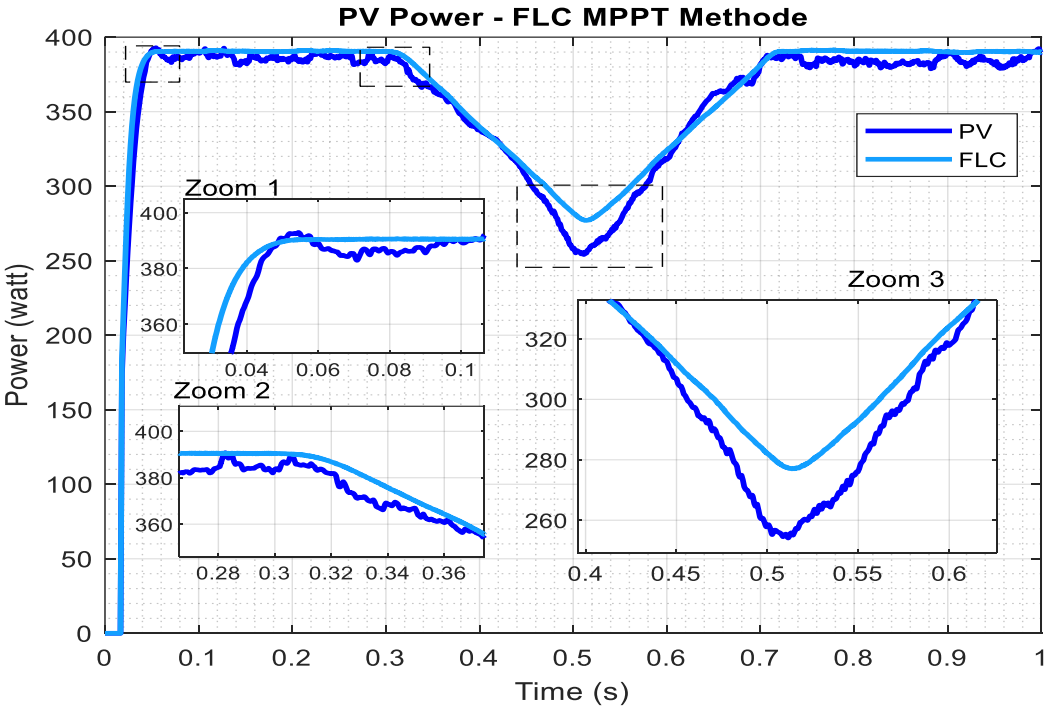


Figure III-27 PV Power - FLC MPPT

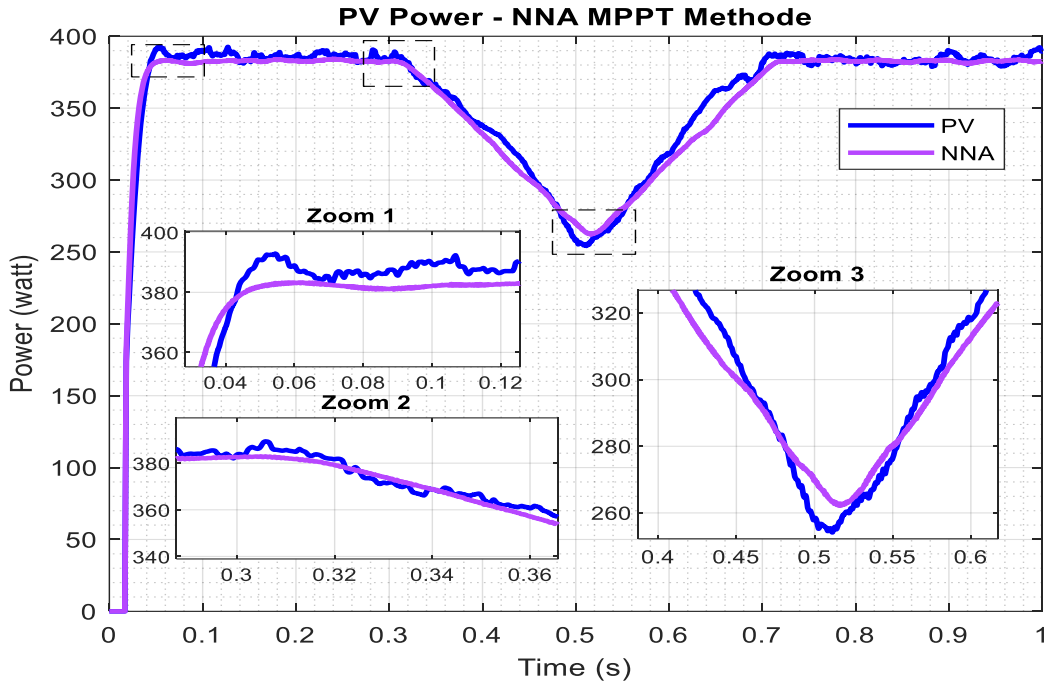


Figure III-28 PV Power - NNA MPPT

The simulations were run under a deliberately time-varying irradiance profile Figure III-19 that switches rapidly between high and low levels (for example a gradual decrease from 1000 to 700 w/m²), which stresses each MPPT strategy's dynamic response and robustness. This test profile ensures that the comparative evaluation reflects both tracking accuracy during steady intervals and the algorithms' transient behavior during fast changes.

Figure III-20 illustrates the photovoltaic (PV) power profile together with the output waveforms of the different MPPT algorithms under standard test conditions. The PV power curve serves as a reference baseline for performance comparison, representing the theoretical maximum power envelope toward which all algorithms aim to converge. Any departure from this envelope observed in subsequent figures reflects transient power losses and tracking inaccuracies, particularly during variations in solar irradiance.

Figure III-21: The PSO-based MPPT demonstrates consistently high tracking accuracy across the simulated windows, with reported efficiencies in Table III-2 ranging from ~99.13% to 99.99% depending on the interval (Table III-2). PSO also shows relatively fast mean

convergence in our tests, reflecting its effective balance of exploration and exploitation for this problem. The small residual oscillations observed after rapid irradiance steps are expected for population-based methods and could be reduced slightly by tuning inertia/acceleration parameters or adding a final local search stage.

Figure III-22: The Grey Wolf Optimizer converges reliably toward near-optimal operating points but settles slightly slower than PSO during fast irradiance drops. This behavior is linked to the encircling/exploitation phase that may limit quick adaptation under sudden changes.

Figure III-23: The ACO approach gives good tracking performance with moderate settling times and efficiencies typically around the high-98% range (Table III-2). ACO's path-reinforcement mechanism helps avoid local peaks, which is advantageous under multi-peak conditions; however, it can produce slightly longer startup oscillations when initial pheromone information is sparse.

Figure III-24: The Cuckoo Search implementation in these simulations shows lower tracking efficiency compared with other metaheuristics, CS's heavy-tailed Lévy moves improve global search but in this configuration appear to cause larger step sizes during transients, producing higher instantaneous tracking losses. For real-time MPPT, reducing the step amplitude or hybridizing CS with a local fine-tuner would likely improve steady-state accuracy.

Figure III-25: HHO achieves moderate performance: while it reaches good power values in some intervals, its efficiency shows larger variation across windows (Table III-2). The dynamic switching between exploration and multiple siege modes explains this variability.

Figure III-26: The Horse Herd Optimization (HOA) results are among the best in terms of consistency and peak efficiency across the simulated windows; Table III-2 reports several intervals with efficiencies above 99% for HOA. HOA's age-grouped behavioral rules appear to provide a good balance between global search and local refinement, producing both fast convergence and small steady-state errors in this setup.

Figure III-27: illustrates the PV output power obtained using the Fuzzy Logic Control (FLC)–based MPPT under rapidly varying irradiance conditions. The FLC algorithm demonstrates excellent dynamic behavior, characterized by very fast convergence to the maximum power point and negligible steady-state oscillations.

Thanks to its rule-based structure and the absence of an explicit mathematical model, the FLC-MPPT adapts efficiently to sudden irradiance variations. The extracted power closely follows the theoretical MPP envelope throughout the simulation intervals, indicating high tracking precision and strong robustness.

As reported in Table III-2, the FLC-MPPT achieves near-unity efficiency across all time windows, confirming its effectiveness under uniform solar irradiance variations. These results highlight the suitability of fuzzy logic controllers for real-time MPPT applications, especially in systems requiring fast response and reduced computational complexity.

Figure III-28: presents the PV power waveform obtained using the Neural Network Algorithm (NNA)–based MPPT. The neural controller exhibits smooth and stable tracking behavior, with rapid adaptation to irradiance changes and minimal transient overshoot.

The learning capability of the neural network enables accurate nonlinear mapping between PV operating conditions and the optimal duty cycle, resulting in high MPP tracking accuracy. Compared to metaheuristic approaches, the NNA-MPPT produces very low oscillations around the MPP, which contributes to improved steady-state performance.

According to Table III-2, the NNA-based MPPT achieves efficiencies exceeding 99% during most operating intervals, confirming its strong potential for intelligent MPPT control in photovoltaic systems. However, its performance remains dependent on the quality of training data and network tuning, which may increase implementation complexity compared to classical techniques.

1) MPP Algorithms comparison

The comparison of simulation results is depicted in Figure III-29, to enable a more thorough evaluation of the performance of the proposed MPPT algorithms. A comprehensive analysis of the algorithm's performance is presented in Table III-2.

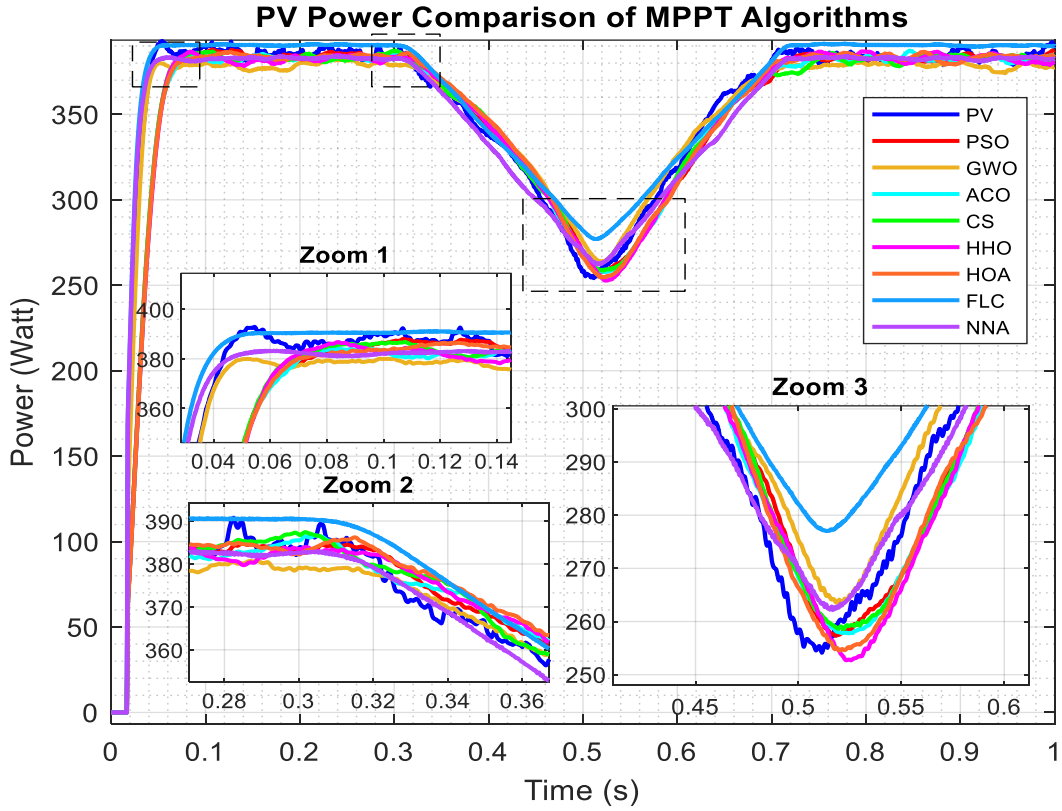


Figure III-29 Comparison of MPPT Algorithms

Figure III-29 together with Table III-2, provides a comprehensive comparison of all MPPT techniques in terms of extracted power (P-MPP), convergence time (Tr), and efficiency under uniform varying irradiance conditions.

Among all tested algorithms, PSO and HOA remain the best-performing metaheuristic methods, offering an effective compromise between tracking accuracy and convergence speed. PSO achieves the highest average efficiency, while HOA shows strong consistency across different operating intervals.

In contrast, intelligent control-based methods (FLC and NNA) outperform most metaheuristic approaches in terms of tracking speed and steady-state accuracy. The FLC-MPPT exhibits the fastest response and near-ideal power extraction, whereas the NNA-MPPT provides highly stable tracking with reduced oscillations, particularly during steady irradiance periods.

Although the efficiencies reported for FLC slightly exceed 100% in some intervals, this behavior can be attributed to numerical resolution, interpolation effects, and reference MPP estimation errors during rapid irradiance transitions, a phenomenon commonly reported in simulation-based MPPT studies. Overall, these results confirm the superiority of intelligent controllers in terms of dynamic performance, while metaheuristic algorithms remain attractive for global optimization and partial shading scenarios.

Table III-2 comprehensive analysis of the algorithm's

	t(s)	0.04-0.06	0.2-0.3	0.52-0.6	0.7-0.75	0.8-0.86	0.9-0,99
	P-PV (watt)	391.08	390,49	254,39	379,07	385,11	389,45
PSO	**P-MPP (w)**	363,5	385,96	255,64	377,87	385.07	388.03
	Tr (s)	0,046	0,25	0,56	0,72	0,81	0.91
	Efficiency (%)	99,13%	99,89%	99,88%	99,74%	99,99%	99,69%
GWO	**P-MPP (w)**	377.09	379.77	261,3	375,21	379,34	374,67
	Tr (s)	0.041	0,29	0,58	0,74	0,85	0,96
	Efficiency (%)	98,86%	98,69%	98,21%	97,49%	98,23%	97,69%
ACO	**P-MPP (w)**	362.11	381.56	257.63	376.82	382	385,52
	Tr (s)	0.042	0,24	0,57	0,73	0,82	0,93
	Efficiency (%)	97,63%	98,11%	98,02%	98,48%	98,59%	98,13%
CS	**P-MPP (w)**	355,89	380,63	259,09	374,91	372,47	379,01
	Tr (s)	0,049	0,30	0,60	0,75	0,86	0,99
	Efficiency (%)	96,73%	96,73%	96,73%	96,73%	96,73%	96,73%
HHO	**P-MPP (w)**	349,58	383,56	358,34	376,97	380,26	381,56
	Tr (s)	0,046	0,29	0,58	0,74	0,85	0,96
	Efficiency (%)	96,54 %	98,21 %	97,50 %	97,57 %	97,91 %	97,59 %
HOA	**P-MPP (w)**	358,89	384,09	255,59	378,69	379,98	383.29
	Tr (s)	0,042	0,25	0,56	0,73	0,82	0,92
	Efficiency (%)	97,01%	98,99%	99,29%	99,78%	99,03%	98,79%

FLC	**P-MPP (w)**	390.7	390.61	277.17	384.12	390.43	390.13
	Tr (s)	0.04	0.021	0.054	0.72	0.81	0.91
	Efficiency (%)	99.94 %	100 %	101 %	100 %	100 %	100 %
NNA	**P-MPP (w)**	382.54	382.91	263.7	378.55	383.85	383.92
	Tr (s)	0.04	0.02	0.051	0.711	0.802	0.915
	Efficiency (%)	98.12 %	97.31%	98.91 %	99.92 %	99.29 %	99.13 %

At t = 0.3 s to t = 0.5 s, significant power variations occur as the irradiance gradually decreases from 1000 to 700 W/m², followed by an increase from t = 0.5 s to t = 0.8 s. During this highly dynamic interval, the PSO-based MPPT achieves the highest efficiency among the metaheuristic algorithms (99.69%), followed by HOA (98.79%), ACO (98.13%), GWO (97.68%), HHO (97.59%), and CS (96.73%), respectively. Moreover, the PSO-MPPT tracker reaches the maximum power point in the shortest convergence time compared with the other population-based optimization techniques.

With the inclusion of intelligent control–based MPPT strategies, namely Fuzzy Logic Control (FLC) and Neural Network Algorithm (NNA), further improvements in dynamic response and steady-state accuracy are observed. The FLC-MPPT exhibits very fast convergence and power extraction that closely matches the theoretical MPP throughout the irradiance transitions, while the NNA-MPPT provides smooth and stable tracking, particularly during steady operating intervals, with reduced oscillations around the MPP.

Overall, the results indicate that, under both increasing and decreasing irradiance conditions, PSO remains the most effective metaheuristic technique, offering an excellent compromise between convergence speed and tracking accuracy. However, FLC and NNA demonstrate superior transient performance and steady-state behavior, highlighting the advantages of intelligent controllers for real-time MPPT applications. Meanwhile, the HOA algorithm maintains robust and consistent performance, achieving an average efficiency of 98.95%, despite slightly slower convergence.

III.6.1.2 Non-Uniform Irradiance Condition

The MPP tracking under non-uniform irradiance conditions, specifically partial shading, is known to be a challenging task due to the presence of multiple peaks in the I-V/P-

V characteristic curves. The number of peaks depends on the number of shaded modules in the PV array. To comprehensively evaluate the global peak tracking capabilities of the proposed MPPT algorithm, four different shading patterns were applied to the four PV arrays connected in series. The irradiance arrangements of these shading patterns are 1000, 800, 600, 300 w/m² respectively, While their corresponding characteristic curve are displayed in Figure III-30, The simulation results of actual power accumulated by the PV system under PSC are shown in Figures III.31, III.32, III.33, III.34, III.35, III.36, III.37 and III.38, respectively. These results were obtained using the PSO, GWO, AOC, CS, HOA, HHO and AI algorithms FLC, NNA.

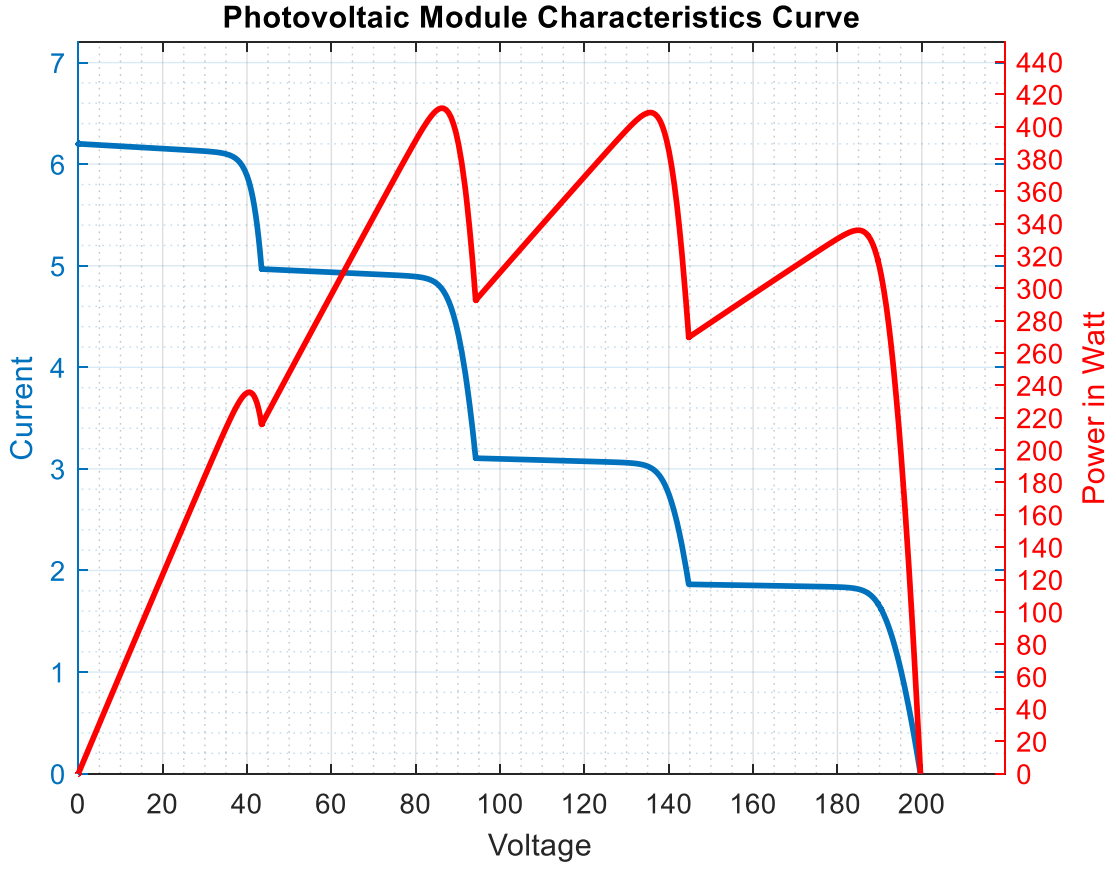


Figure III-30 PV Characteristic Curves of the Studied PSC Case

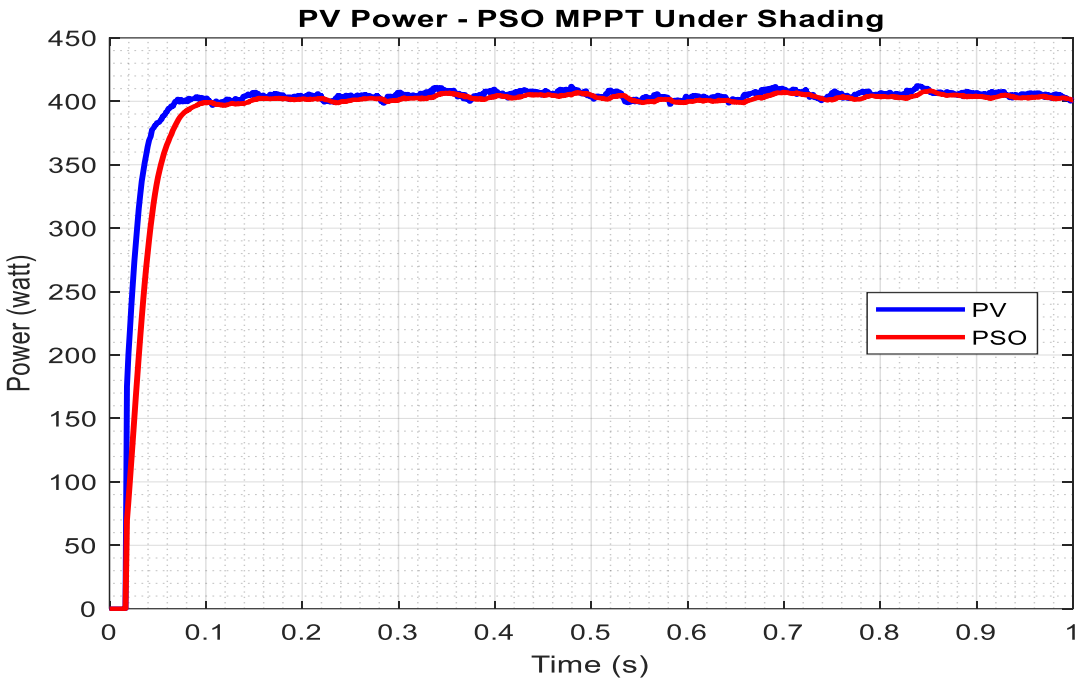


Figure III-31 PV Power-PSO MPPT under PSC

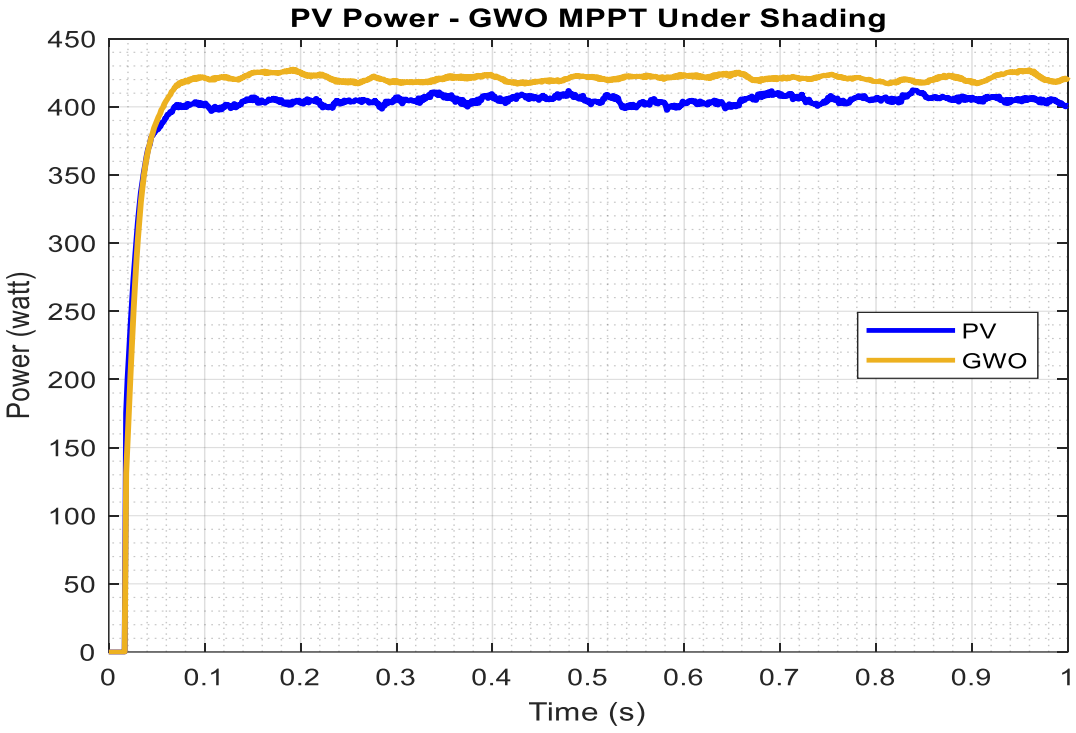


Figure III-32 PV Power-GWO MPPT under PSC

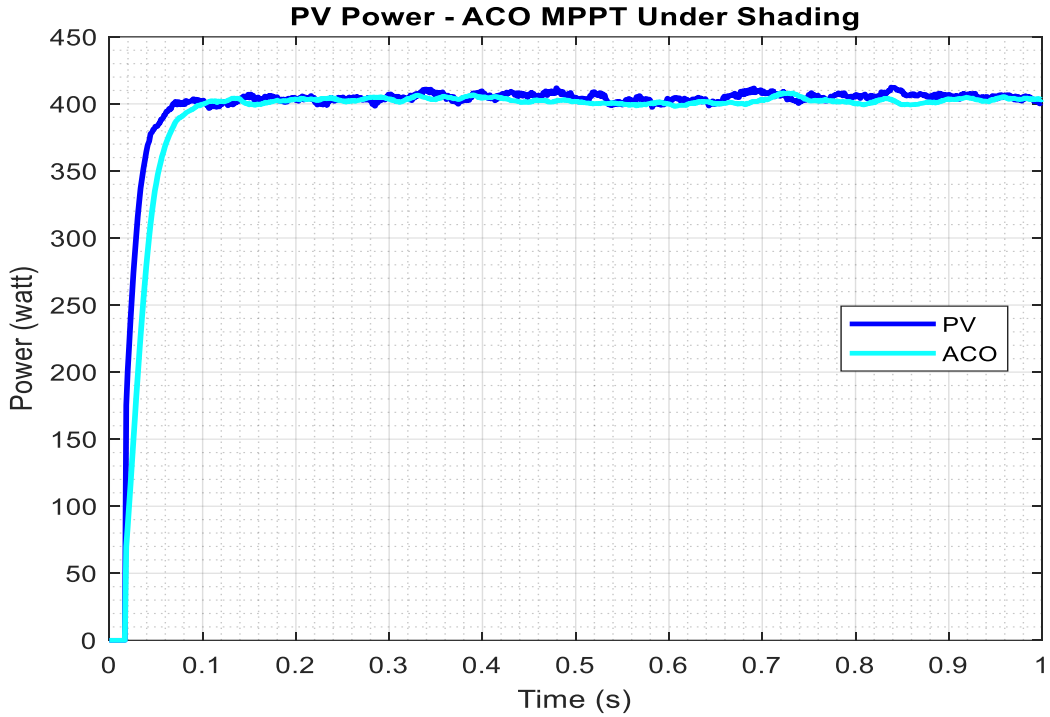


Figure III-33 PV Power-ACO MPPT under PSC

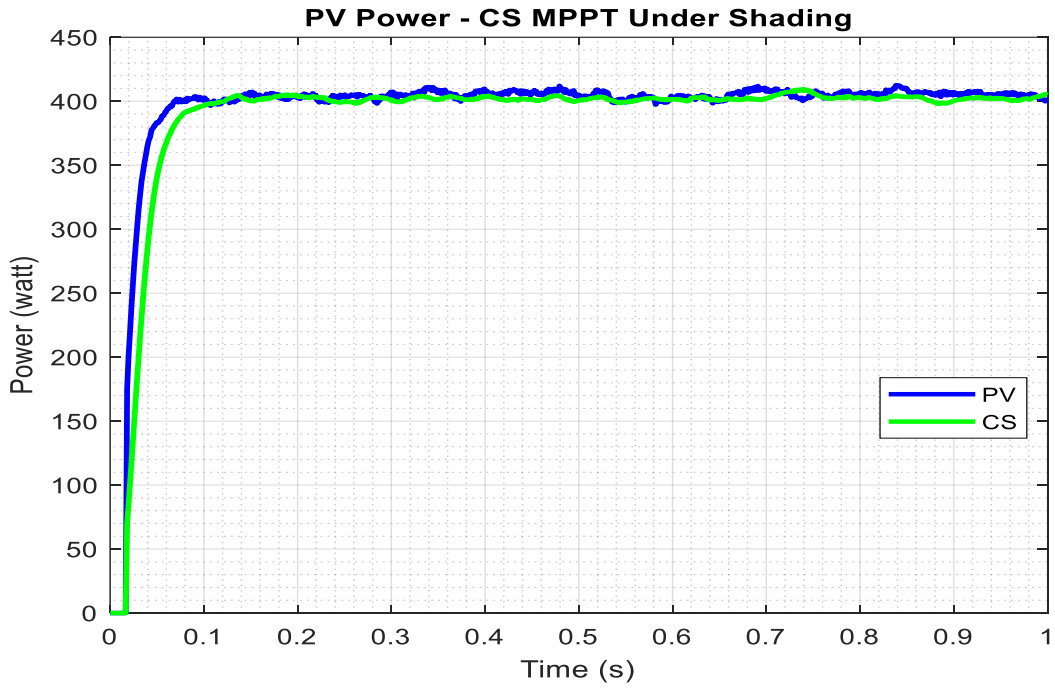


Figure III-34 PV Power-CS MPPT under PSC

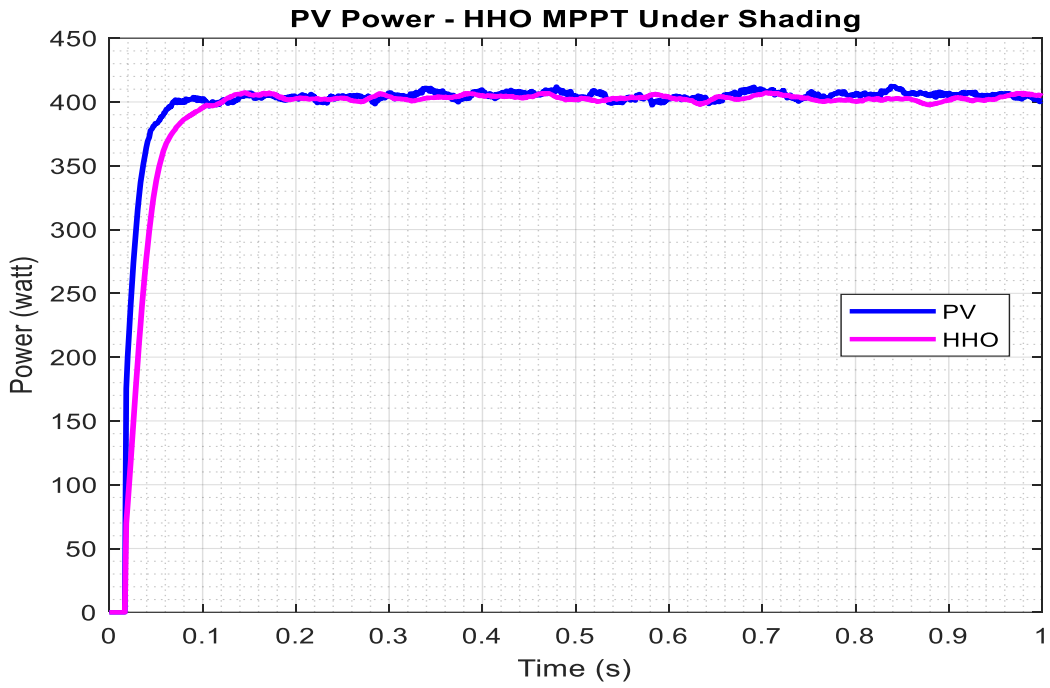


Figure III-35 PV Power-HHO MPPT under PSC

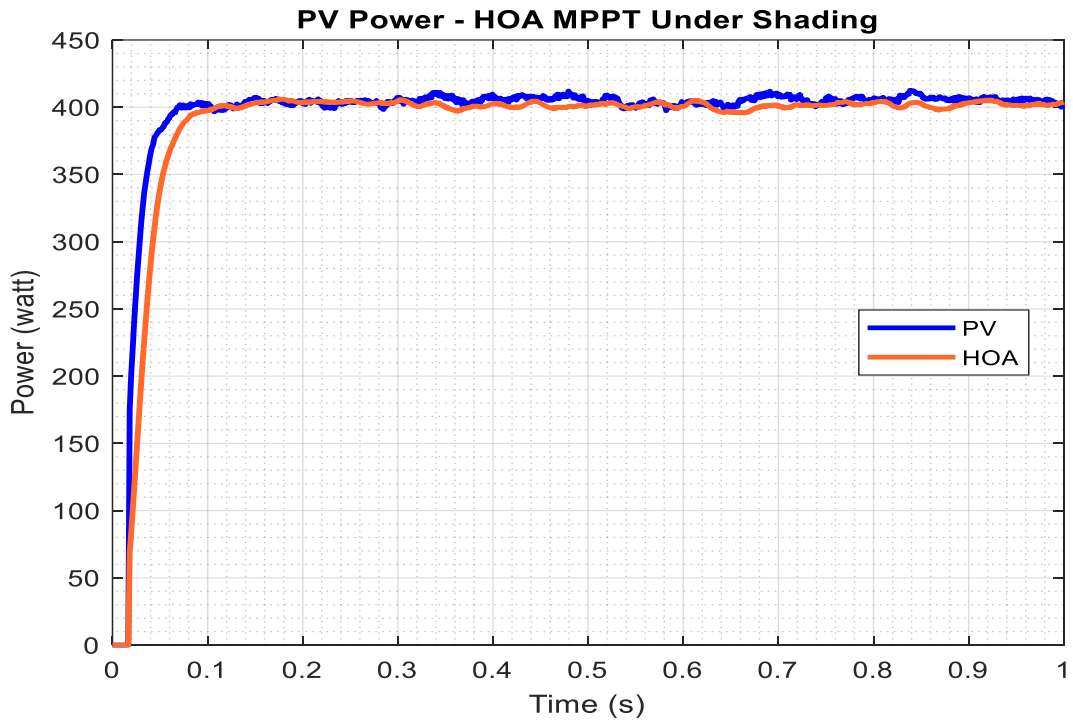


Figure III-36 PV Power-HOA MPPT under PSC

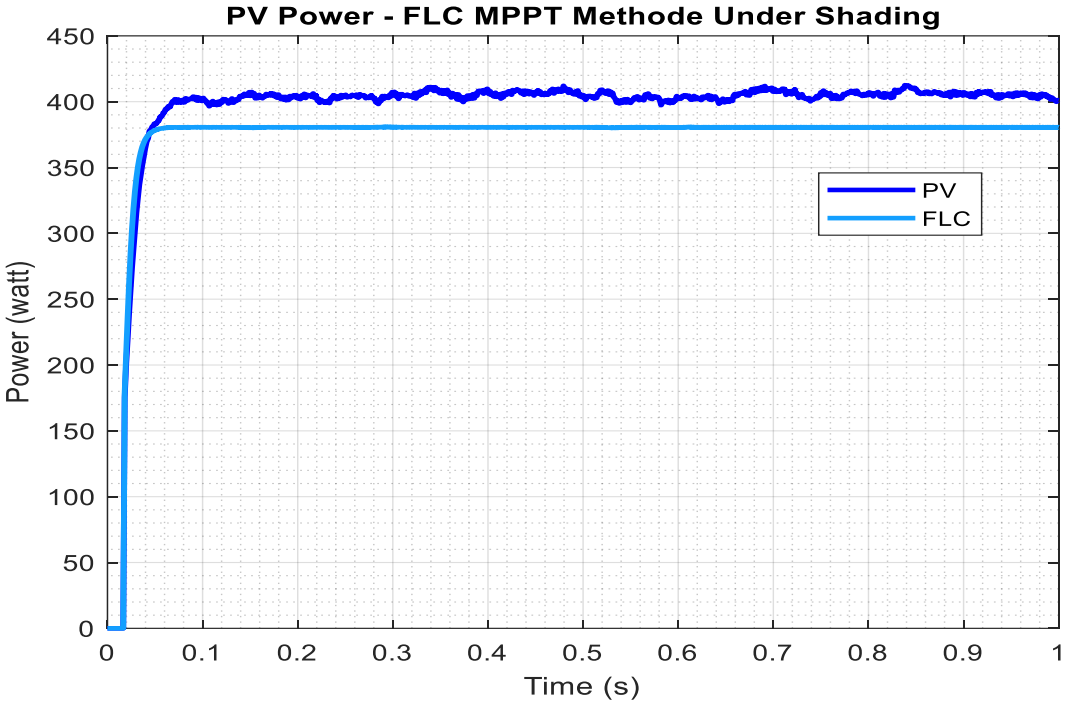


Figure III-37 PV Power-FLC MPPT under PSC

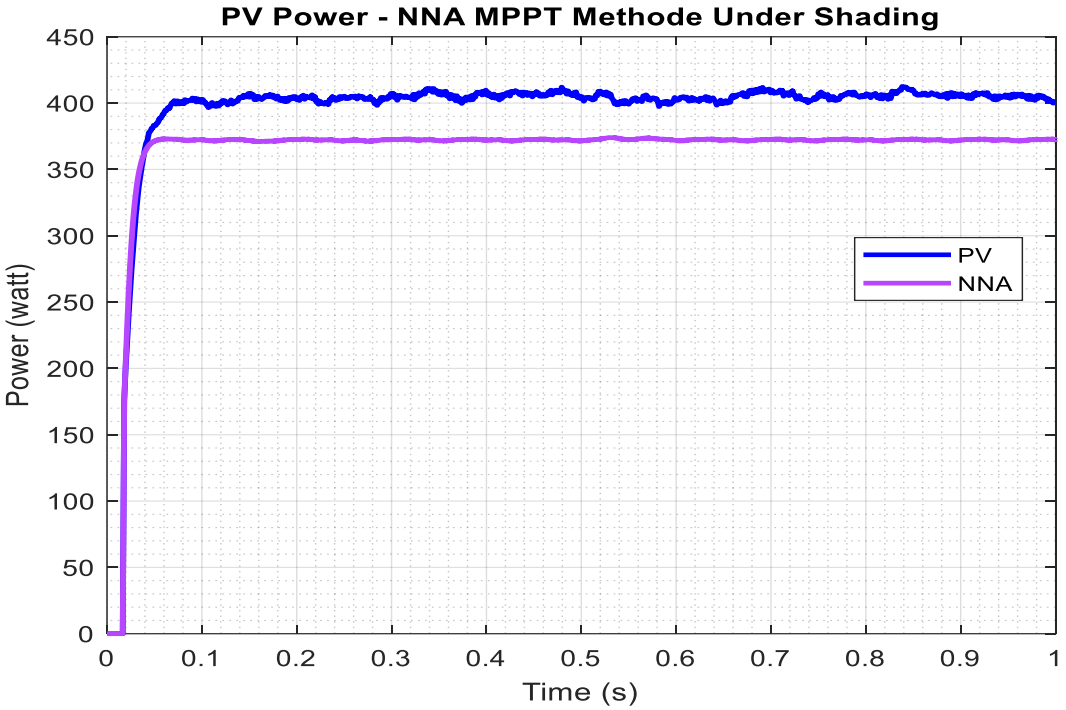


Figure III-38 PV Power-NNA MPPT under PSC

Figure III-30 illustrates the I–V and P–V characteristics of the PV array under partial shading conditions, where different irradiance levels are applied to the series-connected modules. As expected, the P–V curve exhibits multiple local maximum power points (LMPPs) in addition to a single global maximum power point (GMPP). This multi-peak behavior significantly increases the complexity of MPPT operation and highlights the necessity of global search–based MPPT strategies for accurate GMPP tracking.

Figure III-31 shows the PV output power obtained using the PSO based MPPT under partial shading conditions. The algorithm successfully avoids convergence to local maxima and rapidly tracks the global maximum power point. Owing to its strong exploration capability and cooperative particle behavior, PSO demonstrates fast convergence, limited oscillations, and high tracking accuracy, making it one of the most effective MPPT techniques under PSC.

Figure III-32 presents the PV power response of the Grey Wolf Optimization (GWO) based MPPT. The GWO algorithm is able to locate the GMPP despite the presence of multiple local peaks. However, compared to PSO, it exhibits slightly slower convergence and larger transient oscillations, which can be attributed to its encircling and exploitation strategy. Nevertheless, GWO demonstrates reliable global tracking capability under PSC.

Figure III-33 depicts the PV power obtained using the Ant Colony Optimization (ACO) based MPPT. The algorithm successfully converges to the GMPP by exploiting its probabilistic path-search mechanism. While ACO effectively avoids local maxima, its convergence speed is moderate, and small oscillations are observed during the transient phase, particularly under abrupt irradiance changes.

Figure III-34 illustrates the performance of the Cuckoo Search (CS) based MPPT under partial shading. Although CS is capable of escaping local maxima due to its Lévy flight mechanism, it exhibits longer settling times and larger power fluctuations during convergence. This behavior results in increased transient losses, indicating that CS requires further parameter tuning or hybridization to improve its real-time MPPT performance under PSC.

Figure III-35 shows the PV power response obtained using the Harris Hawks Optimization (HHO) algorithm. The HHO based MPPT is able to reach the GMPP; however, its performance is characterized by noticeable power oscillations and variable convergence behavior, depending on the active exploration and exploitation modes. These characteristics lead to moderate tracking accuracy compared to PSO and HOA.

Figure III-36 presents the PV output power using the Horse Herd Optimization Algorithm (HOA) based MPPT. HOA demonstrates robust GMPP tracking, combining good convergence speed with improved stability. Compared to CS and HHO, HOA exhibits reduced oscillations and more consistent tracking performance, making it a strong alternative to PSO under partial shading conditions.

Figure III-37 illustrates the PV power obtained using the Fuzzy Logic Control (FLC) based MPPT. Although FLC shows a fast response, it converges to a local maximum power point rather than the GMPP. This limitation arises from the rule-based nature of the controller, which lacks global search capability, rendering FLC unsuitable for standalone operation under partial shading conditions.

Figure III-38 shows the PV power response of the Neural Network Algorithm (NNA) based MPPT under PSC. The NNA demonstrates smooth and stable tracking behavior but converges to a local optimum, failing to identify the GMPP. This limitation is primarily due to the neural network being trained under uniform irradiance conditions, which restricts its generalization ability in multi-peak operating scenarios.

2) MPP Algorithms comparison under PSC

The comparison of simulation results is depicted in Figure III-39, to enable a more thorough evaluation of the performance of the proposed MPPT algorithms. A comprehensive analysis of the algorithm's performance in both uniform and under PSC is presented in Table III-3.

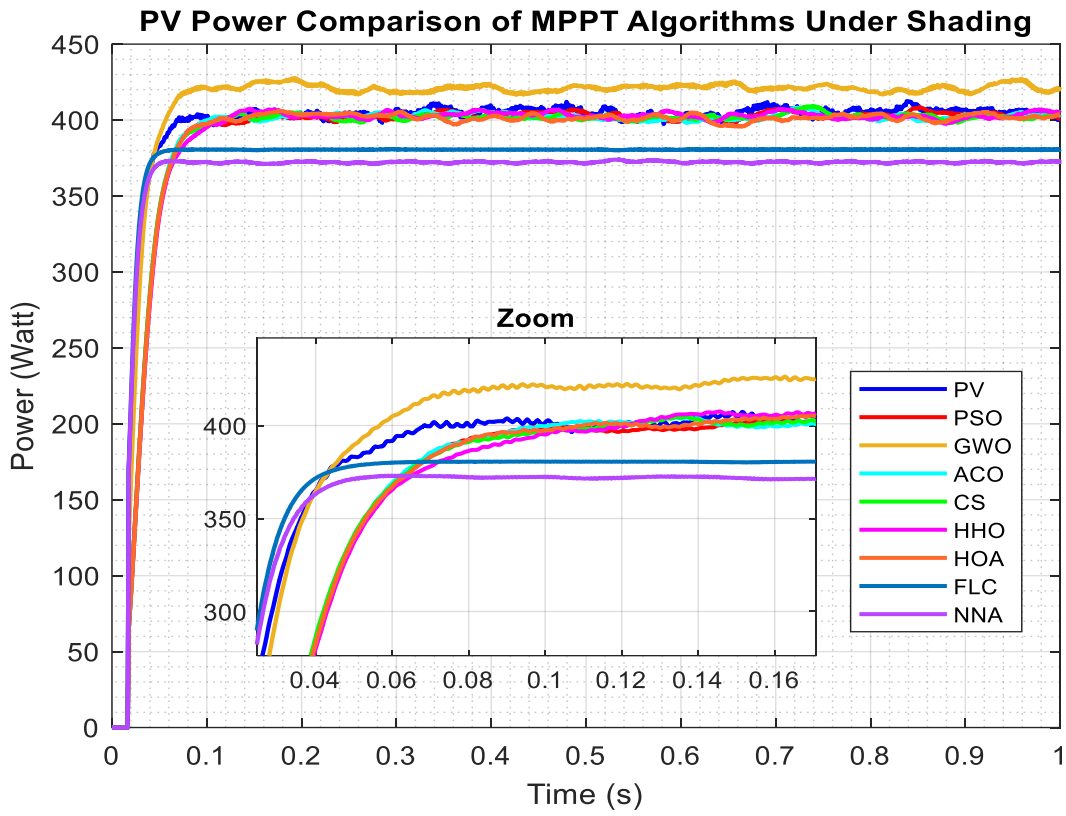


Figure III-39 Comparison of MPPT Algorithms under PSC

Figure III-39 provides a comparative evaluation of all MPPT algorithms under partial shading conditions. The results clearly indicate that metaheuristic-based MPPT techniques outperform intelligent control–based methods in terms of global maximum power point tracking.

Among the tested algorithms, PSO exhibits the best overall performance, achieving the fastest convergence and highest tracking accuracy. HOA follows closely, offering a good balance between convergence speed and stability. GWO and ACO demonstrate reliable GMPP tracking with moderate convergence rates, while CS and HHO show increased oscillations and longer settling times.

In contrast, FLC and NNA fail to guarantee GMPP tracking, as they converge to local maxima despite their fast dynamic response. These results confirm that global optimization

capability is essential for MPPT operation under partial shading conditions, and position PSO and HOA as the most suitable techniques for practical PSC applications.

Table III-3 Comparative Performance of MPPT Techniques under Uniform and Partial Shading Conditions

MPPT Technique	Performance under Uniform Irradiance (USI)	Performance under Partial Shading Conditions (PSC)	Main Observation
PSO	Excellent tracking accuracy, fast convergence, high efficiency	Excellent GMPP tracking, fast convergence, robust behavior	Best overall performance in both cases
HOA	Very good accuracy, low oscillations, stable response	Very good GMPP tracking, slightly slower than PSO	Strong and consistent in USI and PSC
GWO	Good tracking accuracy, moderate convergence speed	Good GMPP tracking, slower transient response	Reliable but slower under PSC
ACO	Good steady-state performance, moderate oscillations	Good GMPP tracking, moderate convergence	Acceptable compromise solution
HHO	Moderate performance, variable convergence	Moderate GMPP tracking, noticeable oscillations	Sensitive to dynamic conditions
CS	Lower tracking accuracy, higher oscillations	Moderate GMPP tracking, long settling time	Needs tuning or hybridization
FLC	Excellent tracking, very fast response, near-unity efficiency	Tracks local MPP only, fails to reach GMPP	Suitable only for uniform irradiance
NNA	Very good tracking, smooth response	Tracks local MPP only, limited generalization	Requires retraining for PSC

From the comparison presented in Table III-3, it can be concluded that the performance of MPPT techniques strongly depends on the operating irradiance conditions. Intelligent control–based methods such as FLC and NNA provide excellent tracking accuracy and fast response under uniform irradiance; however, their effectiveness degrades under partial shading

due to their local optimization nature. In contrast, metaheuristic-based MPPT algorithms, particularly PSO and HOA, demonstrate robust global maximum power point tracking under both uniform and partial shading conditions, making them more suitable for practical photovoltaic systems exposed to non-uniform environmental conditions.

III.7 Conclusion

This chapter established the fundamental principles essential for maximizing photovoltaic (PV) system efficiency, emphasizing the critical role of Maximum Power Point Tracking (MPPT) and the enabling function of DC–DC converter topologies. It was highlighted that MPPT algorithms serve as a vital interface, ensuring continuous extraction of maximum available power under dynamically varying solar irradiance and temperature conditions.

The core contribution of this chapter lies in the comparative performance analysis of multiple MPPT techniques, including six advanced metaheuristic optimization algorithms PSO, GWO, ACO, CS, HHO, and HOA as well as intelligent control–based approaches, namely Fuzzy Logic Control (FLC) and Artificial Neural Network (ANN). Following a detailed presentation of the theoretical foundations and PV system modeling, all algorithms were subjected to rigorous simulation-based evaluation under both uniform irradiance conditions and partial shading conditions (PSC). Key performance metrics such as response time, tracking accuracy, convergence behavior, and efficiency were analyzed to provide meaningful practical insights.

Under uniform irradiance conditions, all investigated MPPT techniques demonstrated effective tracking of the maximum power point. In particular, the FLC and ANN-based MPPT methods exhibited very fast dynamic response and minimal steady-state oscillations, resulting in high tracking accuracy and efficiency. Among the metaheuristic algorithms, PSO and HOA consistently achieved superior performance, combining rapid convergence with high steady-state efficiency.

However, under partial shading conditions, where the PV characteristics exhibit multiple local maxima, the performance of MPPT techniques was found to depend strongly on

their global search capability. The simulation results revealed that metaheuristic-based MPPT algorithms successfully tracked the global maximum power point (GMPP), with PSO emerging as the most robust and reliable method, followed closely by HOA, which demonstrated stable tracking with reduced oscillations. In contrast, despite their excellent performance under uniform irradiance, the FLC and ANN-based methods converged to local maxima under PSC, highlighting their limitations in multi-peak operating scenarios.

Overall, the comparative analysis confirms that no single MPPT technique is universally optimal for all operating conditions. Intelligent control–based MPPTs are highly effective under uniform irradiance, while metaheuristic optimization techniques particularly PSO and HOA offer superior robustness under partial shading conditions. These findings provide valuable guidelines for selecting appropriate MPPT strategies based on environmental conditions and system requirements, and they motivate future developments toward hybrid or adaptive MPPT solutions.

While these advancements significantly enhance energy harvesting during sunlight hours, the intermittent nature of solar power necessitates complementary solutions to ensure continuous and reliable operation. Therefore, the focus of this thesis now transitions from individual PV optimization to system-level integration. The next chapter will address Hybrid Energy Systems (HES) by integrating the optimized PV system with wind energy and energy storage technologies, alongside the development of comprehensive Energy Management Strategies (EMSs) to guarantee a stable, reliable, and continuous energy supply.

Chapter IV: Modeling, Control, and Integration of a PV/Wind/HESS Microgrid with Energy Management Strategy

IV.1 Introduction

This chapter focuses on the modeling and energy management strategy (EMS) of a newly developed standalone hybrid renewable energy system (HRES), proposed to address the inherent intermittency of renewable energy sources. Precise modeling of each system component is a critical prerequisite for accurate performance assessment and the implementation of reliable energy management schemes.

The proposed hybrid microgrid adopts an innovative architecture that combines photovoltaic (PV) generation, a wind energy conversion system based on a Permanent Magnet Synchronous Generator (PMSG), and a hybrid energy storage system (HESS) consisting of a battery and a supercapacitor. This coordinated integration is designed to ensure continuous and stable power supply under fluctuating environmental conditions. In this configuration, the PV array serves as the main energy source, while the wind turbine operates as a supplementary generator, enhancing supply reliability during periods of reduced solar availability. The HESS plays a key role in power conditioning, with the battery responsible for long-term energy storage and the supercapacitor providing rapid power support for transient load variations and DC-bus voltage stabilization.

A central contribution of this chapter is the design and assessment of an EMS aimed at efficient power flow regulation and DC-bus stability maintenance. The proposed strategy is based on Fuzzy Logic Control (FLC), chosen for its robustness, adaptability, and effectiveness in handling system nonlinearities and uncertainties. A comprehensive comparative study is carried out to evaluate the performance of the FLC-based EMS in optimizing power allocation between the HESS components and the load, thereby ensuring reliable operation across a wide range of operating conditions.

The remainder of the chapter is organized as follows: first, the overall HRES architecture and detailed component models are presented. Next, the EMS framework and the proposed FLC-based control strategy are described. Finally, simulation results are discussed to validate the effectiveness of the EMS in maintaining energy balance, stabilizing battery operation, and improving overall system efficiency under varying photovoltaic irradiance levels, wind speeds, and load demands.

IV.2 Proposed System Description

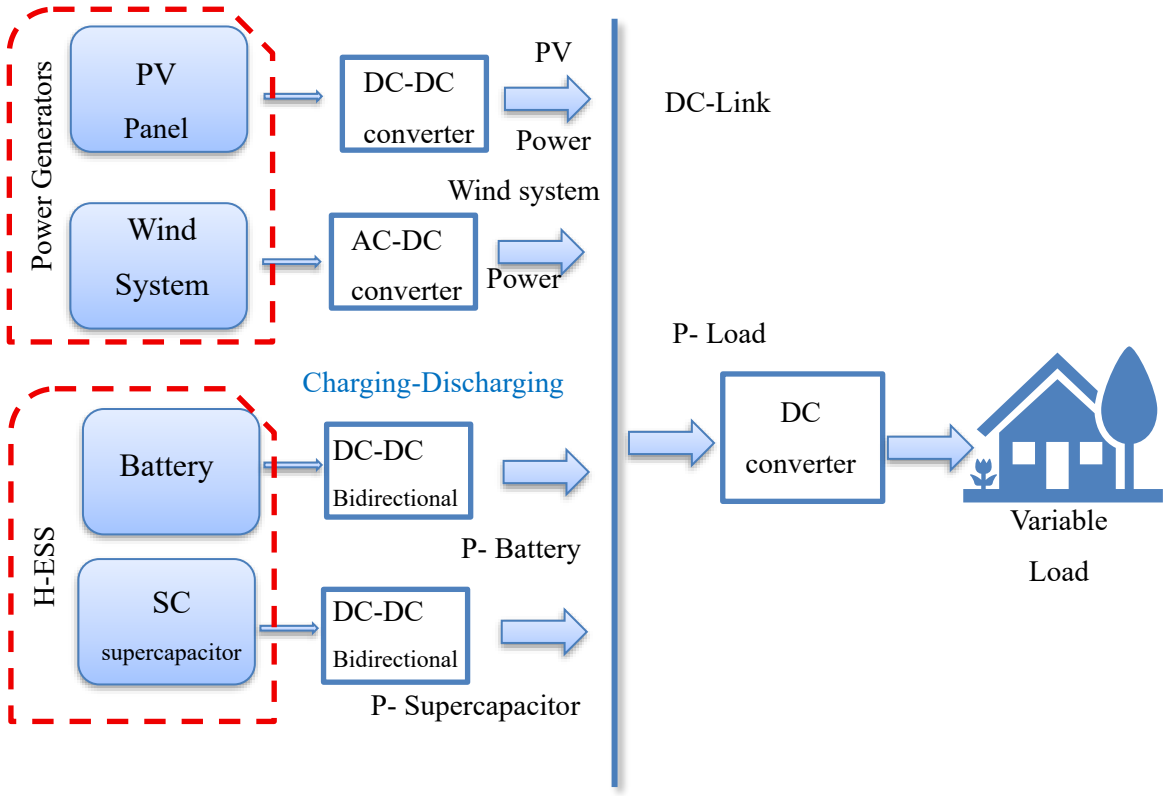
The studied system is a standalone hybrid renewable energy system (HRES) that combines photovoltaic (PV) generation with a wind energy conversion system (WECS) based on a permanent magnet synchronous generator (PMSG). To guarantee a reliable and continuous power supply, the system incorporates a hybrid energy storage system (HESS) composed of a battery and supercapacitors (SCs). The integration of supercapacitors is particularly effective in compensating for short-term power fluctuations caused by abrupt changes in wind conditions or load demand. By absorbing high-frequency power variations, the SCs alleviate operational stress on the battery, thereby extending its lifespan and reducing maintenance requirements.

An advanced energy management strategy (EMS) is implemented to maintain balance between power generation and consumption. This strategy coordinates the operation of the renewable sources and the storage elements, allowing the system to adapt efficiently to dynamic load conditions. As illustrated in Figure IV-1, both the PV array and the wind generation unit are connected to a common 350 V DC bus through dedicated DC/DC converters. This shared DC-bus architecture ensures regulated voltage levels and stable power delivery to the variable load.

The wind energy subsystem utilizes a PMSG, chosen for its high efficiency, compact structure, and suitability for advanced control schemes, including maximum power point tracking (MPPT). MPPT techniques are applied to both the PV and wind subsystems to maximize energy harvesting under fluctuating environmental conditions. The HESS operates under a coordinated control framework that dynamically allocates power between the battery and the supercapacitor according to system demands. During transient operating conditions,

the supercapacitor provides rapid power support to absorb or supply short-term energy imbalances, thereby reducing battery cycling stress and depth of discharge. Meanwhile, the DC/DC converters interfacing the PV and wind systems are regulated by the EMS to maintain DC-bus voltage stability and ensure overall system robustness.

Figure IV-1 System Proposed



Simulation results demonstrate that the proposed configuration effectively balances energy supply and demand, enhances overall system efficiency, and improves the durability and operational performance of the energy storage components.

IV.3 Modelling of System Components

IV.3.1 Wind Energy Model

The mechanical power output of the wind turbine is expressed as [128]:

$$P_w = \frac{1}{2}\rho\pi R^2 V_w^3 C_p(\lambda,\beta) \quad \text{(IV.1)}$$

Where:

- ρ: Air density (kg/m³),
- R: Radius of the turbine blades (m),
- V_W : Wind speed (m/s),
- C_p: Power coefficient, dependent on the pitch angle (β) and the tip-speed ratio (λ).

The tip-speed ratio (λ) is defined as:

$$\lambda = \frac{W_r.R}{V_w} \quad \text{(IV.2)}$$

Where:

- W_r: Turbine angular speed (rad/s).

The power coefficient $C_p(\lambda,\beta)$is typically determined using experimental data and is expressed as:

$$C_p(\lambda,\beta) = C_1\left(\frac{C_2}{\lambda_i} - C_3\beta - C_4\right)e^{-\left(\frac{C_5}{\lambda_i}\right)} + C_6\lambda \quad \text{(IV.3)}$$

With:

$$\frac{1}{\lambda_i} = \frac{1}{\lambda+0.08\beta} - \frac{0.035}{1+\beta^3} \quad \text{(IV.4)}$$

Constants C_1 to C_6 are obtained through experimental testing and depend on the specific turbine design [128].

IV.3.1.1 PMSG Modelling

The PMSG converts mechanical energy from the turbine into electrical energy. Its operation is modelled using the Park transformation in the d-q reference frame [128]:

$$V_{sd} = R_s i_d + \frac{d\lambda_d}{dt} - w_e \lambda_q \quad \text{(IV.5)}$$

$$V_{sd} = R_s i_q + \frac{d\lambda_q}{dt} - w_e \lambda_d \quad \text{(IV.6)}$$

Where:

- R_s: Stator winding resistance (Ω),
- V_{sd}, V_{sq}: Stator voltages (d-q frame) (V),
- i_d, i_q: Stator currents (d-q frame) (A),
- w_e: Electrical angular speed (rad/s).

The stator flux components are:

$$\lambda_d = L_{sd} i_d + \lambda_m, \ \lambda_q = L_{sq} i_q \quad \text{(IV.7)}$$

Where:

- L_{sd}, L_{sq}: Stator inductances (d-q frame) (H),
- λ_m: Permanent magnet flux linkage (Wb)

IV.3.1.2 Torque Calculation

The electromagnetic torque generated by the PMSG is derived as:

$$T_e = \frac{3}{2} p \left[\lambda_m i_q - \left(L_{sq} - L_{sd} \right) i_q i_d \right] \quad \text{(IV.8)}$$

For surface-mounted permanent magnet machines (L_{sq}=L_{sd}), the equation simplifies to:

$$T_e = \frac{3}{2} p(\lambda_m i_q) \quad \text{(IV.9)}$$

Where p is the number of pole pairs in the PMSG [128].

This combination of wind turbine and PMSG equations provides an accurate representation of the wind generation subsystem's dynamics and facilitates effective simulation under varying wind and load conditions, Figure IV-2 depicts the proposed wind power system's schematic.

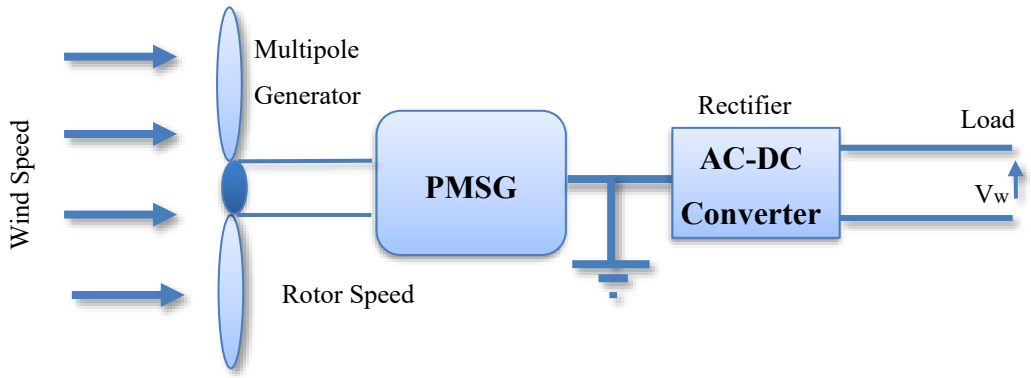


Figure IV-2 Wind Turbine model and PMSG scheme.

Wind electrical system used in the designed system are summarized in Table VI.1.

Table IV-1 Wind electrical system parameters

	Parameters	**Value**
Wind Electrical System	P max	6 kW
	Diameter	2.8 m
	Working wind speed	(3 ~ 25) m/s
	Rated Rotate Speed	180 rpm
	Open-circuit voltage (Voc)	64.2 V

IV.3.2 Photovoltaic (PV) Model

The output power of a PV array depends on several factors, including solar irradiance (G) and cell temperature (Tc). The electrical behavior of a single PV module is represented by the following equation:

$$I = I_{ph} - I_0(e^{\frac{q(V+IR_S)}{nkT}} - 1) + \frac{V+IR_S}{R_p} \quad \text{(IV.10)}$$

Where:

- I : Output current of the module (A),
- I_{ph}: Photogenerated current proportional to irradiance (A),
- I_0: Saturation current of the diode (A),
- q : Electron charge (1.6×10^{-19}C),
- V: Output voltage of the module (V),
- R_s: Series resistance (Ω),
- R_p: Parallel resistance (Ω),
- n: Ideality factor of the diode,
- k: Boltzmann constant (1.38×10^{-23}J/K),T: Absolute temperature (K).

The PVarray used in the designed system are summarized in Table VI.2.

Table IV-2 PV electrical system Parameters

	Parameters	Value
PV module	Maxpower (Watt)	305.226 W
	Max voltage (Vmp)	64.2 V
	Max current (Imp)	5.58A
	Short-circuit current (Isc)	5.96 A
	Open-circuit voltage (Voc)	64.2 V

IV.3.3 Maximum Power Point Tracking (MPPT)

Maximum Power Point Tracking (MPPT) techniques are fundamental for maximizing the energy harvested from renewable energy sources (RES), particularly photovoltaic (PV) arrays and wind energy conversion systems. These algorithms continuously adjust the operating point of each generator to ensure operation at or near its maximum power condition despite variations in environmental parameters. In hybrid renewable energy systems, MPPT also contributes to coordinated power regulation by accounting for the state of charge (SOC) of the hybrid energy storage system (HESS) and the mismatch between generated power and load demand.

A conventional MPPT implementation based on Proportional–Integral (PI) control is depicted in Figure IV-3. In this scheme, an outer control loop generates a reference voltage derived from a voltage-based MPPT technique. Real-time measurements of the generator output voltage and current are used by the MPPT algorithm to identify the optimal operating point under changing conditions.

The PI controller processes the error between the measured voltage and the reference voltage to regulate the input capacitor voltage of the DC–DC boost converter, which corresponds to the generator terminal voltage. By adjusting the pulse-width modulation (PWM) signal, the controller modifies the converter duty cycle, thereby maintaining operation near the maximum power point. Although the converter does not directly control the capacitor current, a feedforward approach can be employed to estimate the appropriate current reference, typically associated with the inductor current of the boost converter.

To further enhance dynamic performance and reduce steady-state voltage and current deviations, a compensation stage is incorporated within the control structure. This stage improves system stability and ensures efficient power transfer. Figure IV-3 illustrates the overall architecture of the PI-based MPPT control scheme.

Additionally, a Limiting Power Tracking (LPT) function is activated when the energy storage system reaches full charge and the available renewable power exceeds the load demand.

Under such conditions, the LPT mechanism regulates the DC-bus voltage by comparing the measured value with a predefined reference. This function constrains the power output of both the PV system and the PMSG-based wind generator, ensuring that the generated power matches the load requirements and thereby enhancing overall system stability and reliability.

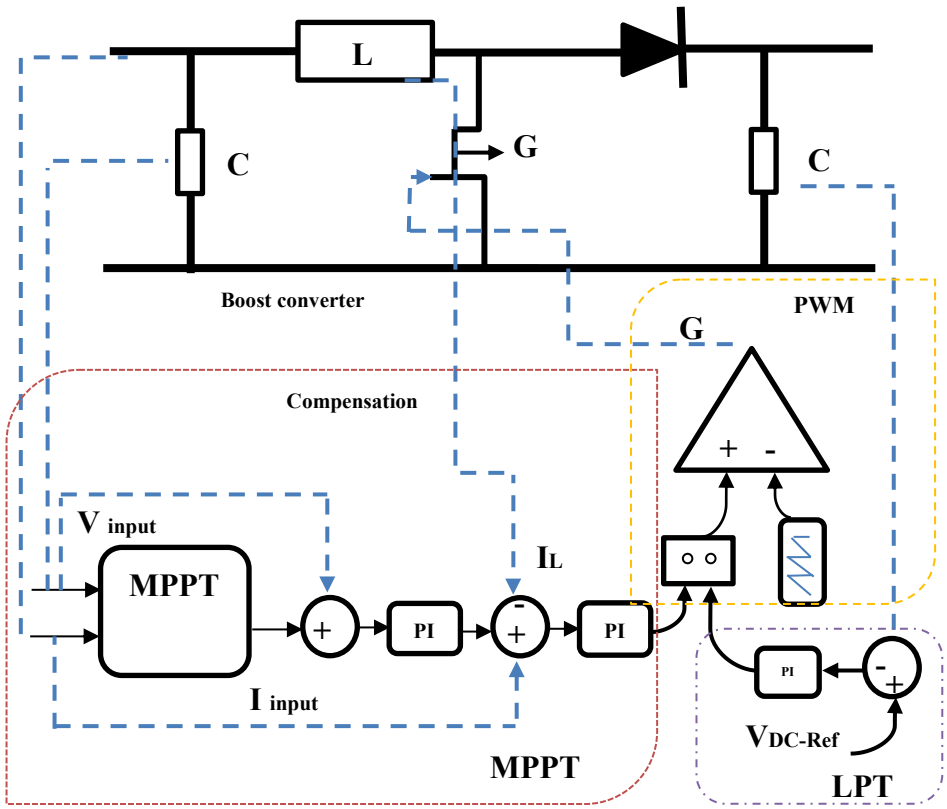


Figure IV-3 block schematic of the MPPT-using PI control.

IV.4 Energy Storage System ESS

IV.4.1 Battery Modelling

Batteries play a vital role in hybrid renewable energy systems due to their high energy density, rapid dynamic response, and low self-discharge rate. These features make them highly suitable for storing excess energy generated by intermittent renewable sources. Figure IV-4 presents the equivalent electrical model used to simulate battery behavior and analyze its dynamic characteristics [87].

Battery voltage varies nonlinearly depending on the charging or discharging phase and the control strategy employed, which is essential for maintaining performance and extending

battery lifespan. During the discharge phase, the terminal voltage of the battery can be expressed as follows:

$$V_b = V_0 + R_b I_b - \frac{kQ_b}{Q_b + \int I_b dt} + A_b e^{B_b \int I_b dt} \quad \text{(IV.11)}$$

The state of charge (SOC) of the battery can be calculated using its rated capacity and the integral of the current over time:

$$SOC = 100\left(1 + \frac{\int I_b dt}{C_{bat}}\right) \quad \text{(IV.12)}$$

In these equations:

B_b denotes the internal resistance of the battery,

V_0 is the open-circuit voltage,

I_b is the battery current,

k represents the polarization voltage,

C_b is the battery capacity,

A_b is the exponential voltage,

Q_b refers to the exponential capacity.

These parameters collectively describe the dynamic electrical behavior of the battery under different operating conditions, which is essential for accurate modeling in control and simulation environments.

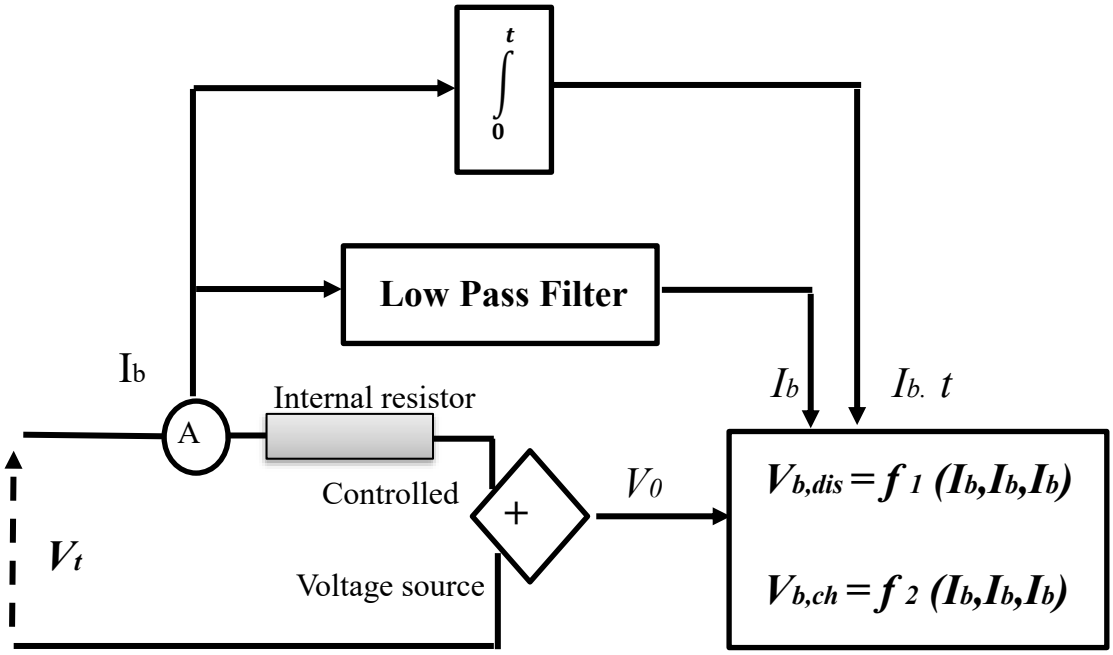


Figure IV-4 Model of battery

The key electrical and physical parameters of the Battery used in the designed system are summarized in Table VI.3.

Table IV-3 Battery electrical system Parameters

Battery	Nominal voltage 240 V. Rated capacity 20 Ah. Battery response time 0.1s, Initial SOC 100 %.

IV.4.2 Supercapacitor (SC):

Supercapacitors (SCs) are energy storage devices characterized by high power density and fast dynamic response. In hybrid energy storage configurations, SCs are deployed to absorb or deliver short bursts of power, thereby reducing the stress on the battery and improving the overall reliability and responsiveness of the system. They help mitigate both the frequency and depth of battery cycling, which directly contributes to extended battery life.

In this work, the Stern model is employed to simulate SC behavior. Figure IV-5 illustrates the corresponding electrical equivalent circuit [87].

The voltage across the supercapacitor is determined as:

$$V_{SC} = \frac{N_s Q_T}{N_p C_{cell}} - R_{SC} I_{SC} \quad \text{(IV.13)}$$

where:

Q_T is the total electric charge (Coulombs),

N_s is the number of SC cells in series,

N_p is the number of SC cells in parallel,

R_{SC} represents the internal resistance,

I_{SC} is the current flowing through the SC.

The stored energy in the supercapacitor depends on both the terminal voltage V_{SC} and the capacitance Q_{SC}, and is computed using the equation:

$$E_{SC} = \frac{Q_{SC} V_{SC}^2}{2} \quad \text{(IV.14)}$$

As the capacitor voltage changes, the energy stored also varies accordingly. The change in stored energy SOC_{SC} can be calculated using the following expression:

$$SOC_{SC} = 100\left(SOC_{SC(t_0)} - \frac{\int I_{SC} dt}{Q_{SC}}\right) \quad \text{(IV.15)}$$

These models are essential for accurately simulating the hybrid energy storage system's performance and for designing control strategies that effectively coordinate battery and SC operation during dynamic system conditions.

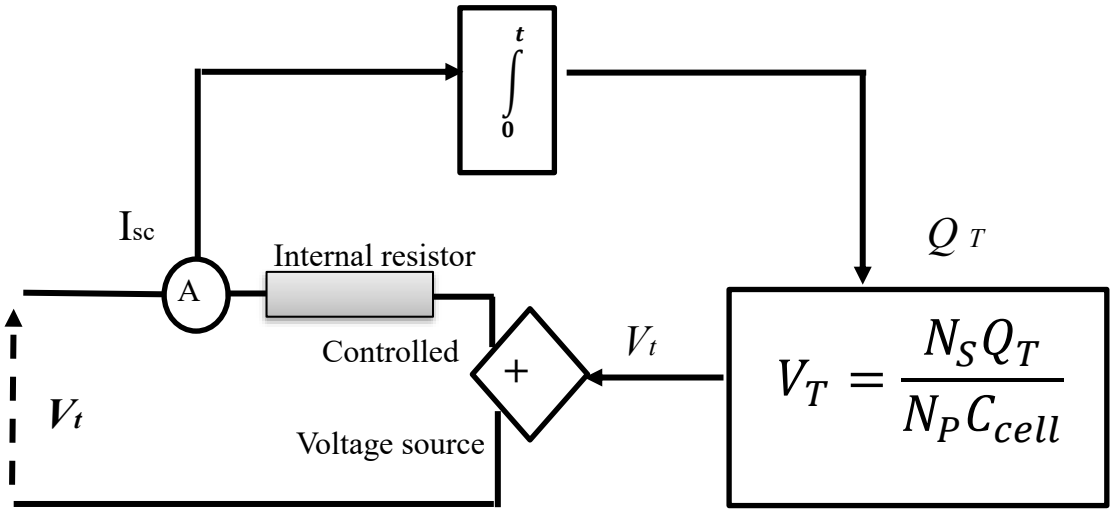


Figure IV-5 Model of SC

The Super Capacitor used in the designed system are summarized in Table VI.4.

Table IV-4 SC electrical system Parameters

Supercapacitor	Rated capacitance 34.666 F, Rated voltage 32.4 V, Number of series capacitors 1, Number of parallel capacitors 1, Operating temperature 25 (Celsius),

IV.4.3 Role of Bidirectional Converters:

Each storage component connects to the 350 V DC bus via bidirectional DC-DC converters, which facilitate energy exchange in both charging and discharging modes:

IV.4.3.1 Charging Mode (Buck Converter):

Transfers energy from the higher voltage DC bus to the ESS device, defined by:

$$P_{charge} = V_{bus}^2 / R_{Load} \quad \text{(IV.16)}$$

IV.4.3.2 Discharging Mode (Boost Converter):

Transfers energy from the ESS to the DC bus, defined by [87]:

$$P_{discharge} = V_{out} . \mathrm{I_{out}} \quad \text{(IV.17)}$$

Where V_{out}, $\mathrm{I_{out}}$ and R_{Load} represent the output voltage, current, and load resistance, respectively.

Table IV-5 Converter electrical system Parameters

DC-DC Converters	*L*-PV=*0.0016*mH, *L*-W=0.0026mH, *L*-SC=0.00103mH, *L*-Bat= 0.0055mH, *C*-DC = 1200µF,

The converter used in the designed system are summarized in Table IV.5.

IV.5 Sizing of the ESS Components

IV.5.1 The Supercapacitor Sizing:

The supercapacitor is sized to handle high power demands during transients. Maximum exchangeable energy [128]:

$$E_{SC} = 0.5\, C_{SC} ({V_{max}}^2 - {V_{min}}^2) \quad \text{(IV.18)}$$

where, $\mathrm{V_{max}}$ and $\mathrm{V_{min}}$ denote the maximum and minimum allowable voltages.

IV.5.2 Battery Sizing:

The battery capacity is proportional to the rated power of the wind turbine, DC-link voltage, and the duration of low wind speed intervals:

$$C_{batt} \infty \frac{P_{wt} \cdot LWD \cdot V_{dc-link}}{C_{SC}} \quad \text{(IV.19)}$$

Final Capacity Calculation for HESS

The hybrid ESS's total energy capacity is determined by the system's rated power and expected operational time, considering a 10% safety margin:

$$E_{HESS} = P_{rated,\ turb} * t * 10\% \quad \text{(IV.20)}$$

For the supercapacitor:

$$E_{SC} = E_{HESS} * A\% \quad \text{(IV.21)}$$

Where A% is the proportion of energy allocated to the supercapacitor.

Finally, the required capacitance of the supercapacitor is calculated as [125]:

$$C = \frac{2E_{CS}}{V^2} \quad \text{(IV.22)}$$

IV.6 HESS Control

In standalone wind energy systems, a hybrid energy storage system (HESS) composed of a battery and a supercapacitor is employed to enhance supply reliability. Owing to their rapid charge–discharge capability, supercapacitors (SCs) are particularly effective in capturing short-duration power fluctuations. This functionality reduces the required battery capacity, mitigates battery degradation, extends operational lifetime, and lowers replacement costs [128]. To achieve effective power sharing, the power exchanged between the wind generation unit and the load is decomposed into two components: a low-frequency component (LFC) and a

transient high-frequency component (THFC). The SC is responsible for compensating the THFC, whereas the battery manages the LFC associated with average power variations.

As illustrated in Figure IV-6, the proposed control strategy consists of three interconnected control loops. The first loop regulates the DC-link voltage, maintaining the DC-bus at a reference value of 350 V. The output of this loop is the total reference current (I-g-ref), which is continuously adjusted to correct any DC-bus voltage deviations. This reference current is then separated into low- and high-frequency components. The LFC is extracted using a low-pass filter and serves as the reference input for the battery control loop, allowing the battery to address long-term power imbalances. In contrast, the high-frequency component is assigned to the supercapacitor control loop, which compensates for rapid and transient power variations.

Each control loop is implemented using a Proportional–Integral (PI) controller to ensure accurate regulation. Pulse-width modulation (PWM) is applied to the output of the battery control loop to generate gating signals for the bidirectional battery converter, where switch S(B-2) is activated during discharge and S(B-1) during charging. Similarly, the supercapacitor bidirectional converter is controlled via PWM-generated gating signals, with switch S(SC-1) enabled for charging and S(SC-2) for discharging [128].

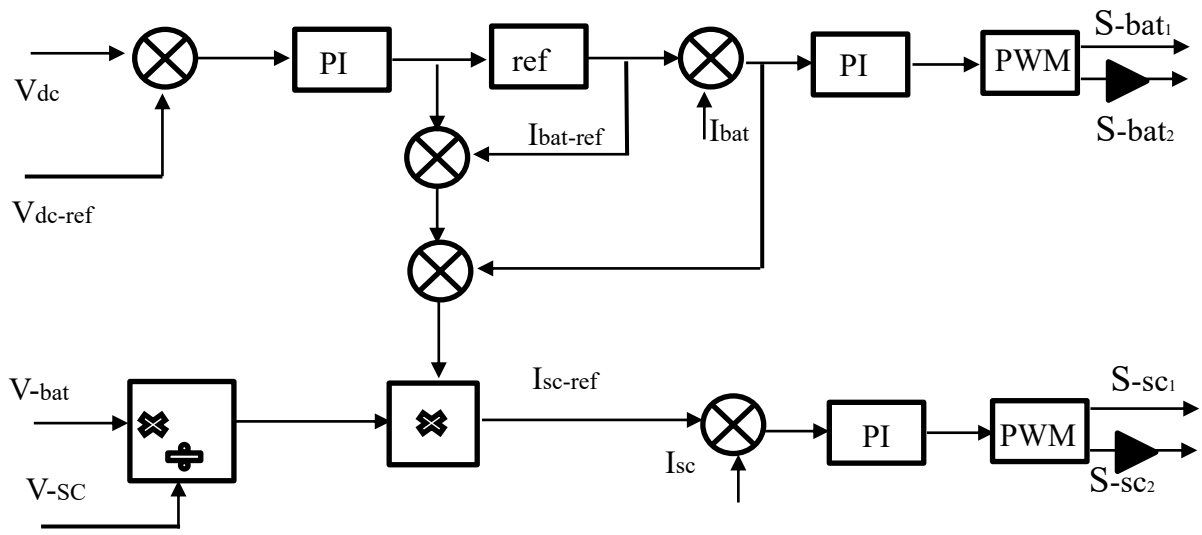


Figure IV-6 Hybrid ESS control scheme.

However, in case when the generator system power is higher than the load demands, even if the battery is fully charged, the extra power will be sent to it. The battery would

deteriorate as a result, so for an improvement an energy management strategy is suggested to address this issue.

IV.7 Fuzzy Logic Energy Management

Figure IV-7 presents the architecture of the proposed Fuzzy Logic Energy Management System (FL-EMS) for a DC microgrid (DCMG) integrating a hybrid energy storage system (HESS). This approach is designed to ensure reliable operation under varying load and generation conditions. The primary objective of the control strategy is to maintain a stable DC-link voltage, despite fluctuations in power supply and demand. This is achieved through a combination of PI control and fuzzy logic-based decision-making.

The PI controller regulates the DC bus voltage by computing the reference current for the bus, denoted as I_{DC-ref}, and sets the target bus voltage at a nominal value, V_{DC-ref}= 350 V. Using the FL-EMS, the converters are supplied with two current references: one for the battery (I_{b-ref}) and one for the supercapacitor (I_{SC-ref}). These references are dynamically adjusted to maintain the DC-link voltage close to its setpoint regardless of load disturbances.

The total current contributions must satisfy the following current balance equations:

$$I_{DC-ref} = I_{b-ref} + I_{SC-ref} \tag{IV.23}$$

$$C_{DC}\frac{dv_{DC}}{dt} = I_b + I_{SC} - I_{Load} \tag{IV.24}$$

In these equations:

I_b, I_{SC}, and I_{Load} represent the currents supplied by the battery, the supercapacitor, and the load, respectively.

C_{DC} denotes the capacitance of the DC bus, which governs the voltage stability and energy distribution capability across system components.

To smooth out rapid fluctuations in SC voltage, a low-pass filter is applied to the DC bus current as an additional layer of control. This filtering process aids in regulating instantaneous voltage transients, ensuring that high-frequency power components are primarily absorbed or released by the supercapacitor.

The system determines the reference currents I_{SC-ref} and I_{b-ref}. by considering the state of charge (SOC) of both the battery ($SOC_{Battery}$) and the supercapacitor (SOC_{SC}). A logic switch selects the appropriate reference current based on SOC thresholds, and the fuzzy logic controller refines the decision by analyzing the system's operating conditions.

Fuzzy logic is particularly well-suited to this application due to its capacity to handle nonlinearities and system uncertainties through linguistic variables and rule-based inference. The developed FL-EMS consists of:

- Three inputs,
- Three outputs,
- A rule base of 27 fuzzy rules, designed specifically to manage power allocation between the renewable energy sources (RES), HESS, and the load.

These rules were designed based on expert intuition and system behavior and are summarized in Table IV-6. The fuzzy logic system was implemented and validated in a MATLAB/Simulink simulation environment.

The fuzzy logic controller (FLC) continuously evaluates the SOC of the storage components and determines the optimal power sharing strategy between the battery and the supercapacitor. The battery is assigned to handle low-frequency, steady-state energy demands, while the supercapacitor addresses high-frequency power transients, thereby minimizing the battery's cycling stress and extending its operational lifespan.

This dynamic energy allocation approach improves overall system efficiency, maintains voltage stability, and enhances the durability of the energy storage units under variable load and renewable generation conditions.

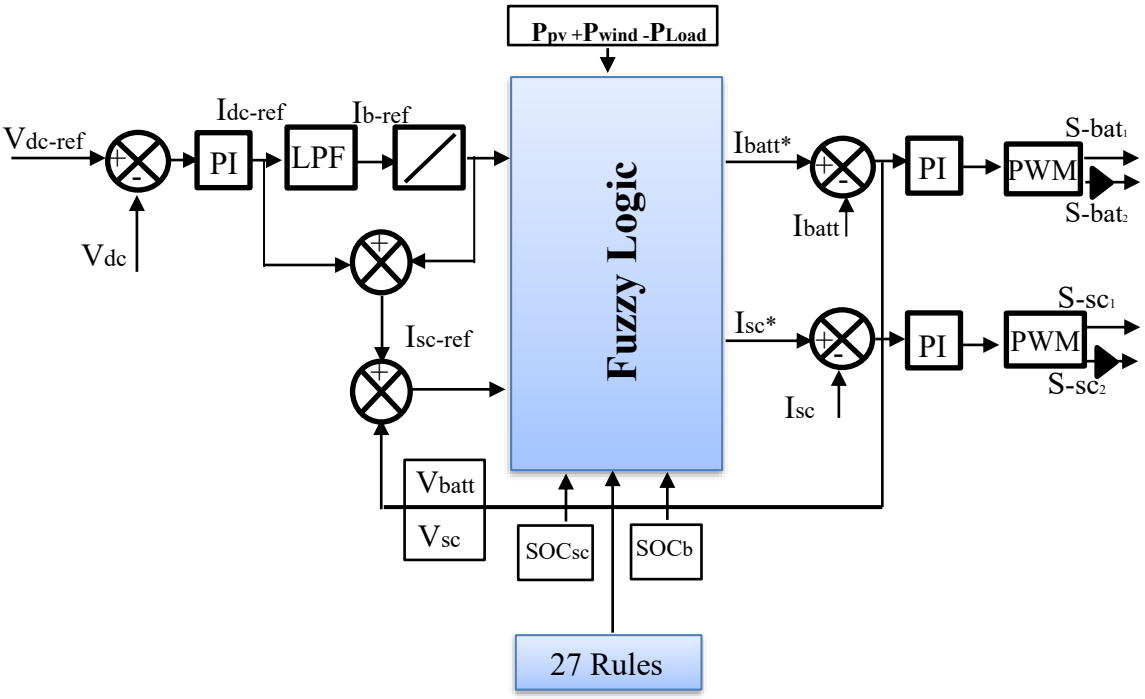


Figure IV-7 Proposed fuzzy logic energy management system

- The Fuzzy Logic Controller analyzes the SOC values and decides how power should be split between the battery and supercapacitor based on 27 fuzzy rules.
- The battery handles low-frequency (steady-state) power demands, while the supercapacitor absorbs high-frequency transients, protecting the battery from stress.
- The goal of this method is to dynamically allocate power between the battery and supercapacitor (SC) to improve system efficiency and protect the battery from high-frequency power fluctuations.

Table IV-6 Fuzzy logic

Rule number	Input variables			Output variables		
	Power	$SOC_{Battery}$	SOC_{SC}	$K_{Battery}$	K_{SC}	**Control mode**
01	Excess	Empty	Empty	ON	ON	MPPT
02	Excess	Empty	Medium	ON	ON	MPPT
03	Excess	Empty	Full	ON	OFF	MPPT
04	Excess	Medium	Empty	ON	ON	MPPT
05	Excess	Medium	Medium	ON	ON	MPPT
06	Excess	Medium	Full	ON	OFF	MPPT
07	Excess	Full	Empty	OFF	ON	MPPT
08	Excess	Full	Medium	OFF	ON	LPT
09	Excess	Full	Full	OFF	OFF	LPT
10	Deficit	Empty	Empty	OFF	ON	LPS
11	Deficit	Empty	Medium	OFF	ON	LPS
12	Deficit	Empty	Full	OFF	ON	LPS
13	Deficit	Medium	Empty	ON	ON	MPPT
14	Deficit	Medium	Medium	ON	ON	MPPT
15	Deficit	Medium	Full	ON	OFF	MPPT
16	Deficit	Full	Empty	ON	OFF	MPPT
17	Deficit	Full	Medium	ON	ON	MPPT
18	Deficit	Full	Full	ON	ON	MPPT
19	Balance	Empty	Empty	ON	ON	LPS
20	Balance	Empty	Medium	ON	ON	LPS

21	Balance	Empty	Full	ON	ON	LPS
22	Balance	Medium	Empty	ON	ON	MPPT
23	Balance	Medium	Medium	ON	ON	MPPT
24	Balance	Medium	Full	ON	ON	MPPT
25	Balance	Full	Empty	ON	ON	LPT
26	Balance	Full	Medium	ON	ON	LPT
27	Balance	Full	Full	OFF	ON	LPT

The control mode outputs have three membership functions in the Fuzzy Logic Energy Management System (Table IV-7):

Table IV-7 Summary of control modes in FL-EMS.

Control Mode	When activated?	Function
MPPT (Maximum Power Point Tracking)	When excess power is available from PV & Wind.	Extracts maximum power and stores it in battery/SC.
LPT (Load Power Tracking)	When power generation is balanced with demand.	Matches energy supply to the load efficiently.
LPS (Load Power Shedding)	When power supply is insufficient due to low SOC or low generation.	Reduces power to non-essential loads to prevent system failure.

IV.8 Simulation Results

To evaluate the performance of the proposed hybrid energy system and validate the applied control strategy FL-EMS the system was tested using MATLAB/Simulink for various scenarios. These scenarios include variations in irradiance and wind velocity.

IV.8.1 Case 1: Variations in Irradiance and Wind Velocity.

The analysis of simulation results for the PV/Wind power generation system and the hybrid Battery/SC ESS under these scenarios is presented in **Table IV-8.** The wind velocity, the irradiance, the power from the PV and Wind system, the battery/SC charging- discharging mode, the load power (P-Load), and DC bus voltage are shown in Figures IV-8, 9, 10, 11, 12, 13, 14 respectively.

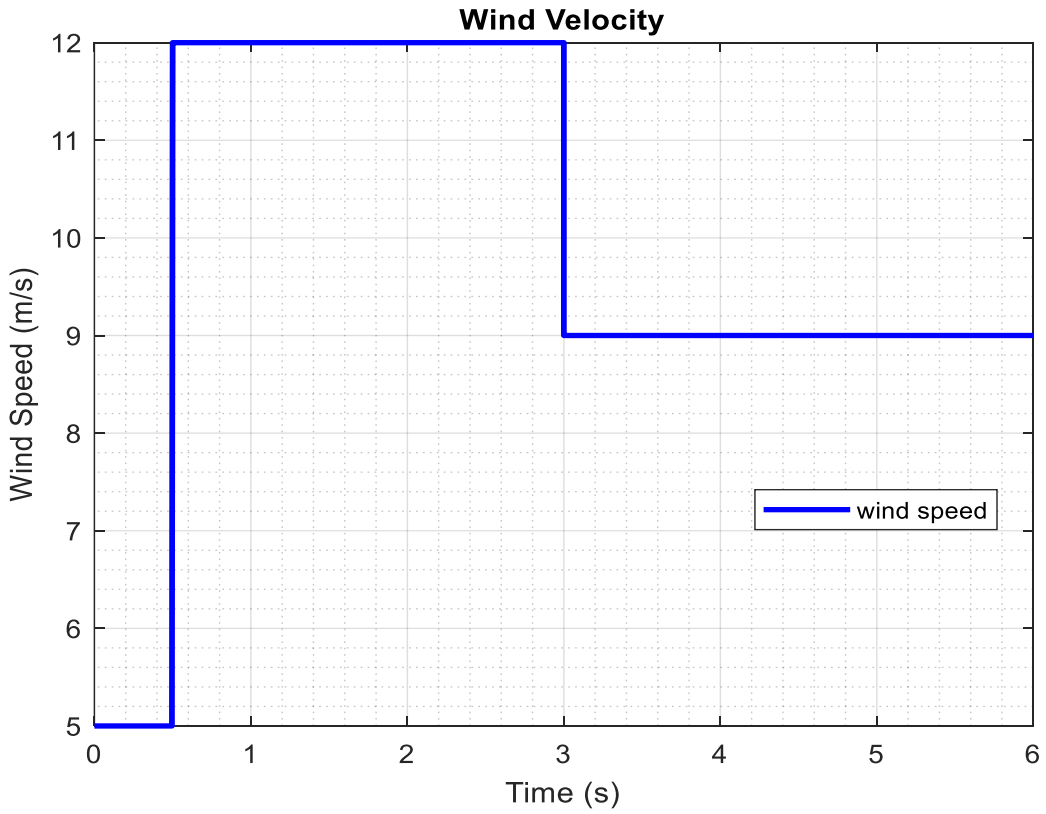


Figure IV-8 Wind Velocity

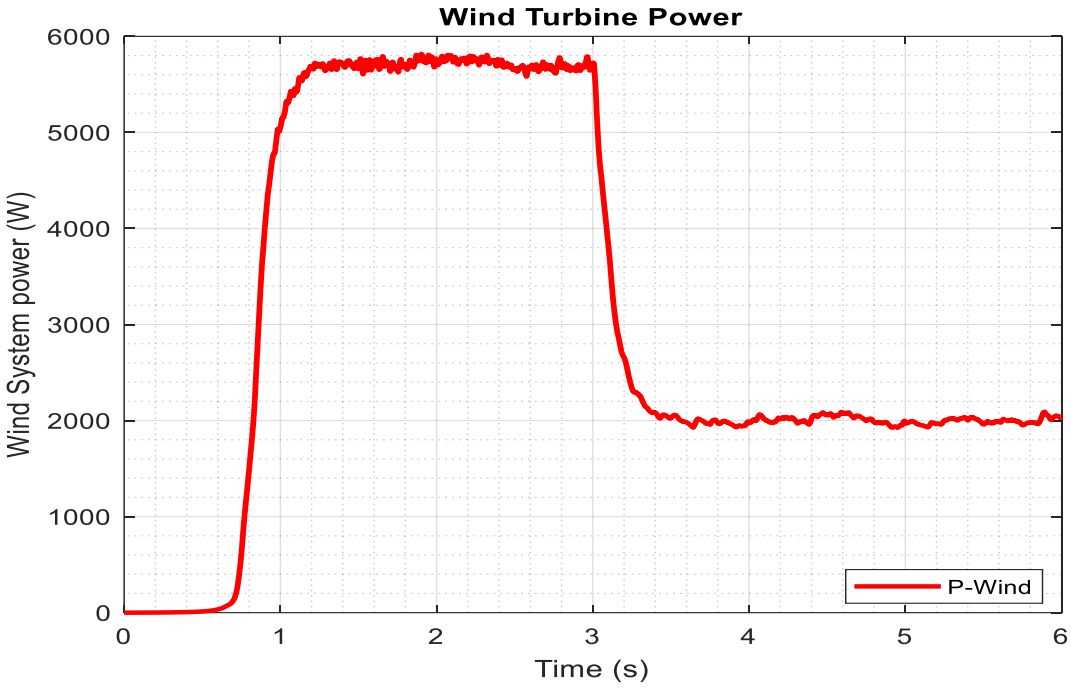


Figure IV-9 Wind system power

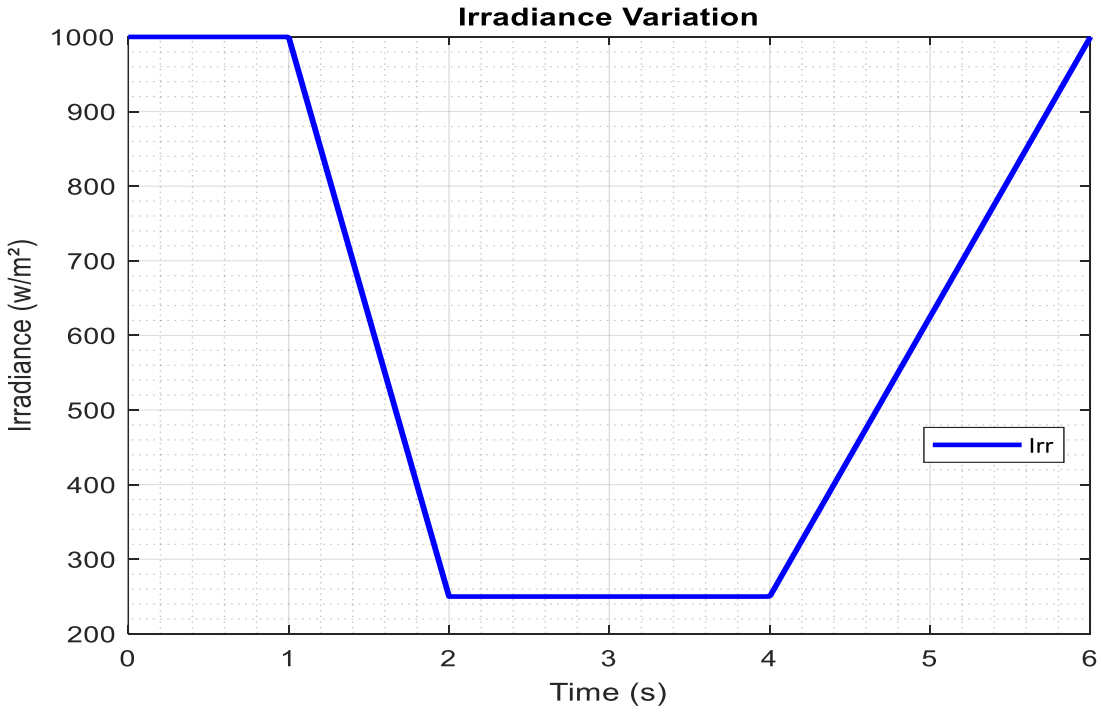


Figure IV-10 irradiance variation

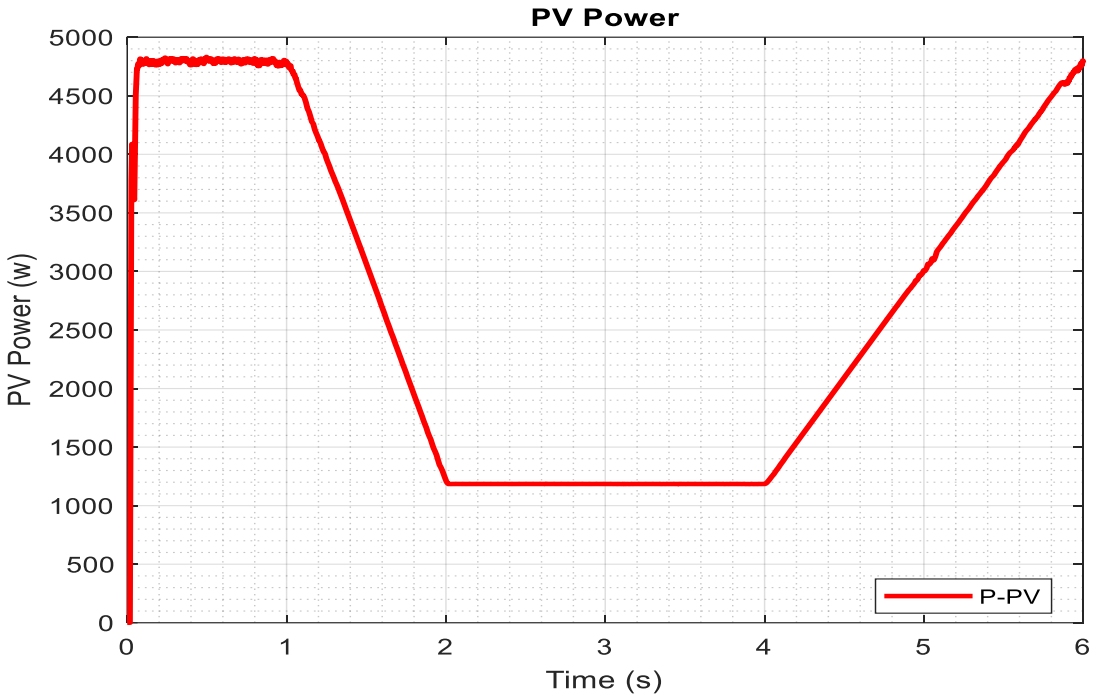


Figure IV-11 PV Power Output

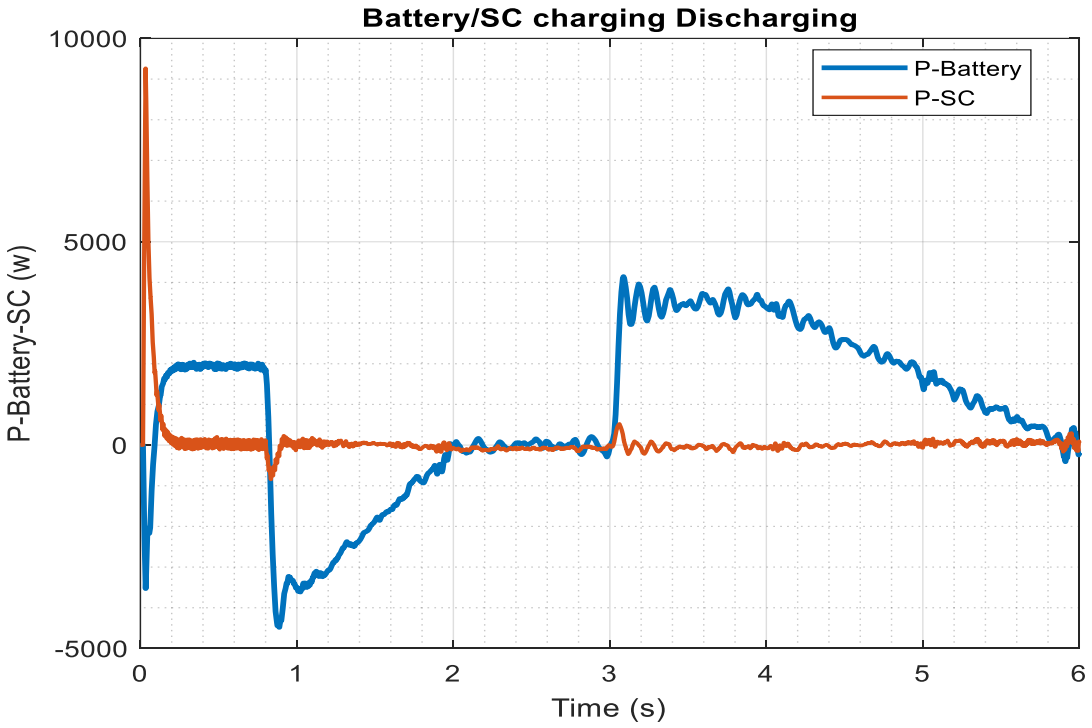


Figure IV-12 Battery/SC Chargin Discharging Modes

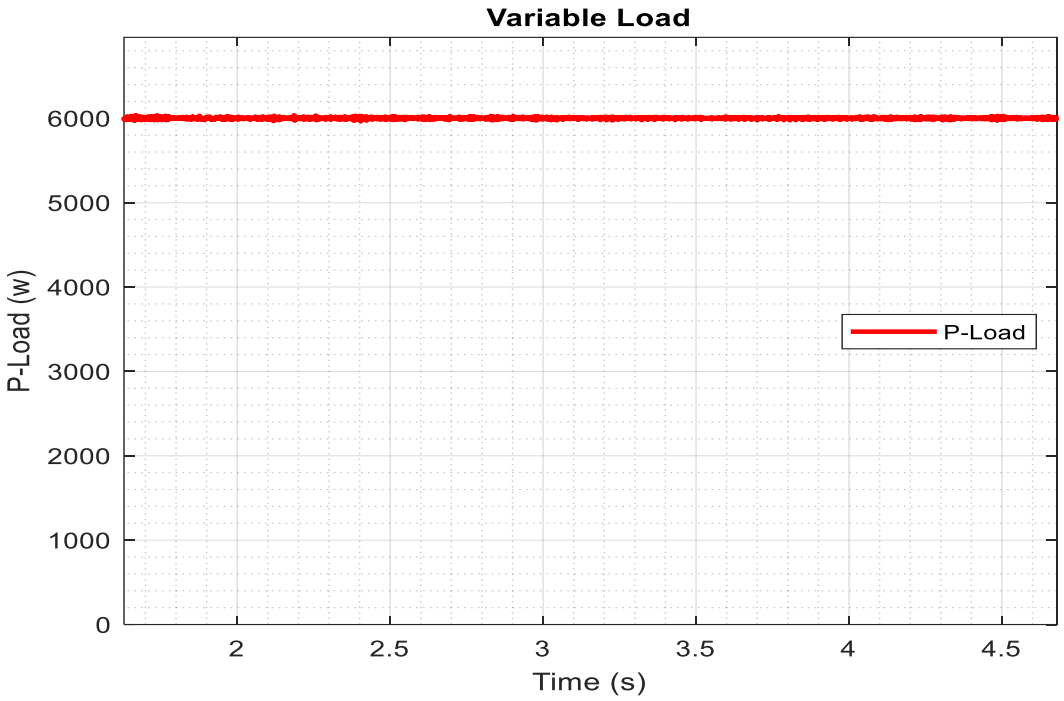


Figure IV-13 Load Power Demand

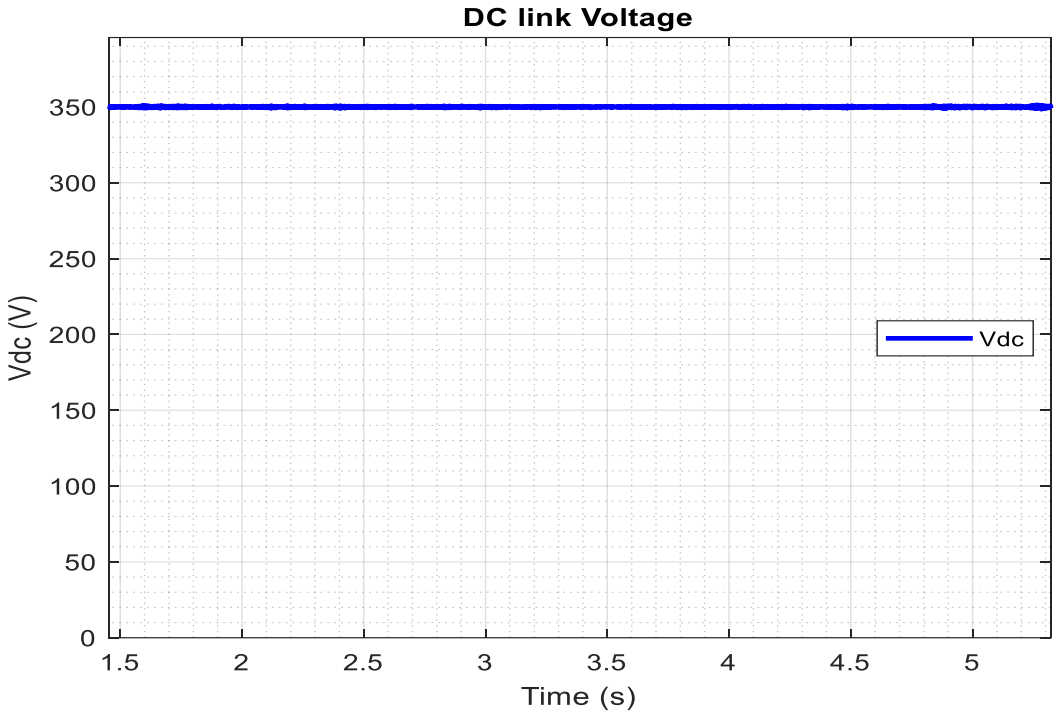


Figure IV-14 Dc voltage

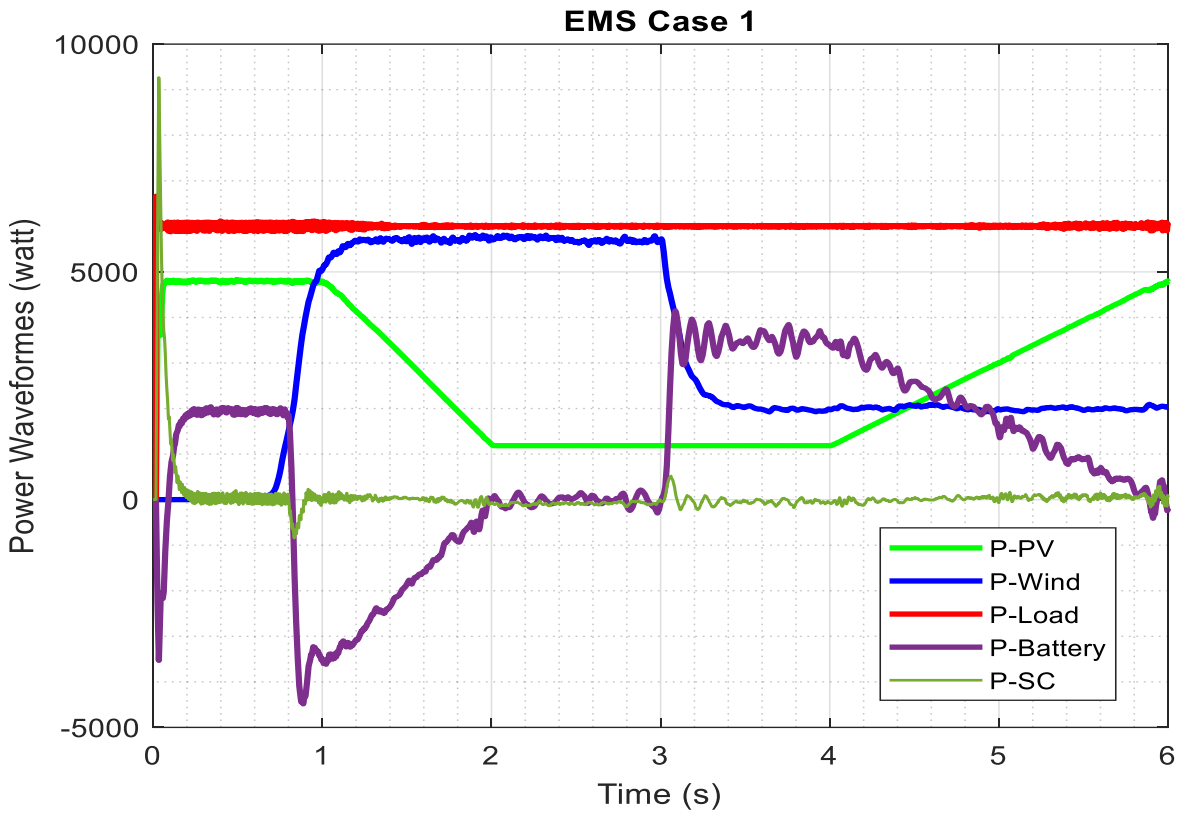


Figure IV-15 Power waveforms case1

Figures IV-8 & IV-9 (Wind velocity & wind power) The wind power output follows the cubic dependence on wind speed, with short gusts creating rapid but limited variations. These transients are managed primarily by the supercapacitor to prevent battery stress, confirming the correct dynamic coupling of turbine and EMS.

Figures IV-10 & IV-11 (Irradiance & PV power) PV power output mirrors the irradiance pattern, with visible dips during abrupt decreases. The MPPT tracks the instantaneous maximum power point effectively, with only minor transient loss during fast irradiance ramps.

Figure IV-12 (Battery / Supercapacitor behavior) The complementary behavior of battery and supercapacitor is evident. The SC responds to high-frequency power fluctuations, while the battery supplies slower energy compensation. This division of roles limits battery current peaks and improves lifespan, validating the fuzzy EMS logic.

Figure IV-13 (Load profile) The mixed load profile tests both steady and transient conditions. When demand rises, the SC supplies the initial surge and the battery follows gradually, keeping the DC bus voltage within tolerance.

Figure IV-14 (DC bus voltage) The DC bus voltage remains tightly regulated around its nominal level. Small dips during transitions are corrected quickly by the fuzzy controller, showing efficient rule activation and converter coordination.

Figure IV-15 (Power waveforms – Case 1) When renewable input decreases, the EMS prioritizes SC discharge for immediate support, followed by battery discharge for sustained deficit. During generation peaks, the SC absorbs excess first, then the battery charges slowly. This two-stage handling smooths the delivered power and reduces battery cycling.

Table IV-8 The results analysis description case 1

Duration	Parameters	Results
Wind Turbine (From t=0 to t=0.5 sec)	Wind velocity: $5\mathrm{m/s}$ $P_{Wind} \approx 40$ W $P_{Wind} < P_{Load}$	Wind power is too low PV power is ≈ 4800 W $P_{Battery} \approx 1800$ W Battery is ON (discharging mode) load power is 6000 W (Surplus power 640 W)
PV Panel (From t=0 to t=1sec)	Irradiance: $1000\ \mathrm{w/m^2}$ $P_{PV} \approx 4800$ W $P_{PV} < P_{Load}$	

<table>
<tr><td>Wind Turbine

(From t=0.5 to t=2sec)</td><td>Wind velocity: 12m/s

$P_{Wind} \approx$ From 10 W to 6000 W

$P_{Wind} < P_{Load}$

$P_{Wind} \approx 6000$ W (t $= 1.2$sec)</td><td rowspan="2">Wind power is increasing to ≈ 6000 W

PV power is decreasing to 2370W

Battery is OFF

$P_{Battery}$ start discharging at (t ≈ 0.8sec)

load power is 6000 W

(Surplus power depends on Battery's capacity)</td></tr>
<tr><td>PV Panel

(From t=1 to t=2sec)</td><td>Irradiance:

(From 1000 to 250 w/m^2)

P_{PV} ≈ Fom 5000 W to 2370W

$P_{PV} < P_{Load}$</td></tr>
<tr><td>Wind Turbine

(From t=2 to t=3 sec</td><td>Wind velocity: 12m/s

$P_{Wind} \approx 6000$ W

$P_{Wind} \approx P_{Load}$</td><td rowspan="2">Wind power is ≈ 6000 W

PV power is ≈ 2370 W

Battery in discharging mode

load power is 6000 W</td></tr>
<tr><td>PV Panel

(From t=2 to t=4sec)</td><td>Irradiance: 250 w/m^2

$P_{PV} \approx 2370$ W

$P_{PV} < P_{Load}$</td></tr>
</table>

Wind Turbine (From t=3 to t=4 sec)	Wind velocity: 9m/s P_{Wind} ≈ From 6000 W to 2000 W $P_{Wind} \approx 2000$ W (t = 3.4sec) $P_{Wind} < P_{Load}$	Wind power is ≈ 2000 W PV power is ≈ 2370 W $P_{Battery} \approx +2400$ W Battery in discharging mode load power is 6000 W (Surplus power 770 W)
PV Panel (From t=3 to t=4sec)	Irradiance: 250 w/m^2 $P_{PV} \approx 2370$W $P_{PV} < P_{Load}$	
Wind Turbine (From t=4 to t=6 sec)	Wind velocity: 9m/s $P_{Wind} \approx 2000$ W $P_{Wind} < P_{Load}$	Wind power is ≈ 2000 W PV power is slowly increasing to ≈ 5000W Battery is ON charging mode $P_{Battery}$ is decreasing while P-PV increases load power is 6000 W
PV Panel (From t=4 to t=6sec)	Irradiance: Increasing from 250 to 1000w/m^2 P_{PV} ≈ Fom 2370 W to 5000W $P_{PV} < P_{Load}$	

The primary goal is to keep the DC-link voltage at 350V and meet the load requirement regardless of changes in irradiance/wind speed.

The DC connection voltage is successfully regulated at 350V.

The supercapacitor's quick response in compensating transient peak powers during irradiance or wind velocity variations, reducing battery charging stresses.

IV.8.2 Case 2: Variations in Irradiance and Wind Velocity and Load Demands

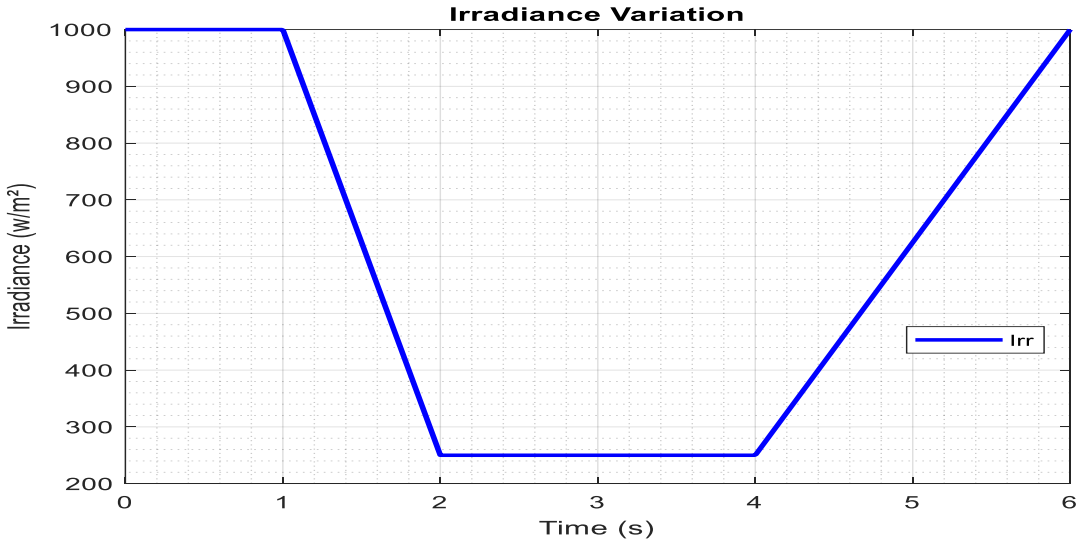


Figure IV-16 Irradiance Variation

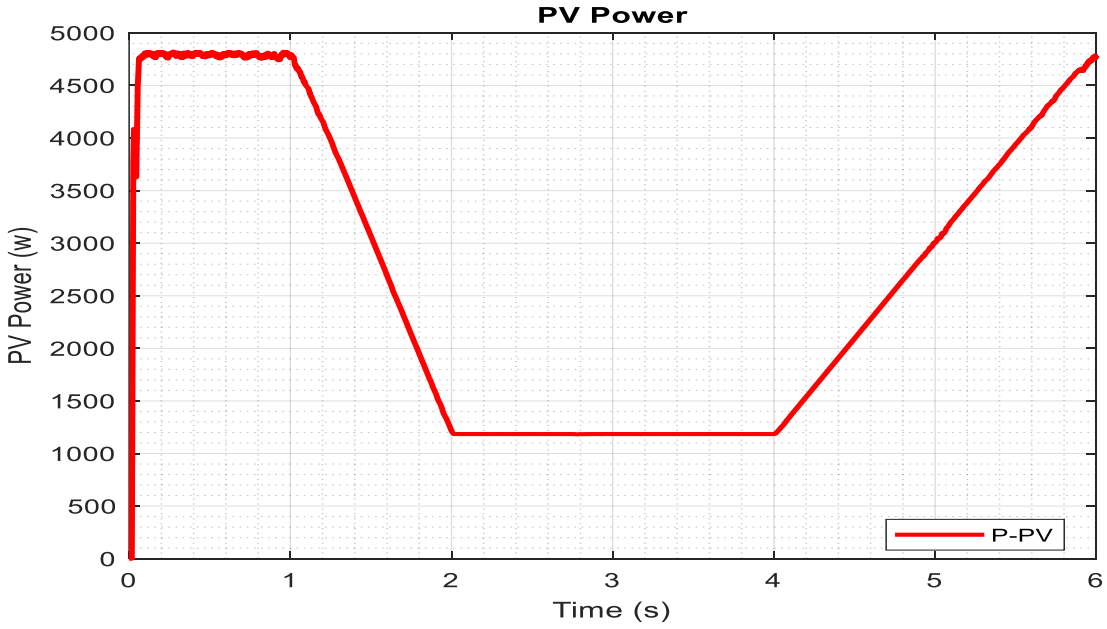


Figure IV-17 PV Power

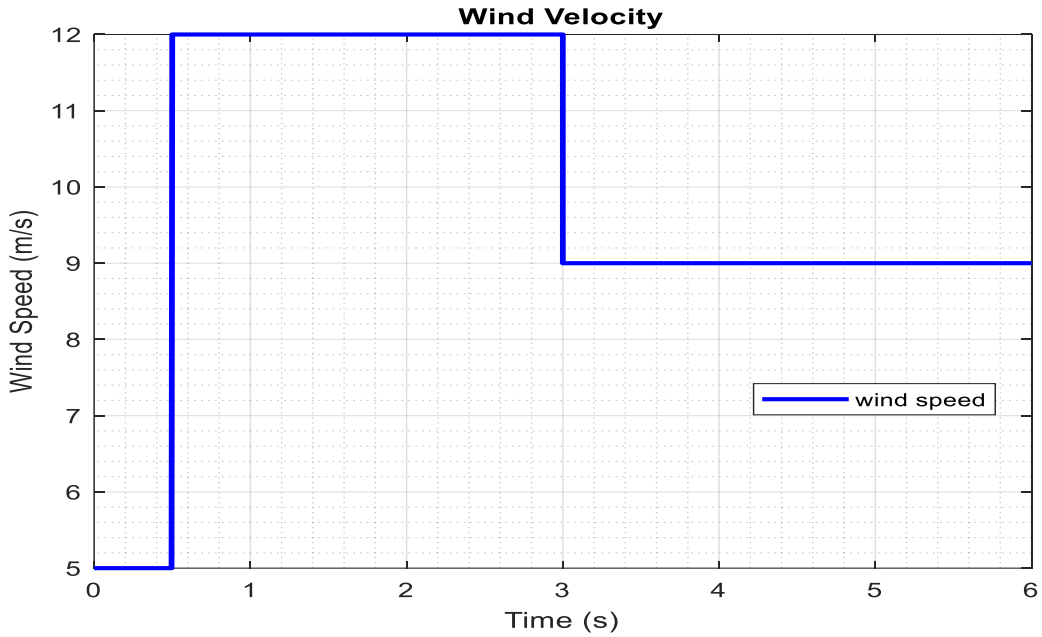


Figure IV-18 wind Velocity

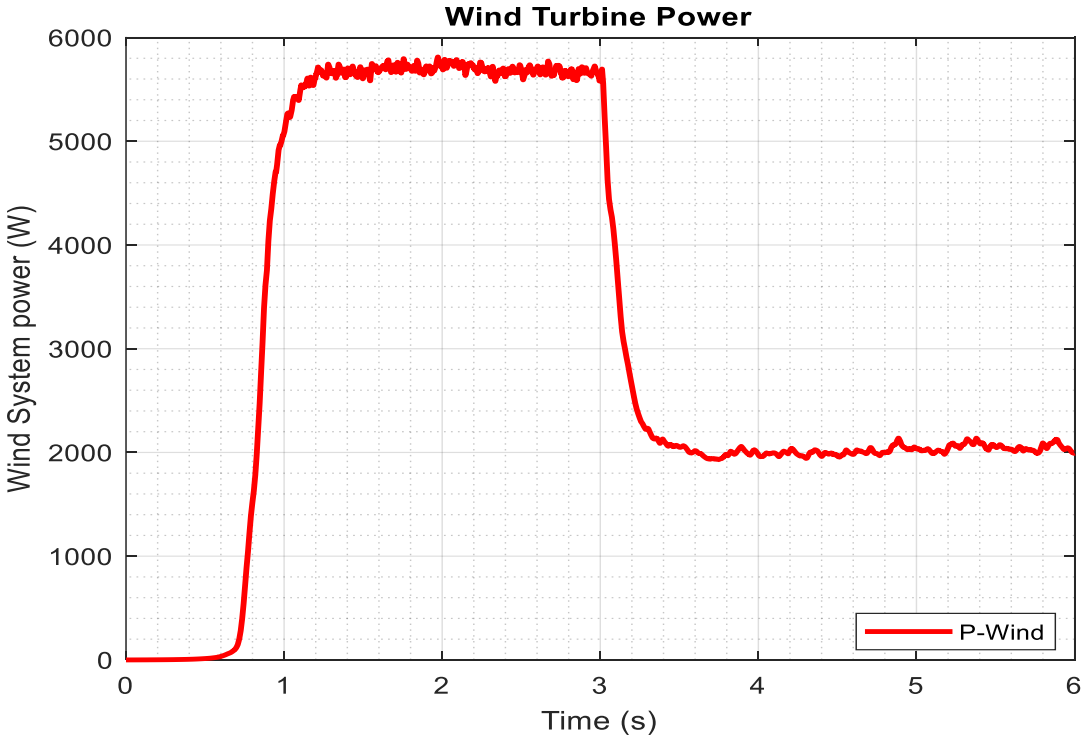


Figure IV-19 Wind system power

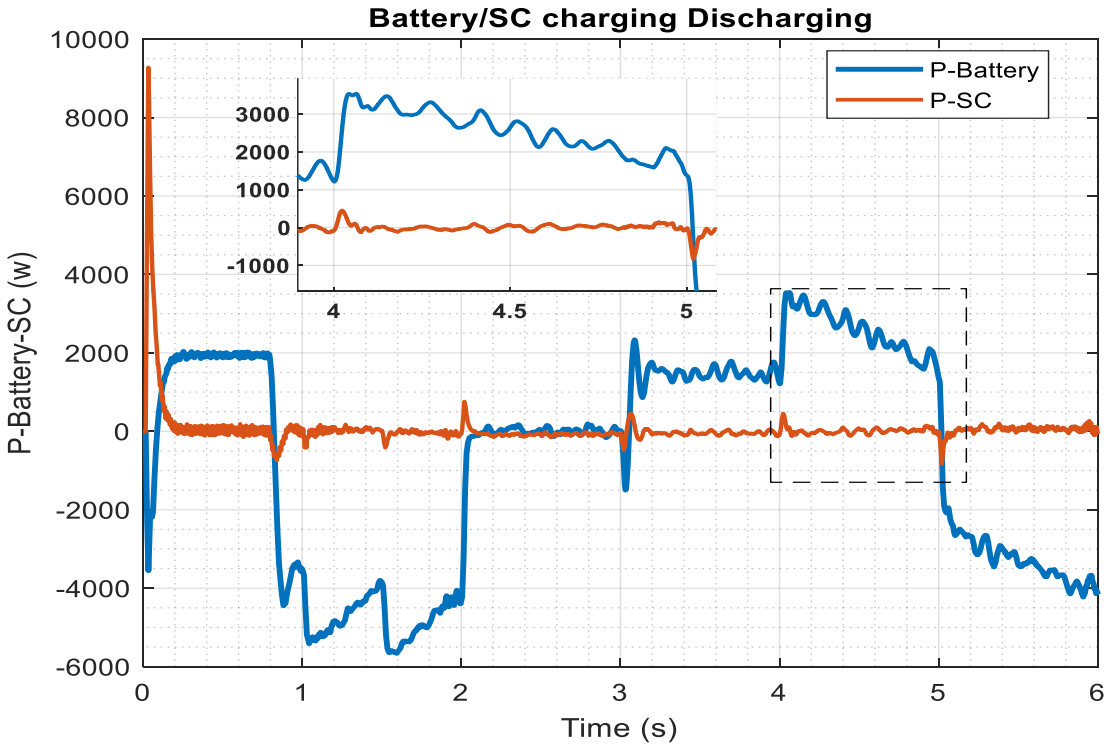


Figure IV-20 ESS Charging/Discharging

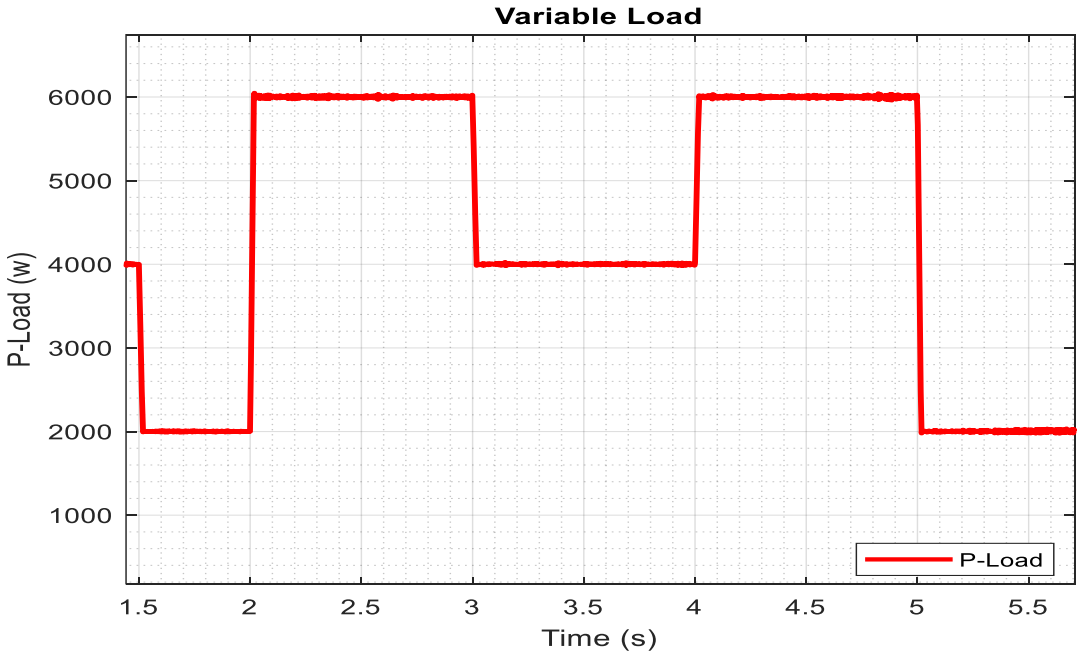


Figure IV-21 Variable Load

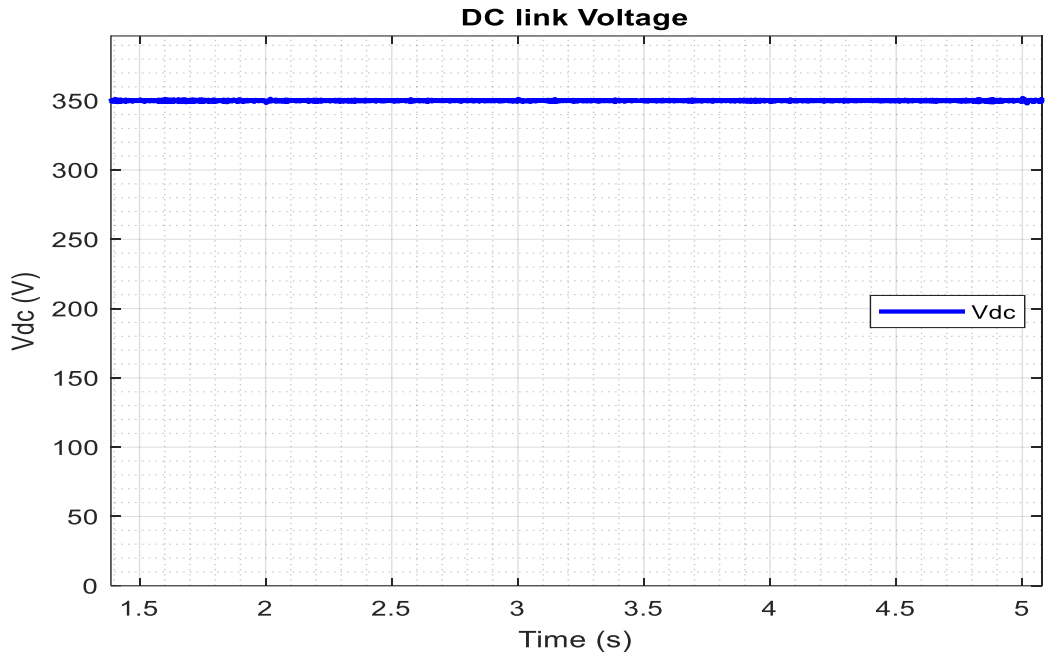


Figure IV-22 DC Bus Voltage

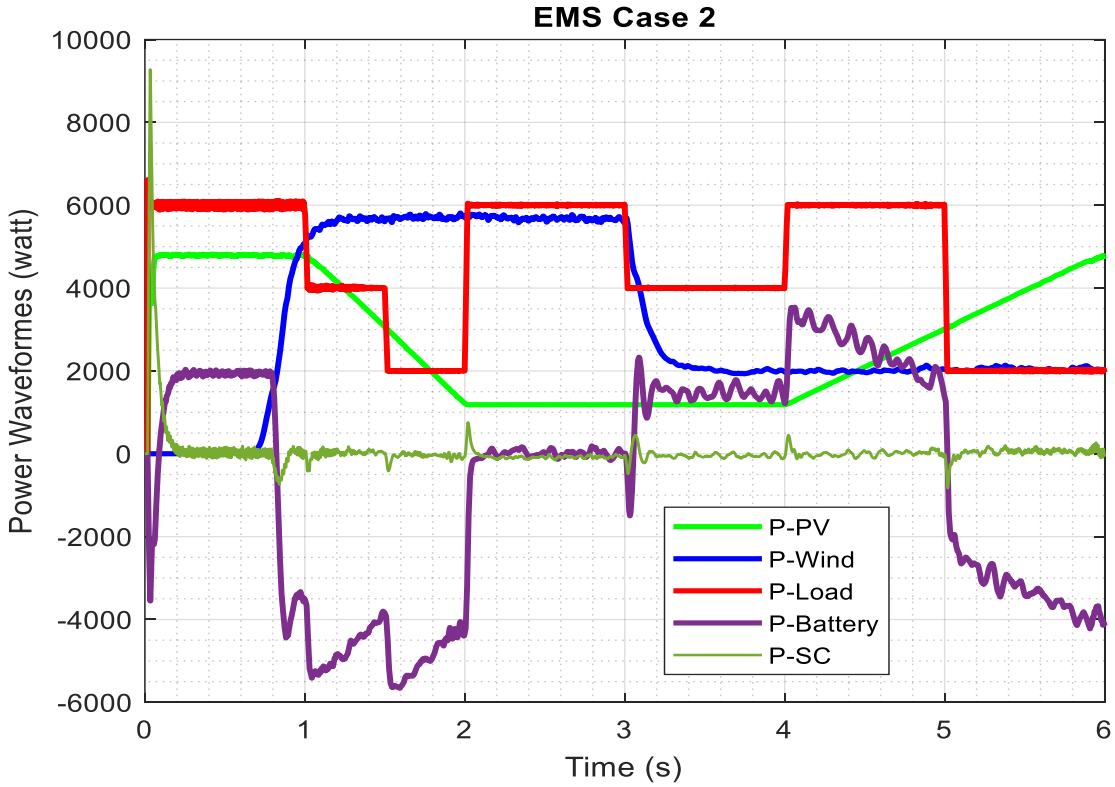


Figure IV-23 Power Waveforms case2

- Irradiance (Fig. 16): Dynamic irradiance profile reflects variations during the test period.
- PV Power (P -PV, Fig. 17): The PV system efficiently tracks the maximum.
- Wind Velocity (Fig. 18): wind profile is used to generate power via the wind turbine.
- Wind Power (P -Wind, Fig. 19): Wind power output increases as wind velocity rises, demonstrating effective MPPT control.
- power under varying irradiance using the MPPT controller.
- Battery/SC Power (Fig. 20): The hybrid ESS effectively manages charging and discharging operations, compensating for power transients and balancing load demand.
- Load Power (Fig. 21): variable load, maintained consistently fulfilled throughout the simulations.
- DC Bus Voltage (Fig. 22): Successfully regulated at 350V, demonstrating system stability and control reliability.
- Power waveforms (Fig 23) of our energy management system case2.

Table IV-9 The results analysis description case 2

Duration	Parameters	Results
Wind Turbine (From t=0 to t=1sec)	Wind velocity: $5m/s$ $P_{Wind} \approx 40$ W $P_{Wind} < P_{Load}$	Wind power is too low PV power is ≈ 4800 W $P_{Battery} \approx 1800$ W Battery is ON (discharging mode) load power is 6000 W (Surplus power 600 W)
PV Panel (From t=0 to t=1sec)	Irradiance: $1000\ w/m^2$ $P_{PV} \approx 4800$ W $P_{PV} < P_{Load}$	

P -Load (From t=0 to t=1sec)	$P_{load} \approx 6000$ W $P_{Load} > P_{PV} + P_{wind}$	
Wind Turbine (From t=0.5 to t=2sec)	Wind velocity: 12m/s $P_{Wind} \approx$ From 10 W to 6000 W $P_{Wind} > P_{Load}$ $P_{Wind} \approx 6000$ W (t $= 1.2$sec)	Wind power is increasing to ≈ 6000 W PV power is decreasing to 2370W Battery in discharging mode $P_{Battery}$ start discharging at (t ≈ 0.8sec) load power is 4000 W and at t= 1.5s 2000W (Surplus power depends on Battery's capacity)
PV Panel (From t=1 to t=2sec)	Irradiance: (From 1000 to 250 w/m^2) $P_{PV} \approx$ Fom 5000 W to 2370W $P_{PV} < P_{Load}$	
P -Load (From t=1 to t=2sec)	$P_{Load} \approx 4000$ W $P_{Load} \approx 2000$ W at t $= 1.5$s	
Wind Turbine (From t=2 to t=3 sec	Wind velocity: 12m/s $P_{Wind} \approx 6000$ W $P_{Wind} \approx P_{Load}$	Wind power is ≈ 6000 W PV power is ≈ 2370 W Battery in discharging mode load power is 6000 W Battery is OFF
PV Panel (From t=2 to t=3sec)	Irradiance: 250 w/m^2 $P_{PV} \approx 2370$ W $P_{PV} < P_{Load}$	

P-Load (From t=2 to t=3sec)	$P_{Load} = 6000w$ $P_{Wind} \approx P_{Load}$	
Wind Turbine (From t=3 to t=4 sec)	Wind velocity: $9m/s$ $P_{Wind} \approx$ From 6000 W to 2000 W $P_{Wind} \approx 2000$ W (t $= 3.4sec$) $P_{Wind} < P_{Load}$	Wind power is ≈ 2000 W PV power is ≈ 1370 W $P_{Battery} \approx +1400$ W Battery in discharging mode load power is 4000 W (Surplus power 770 W)
PV Panel (From t=3 to t=4sec)	Irradiance: $250\ w/m^2$ $P_{PV} \approx 1870W$ $P_{PV} < P_{Load}$	
P-load (From t=3 to t=4sec)	$P_{Load} = 4000w$ $P_{Load} > P_{Wind} + P_{PV}$	
Wind Turbine (From t=4 to t=6 sec)	Wind velocity: $9m/s$ $P_{Wind} \approx 2000$ W $P_{Wind} < P_{Load}$	Wind power is ≈ 2000 W PV power is slowly increasing to $\approx$ 5000W Battery is ON charging mode $P_{Battery}$ is decreasing while P-PV increases Battery is discharging at t=5 sec
PV Panel (From t=4 to t=6sec)	Irradiance: Increasing from 250 to $1000w/m^2$ $P_{PV} \approx$ Fom 2370 W to 5000W $P_{PV} < P_{Load}$	

P-load (From t=4 to t=6sec)	$P_{Load} =$ 4000w at t=4_5 s $P_{Load} > P_{Wind} + P_{PV}$ $P_{Load} =$ 2000w at t=5_6 s $P_{Load} < P_{Wind} + P_{PV}$	load power is 4000 W load power is 2000 W at t=5_6 sec

The primary goal is to keep the DC-link voltage at 350V and meet the load requirement regardless of changes in the load or irradiance/wind speed. The battery should not be harmed by transients or overcharging for this to happen.

The DC connection voltage is successfully regulated at 350V.

The supercapacitor's quick response in compensating transient peak powers during load or wind velocity variations, reducing battery charging stresses, and extending the battery's lifespan to take the lead in making up for any constant drift between generator and load powers.

IV.8.3 Dynamic Load Changes Using Real-Time Data

Test was run under a real data for 24 hours for commercial load profiles during July in city of MEDEA, Algeria Figure IV-24.



Figure IV-24 city of MEDEA, Algeria

Table IV-10 Real data analysis description

Case	July (MEDEA city) 2022		
	Irradiance w/m^2	Wind Velocity m/s	Load Data (Watt)
(00:00a.m →01: 00a.m)	0	7.6000	3999.3
(01:00a.m →02: 00a.m)	0	8	4000
(02:00a.m →03: 00a.m)	0	8.1000	4000.1
(03:00a.m →04: 00a.m)	0	8.1000	4000.1
(04:00a.m →05: 00a.m)	0	8.1000	4000,2
(05:00a.m →06: 00a.m)	0	8	3999.9
(06:00a.m →07: 00a.m)	0	7.9000	3999.6
(07:00a.m →08: 00a.m)	0	8.2000	4000.1
(08:00a.m →09: 00a.m)	576	8.4000	4001.1
(09:00a.m →10: 00a.m)	790	7.9000	4001.9
(10:00a.m →11: 00a.m)	896	7.2000	4002
(11:00a.m →12: 00p.m)	943	6.4000	4003.9
(12: 00p.m →13: 00p.m)	957	5.9000	4003.9
(13: 00p.m →14: 00p.m)	956	5.8000	4002.4
(14: 00p.m →15: 00p.m)	933	5.9000	4001
(15: 00p.m →16: 00p.m)	885	6	4000.5
(16: 00p.m →17: 00p.m)	791	6	3999.8
(17: 00p.m →18: 00p.m)	591	6.1000	3998.4
(18: 00p.m →19: 00p.m)	0	6.3000	3999.1
(19: 00p.m →20: 00p.m)	0	6.4000	3998.6
(20: 00p.m →21: 00p.m)	0	6.3000	3996.8
(21: 00p.m →22: 00p.m)	0	6.3000	3997.3
(22: 00p.m →23: 00p.m)	0	6.2000	3997.1
(23: 00p.m →00: 00a.m)	0	6.2000	3997.4

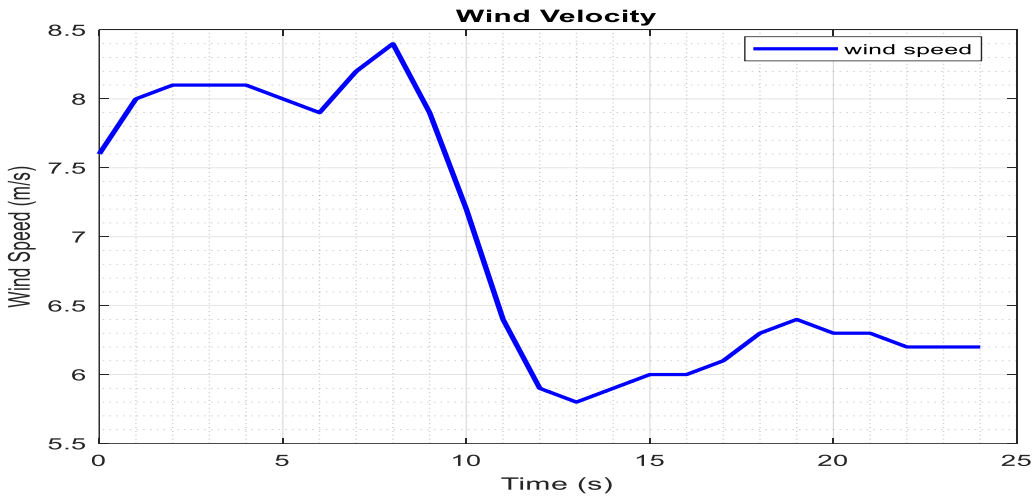


Figure IV-25 Wind velocity for 24h

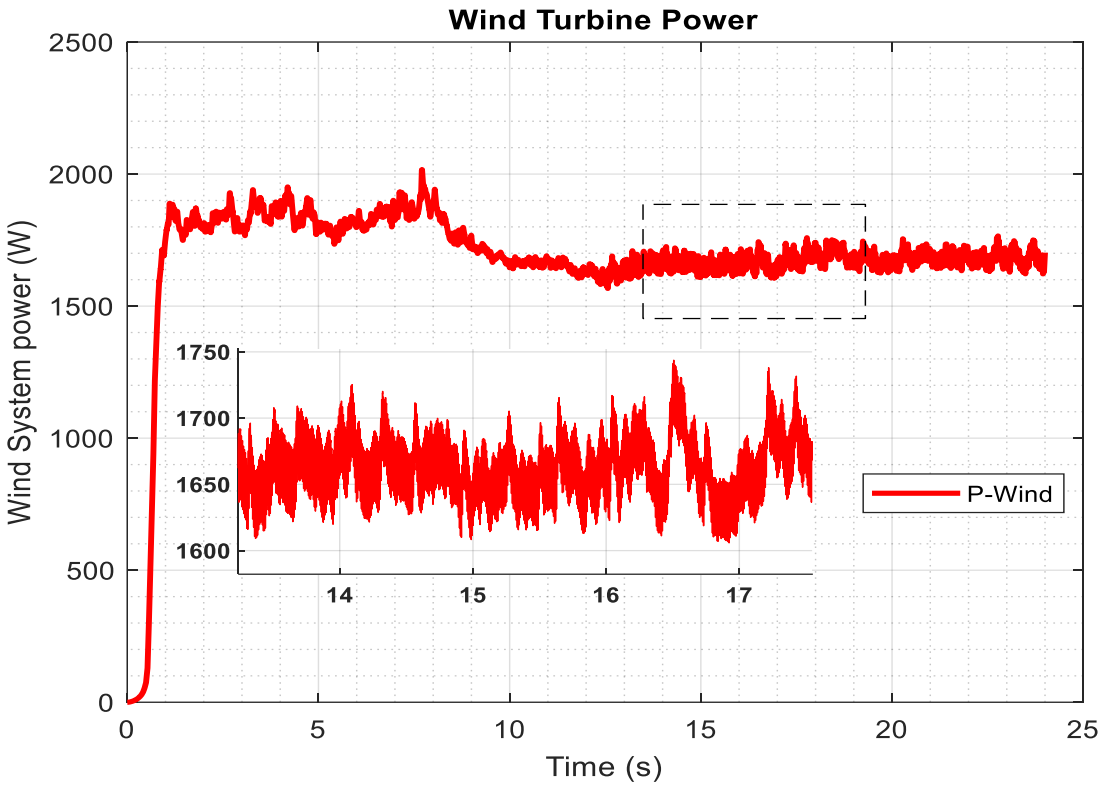


Figure IV-26 wind turbine system power output for 24h

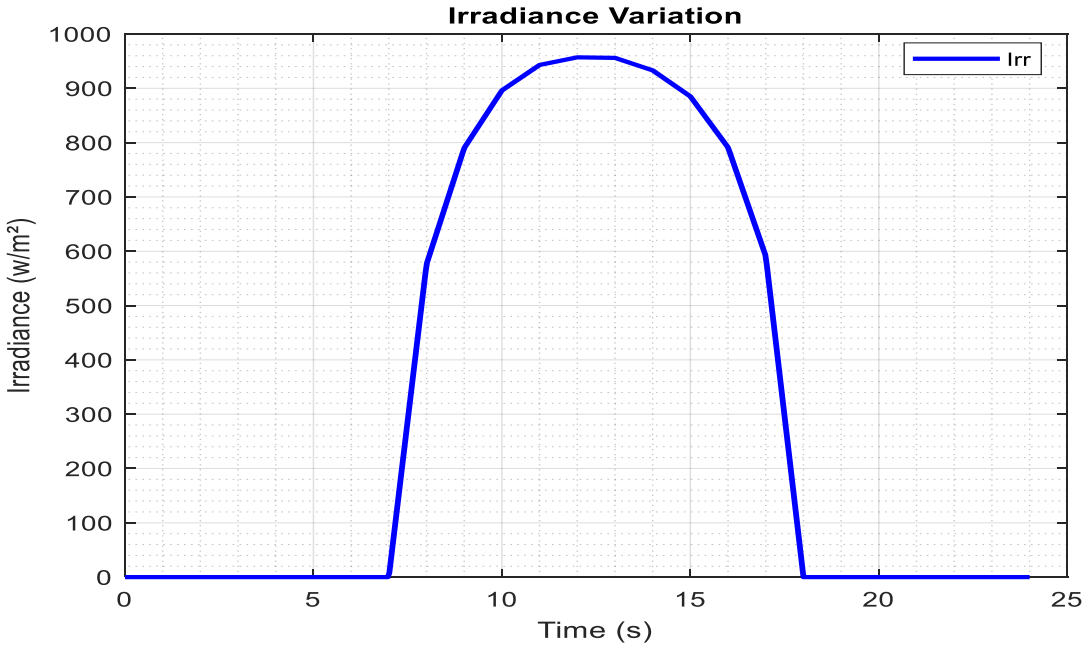


Figure IV-27 irradiance variation for 24 h

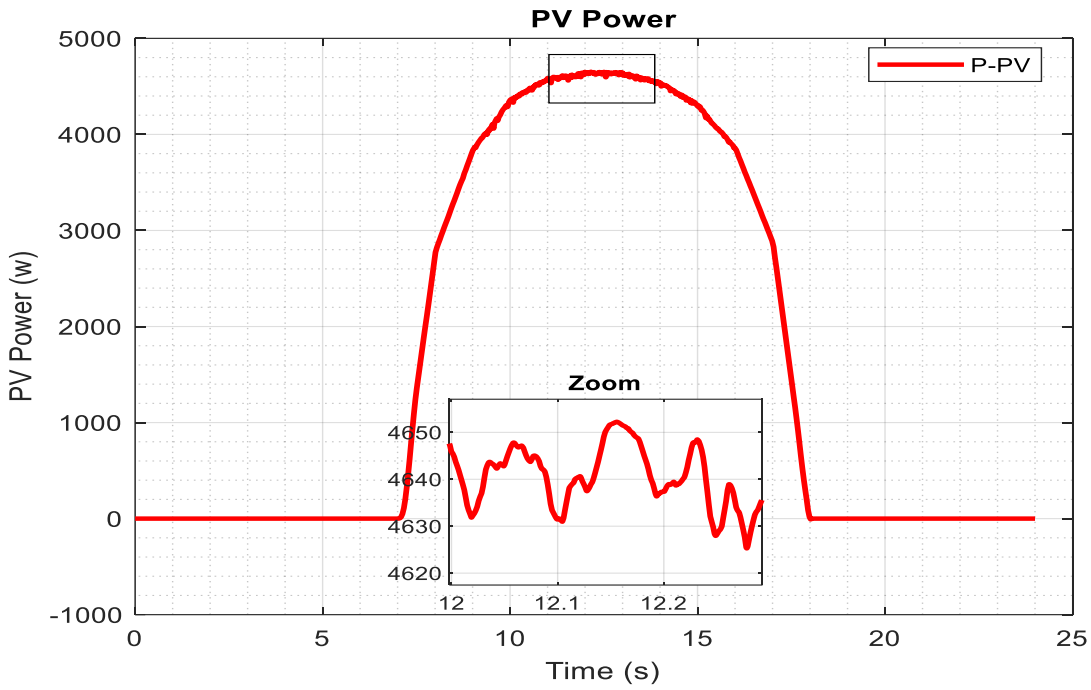


Figure IV-28 PV system Power output for 24h

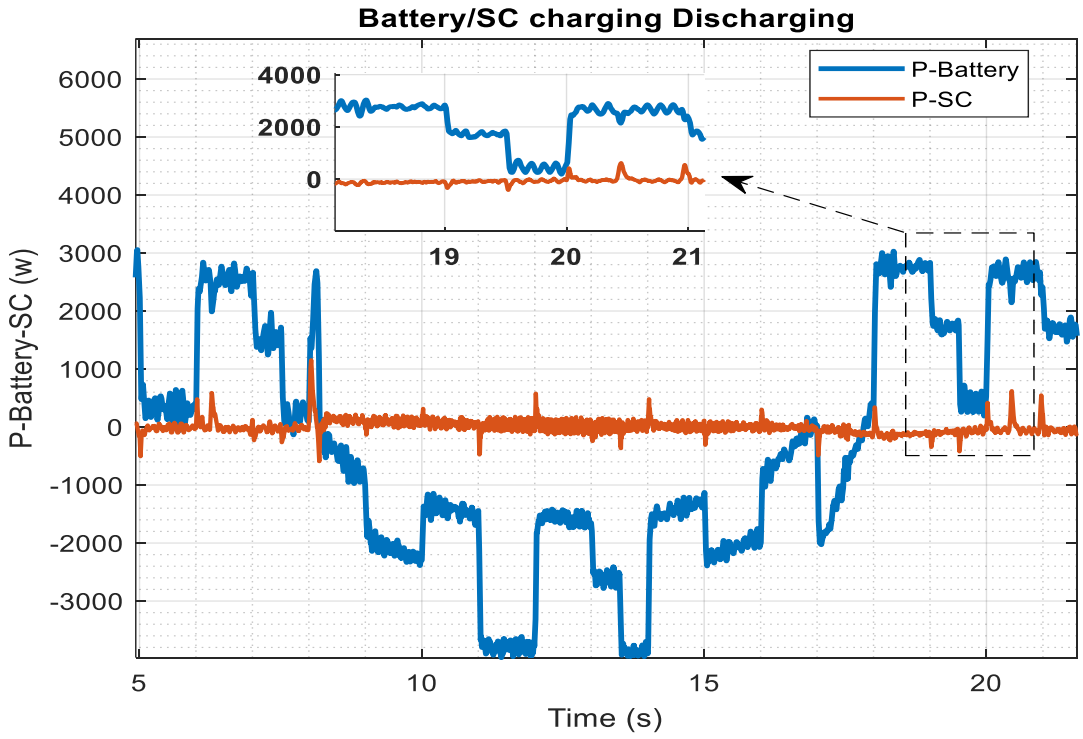


Figure IV-29 Battery/SC Charging-Discharge

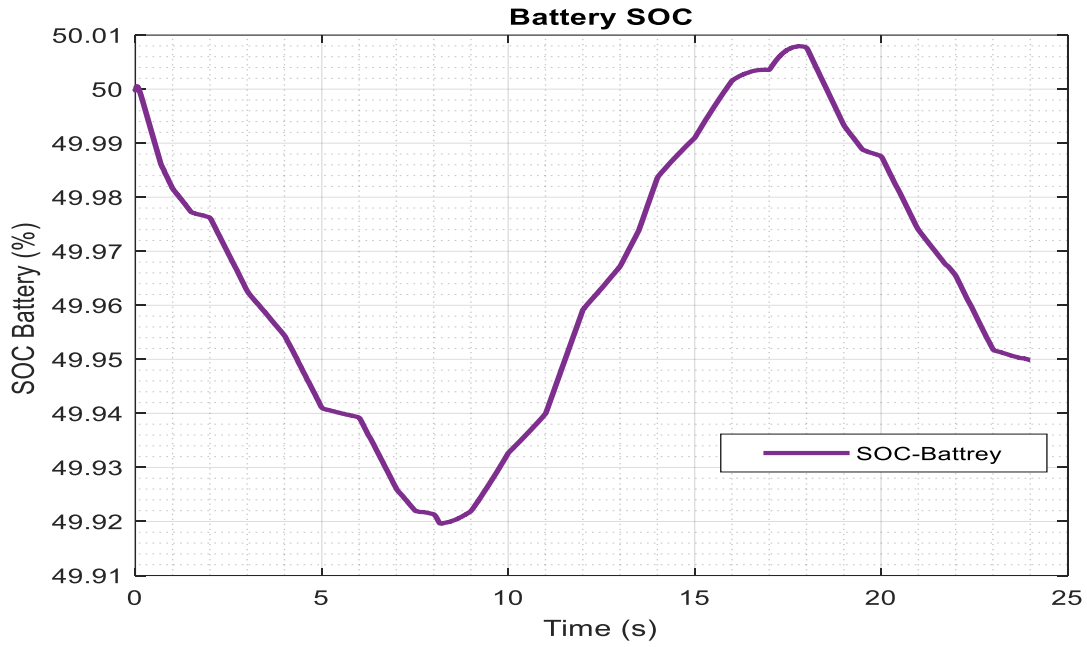


Figure IV-30 battery state of charge SOC%

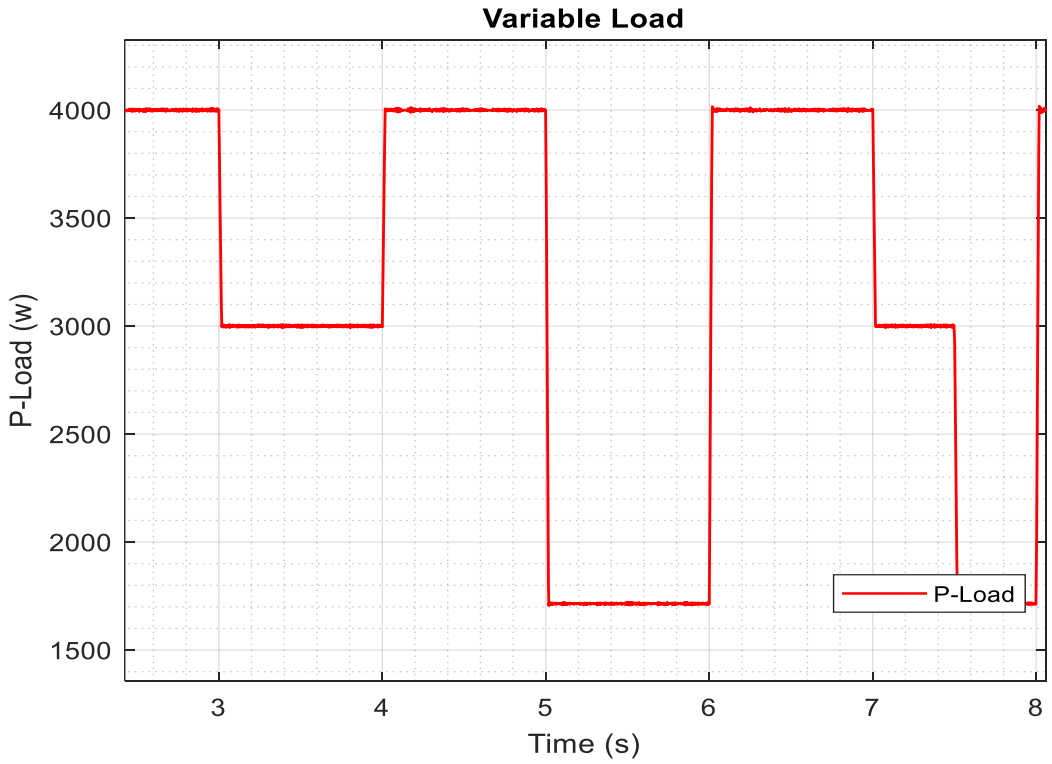


Figure IV-31 Variable Load for 24h

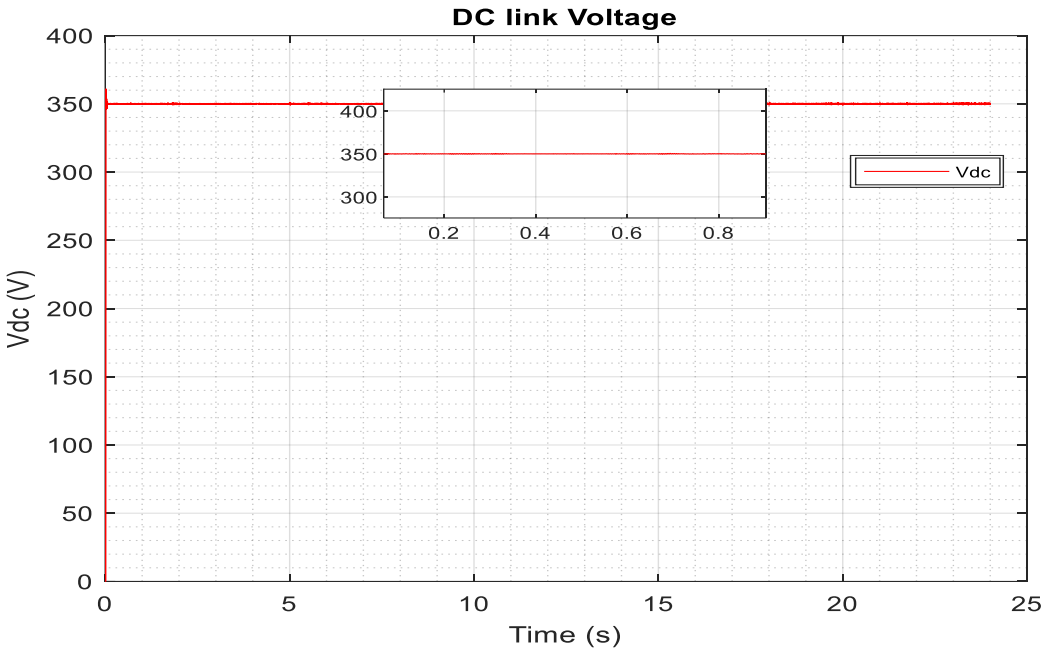


Figure IV-32 DC Voltage

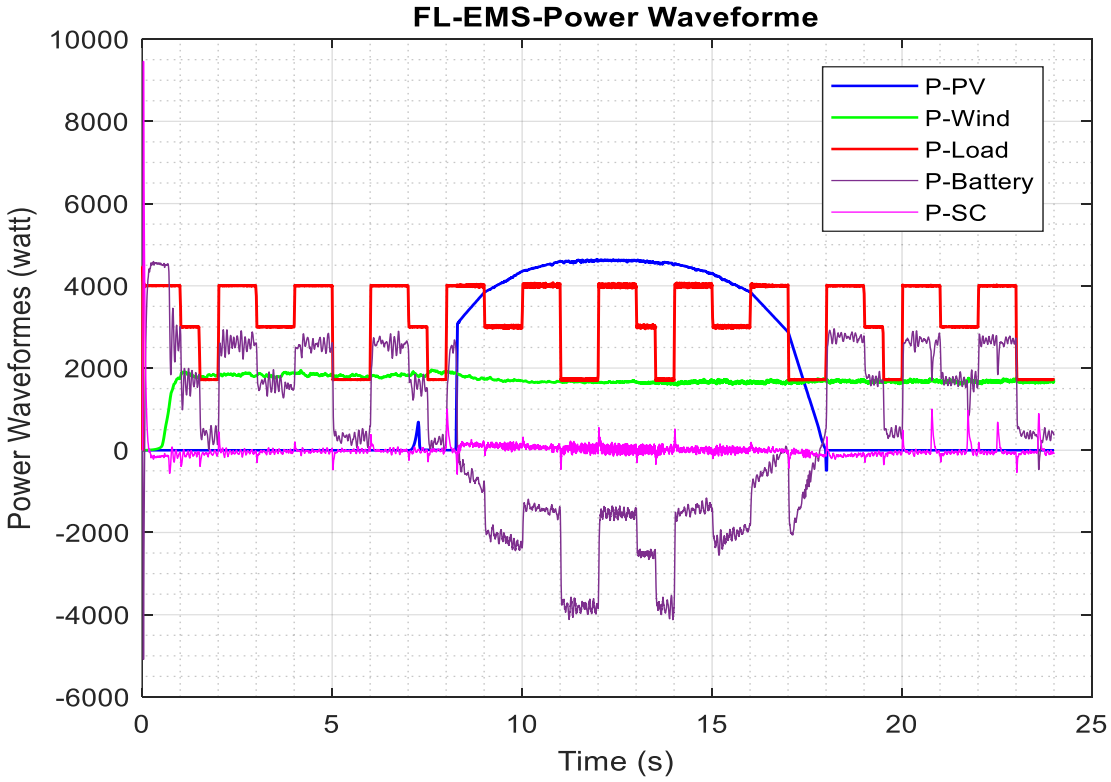


Figure IV-33 power waveforms under Real data

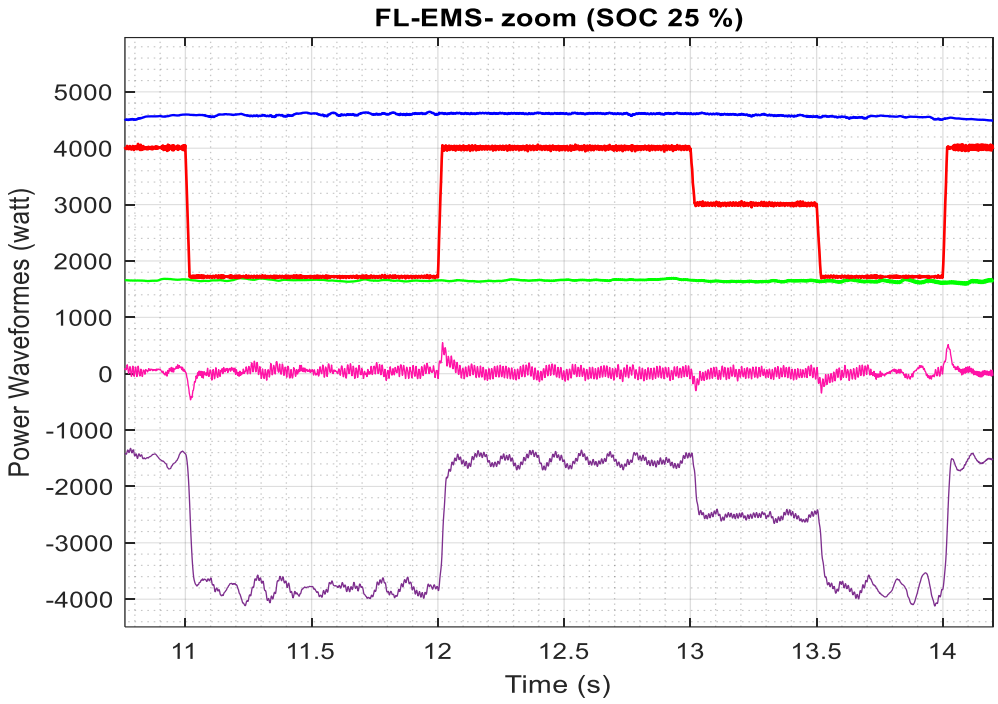


Figure IV-34 FL EMS Zoomed Part 1

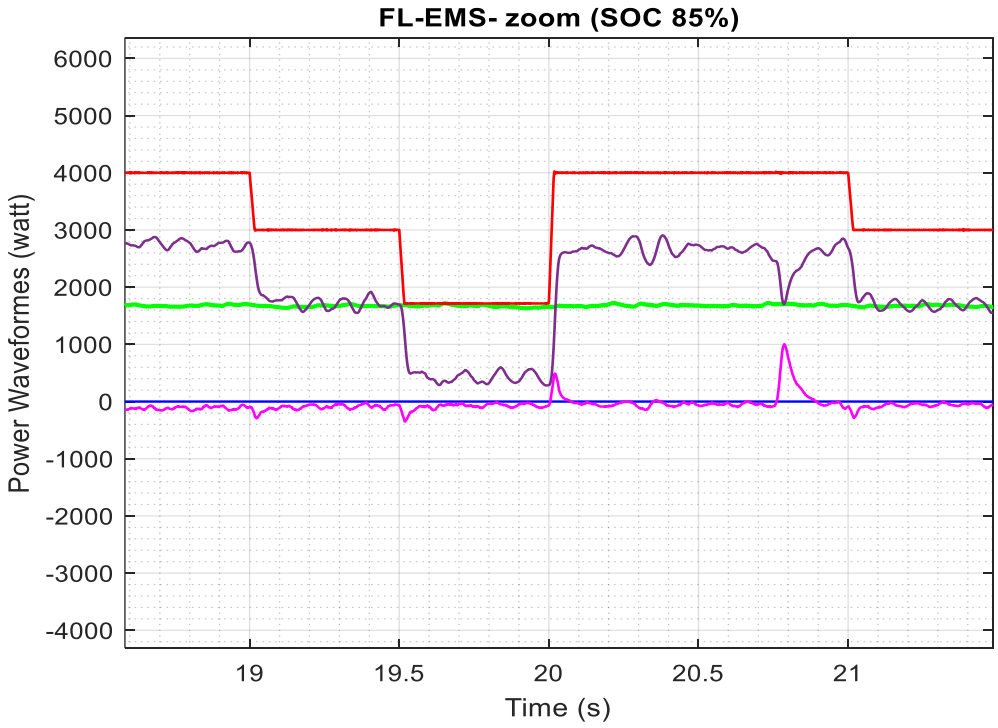


Figure IV-35 FL-EMS Zoomed Part2

- **Observations and Commentary on Figures:**

To evaluate the effectiveness and robustness of the proposed fuzzy logic–based energy management system (FL-EMS), comprehensive simulations were carried out using real 24-hour meteorological and load data for Medea city, Algeria (July). The primary objective of this study is to demonstrate the capability of the FL-EMS to ensure stable DC-link voltage regulation at 350 V, while optimally managing power flows between renewable energy sources (PV and wind), the hybrid energy storage system (battery/supercapacitor), and the load under realistic operating conditions.

Figure IV-25 (Wind Velocity Profile) illustrates the wind speed variation over a 24-hour period. The profile exhibits typical intermittent behavior, with moderate fluctuations during night-time and day-time hours. Such variability highlights the stochastic nature of wind energy and emphasizes the necessity of an intelligent energy management strategy capable of handling rapid changes in generation.

Correspondingly, Figure IV-26 (Wind Turbine Power Output) demonstrates a strong correlation between wind speed and generated power. Despite wind fluctuations, the wind energy conversion system, operating under maximum power point tracking (MPPT), successfully extracts the available power. This confirms the effectiveness of the MPPT strategy and ensures that wind energy is efficiently utilized whenever available.

Figure IV-27 (Solar Irradiance Profile) presents the irradiance variation during the day, characterized by a gradual increase in the morning, a peak around midday, and a decrease toward sunset. This profile is consistent with typical summer conditions in Medea and provides favorable conditions for photovoltaic generation.

As shown in Figure IV-28 (PV Power Output), the photovoltaic system closely follows the irradiance profile, validating the effectiveness of the MPPT control. The PV output reaches its maximum during peak irradiance hours, ensuring optimal energy harvesting and contributing significantly to meeting the load demand and charging the storage system.

The dynamic behavior of the hybrid energy storage system is depicted in Figure IV-29 (Battery and Supercapacitor Charging/Discharging). The results clearly demonstrate the complementary roles of the battery and the supercapacitor:

The battery supplies or absorbs low-frequency, steady-state power, ensuring long-term energy balancing.

The supercapacitor (SC) responds rapidly to high-frequency power fluctuations, absorbing transient peaks and compensating sudden power deficits.

This power-sharing strategy significantly reduces battery current stress and mitigates frequent charge–discharge cycles, thereby extending battery lifespan.

Figure IV-30 (Battery State of Charge – SOC) further confirms the effectiveness of the FL-EMS. The SOC remains within safe operating limits throughout the 24-hour period, with smooth transitions between charging and discharging modes. This behavior demonstrates that the fuzzy logic controller successfully incorporates SOC information into its decision-making process, preventing overcharging or deep discharging conditions.

Figure IV-31 (Variable Load Profile) shows realistic commercial load variations over the day. Despite these continuous changes in load demand, the proposed control strategy ensures uninterrupted power supply.

The most critical performance indicator is illustrated in Figure IV-32 (DC-Link Voltage Response). Despite simultaneous fluctuations in renewable generation and load demand, the DC-link voltage remains tightly regulated around its reference value of 350 V, with minimal ripple and negligible deviation. This result clearly demonstrates:

The capability of the fuzzy logic energy management system to dynamically allocate current references between the battery and the supercapacitor.

The ability to maintain a stable DC-link voltage under real and highly variable conditions strongly validates the robustness and reliability of the proposed FL-EMS.

Figure IV-33 (System Power Waveforms) illustrates the coordinated interaction between PV power, wind power, storage elements, and load demand. The smooth transitions between different operating modes MPPT, load power tracking (LPT), and load power shedding (LPS) highlight the intelligence of the fuzzy rule-based supervisory controller.

The zoomed-in views Figures IV-34 and IV-35 further emphasize the fast dynamic response of the supercapacitor during transient events. The SC effectively buffers sudden power variations, preventing abrupt current changes in the battery and ensuring seamless mode transitions. This confirms that the fuzzy rule base successfully captures expert knowledge and system nonlinearities.

From the presented results, it can be concluded that the proposed fuzzy logic energy management strategy:

Ensures excellent DC-link voltage regulation at 350 V, even under severe renewable intermittency and load fluctuations.

Achieves efficient power sharing between the battery and supercapacitor, assigning low-frequency components to the battery and high-frequency transients to the SC.

Reduces battery stress, enhances system reliability, and prolongs storage system lifetime.

Demonstrates robust performance across all 27 operating scenarios, validating the completeness and effectiveness of the fuzzy rule base.

Overall, the simulation results under real data conditions clearly prove that the proposed FL-EMS provides a robust, intelligent, and reliable energy management solution for DC microgrids with hybrid energy storage systems.

IV.9 Conclusion

This chapter presented the modeling, control, and energy management of a standalone hybrid PV/Wind microgrid incorporating a hybrid energy storage system composed of a battery

and a supercapacitor. Detailed mathematical models of all system components including the photovoltaic generator, wind turbine with PMSG, DC–DC converters, battery, and supercapacitor were developed to accurately capture the dynamic behavior of the overall system and provide a reliable foundation for control and performance evaluation.

A major contribution of this chapter is the design and implementation of a fuzzy logic–based energy management system (FL-EMS) aimed at ensuring stable DC-link voltage regulation while optimally coordinating power flows among renewable sources, storage elements, and the load. The proposed FL-EMS combines conventional PI control with a supervisory fuzzy logic controller that dynamically allocates current references to the battery and supercapacitor based on system power balance and state-of-charge conditions. This structure effectively addresses system nonlinearities, uncertainties, and the intermittent nature of renewable energy sources.

Simulation results under multiple operating scenarios varying irradiance, wind speed, and load demand demonstrated the robustness and effectiveness of the proposed control strategy. The DC-link voltage was consistently regulated around its nominal value of 350 V with minimal ripple, even during rapid transitions in generation and load. The hybrid energy storage system exhibited a clear and efficient power-sharing behavior: the supercapacitor compensated high-frequency transient power components, while the battery handled low-frequency and steady-state energy demands. This complementary operation significantly reduced battery current stress and mitigated excessive charge–discharge cycling.

Furthermore, simulations based on real 24-hour meteorological and load data for Medea city, Algeria, confirmed the practical applicability of the proposed system. The FL-EMS successfully maintained power balance and voltage stability throughout the day despite severe renewable intermittency and realistic load variations. The battery state of charge remained within safe operating limits, demonstrating effective protection against overcharging and deep discharging, while smooth transitions between MPPT, load power tracking, and load power shedding modes highlighted the intelligence and completeness of the fuzzy rule base.

In summary, the results presented in this chapter validate that the proposed fuzzy logic energy management strategy provides a robust, intelligent, and efficient solution for standalone DC microgrids with hybrid energy storage systems. By ensuring excellent DC-link voltage stability, improving power quality, reducing battery degradation, and enhancing overall system reliability, the developed FL-EMS represents a significant contribution toward the practical deployment of renewable-based autonomous microgrids.

Chapter V: General Conclusion

This research focused on the development, modeling, and performance evaluation of advanced energy management and control strategies for a standalone hybrid renewable microgrid integrating photovoltaic (PV) and wind energy sources, supported by a Hybrid Energy Storage System (HESS) composed of a battery and a supercapacitor. In the context of the growing global demand for sustainable, autonomous, and reliable power supply particularly in remote and off-grid areas this work contributes to the advancement of intelligent control solutions capable of enhancing system efficiency, operational stability, and resilience against the inherent intermittency of renewable energy resources.

The primary objective of this thesis was to improve the efficiency and reliability of PV-based and hybrid renewable energy systems through the comparative evaluation of advanced Maximum Power Point Tracking (MPPT) techniques and the design of optimized energy management strategies. This objective was motivated by the limitations of conventional MPPT methods, especially their reduced effectiveness under rapidly changing environmental conditions and complex operating scenarios such as partial shading, as well as by the need for coordinated management of multiple renewable sources and storage technologies to ensure continuous and stable energy supply.

To address these challenges, the research was structured around two main directions. The first focused on the development and evaluation of advanced MPPT algorithms, while the second addressed the design and implementation of an intelligent hybrid renewable energy system with an effective Energy Management Strategy (EMS).

In the first part of this work, a comprehensive comparative study of metaheuristic-based and artificial intelligence (AI)-based MPPT techniques was conducted. The investigated methods included Particle Swarm Optimization (PSO), Grey Wolf Optimization (GWO), Ant Colony Optimization (ACO), Cuckoo Search (CS), Harris Hawks Optimization (HHO), Horse Herd Optimization Algorithm (HOA), as well as AI-based approaches using Fuzzy Logic Control (FLC) and Artificial Neural Networks (ANN). These algorithms were evaluated under

both uniform irradiance conditions and partial shading conditions (PSC) to assess their dynamic behavior, convergence characteristics, and tracking accuracy.

The results demonstrated that under uniform irradiance conditions, all investigated MPPT techniques were capable of effectively tracking the maximum power point, with FLC and ANN-based MPPTs exhibiting very fast convergence and minimal steady-state oscillations. Among the metaheuristic approaches, PSO and HOA consistently achieved high tracking accuracy and efficiency, outperforming the other optimization-based techniques.

However, under partial shading conditions characterized by multi-peak P–V characteristics the performance of MPPT techniques was found to strongly depend on their global search capability. In this context, metaheuristic-based MPPT algorithms successfully tracked the Global Maximum Power Point (GMPP), with PSO emerging as the most robust and reliable technique, followed closely by HOA, which demonstrated stable convergence and reduced oscillations. In contrast, despite their excellent performance under uniform conditions, FLC and ANN-based MPPTs converged to local maxima under PSC, highlighting their inherent limitations in multi-peak operating environments without additional adaptation or hybridization.

The second major contribution of this thesis lies in the design and implementation of a hybrid renewable energy system combining PV and wind energy sources with battery and supercapacitor storage. An intelligent Energy Management Strategy based on Fuzzy Logic Control (FLC-EMS) was developed to coordinate power flow among generation units, storage elements, and loads. The proposed EMS effectively ensured power balance, enhanced system stability, and extended storage component lifespan under varying load demands and environmental conditions. Simulation and real-time validation results confirm the robustness, adaptability, and reliability of the proposed hybrid energy management framework.

Overall, the findings of this research demonstrate that no single control or MPPT strategy is universally optimal for all operating conditions. Intelligent MPPT techniques such as FLC and ANN are highly effective under uniform irradiance, while metaheuristic optimization algorithms particularly PSO and HOA offer superior robustness under partial

shading conditions. The hybrid energy architecture and the proposed EMS provide a scalable and reliable solution for integrating diverse renewable sources and storage technologies.

Collectively, this work contributes to the advancement of hybrid renewable energy systems by providing practical guidelines for MPPT selection, robust energy management solutions, and a comprehensive framework for autonomous microgrid operation. These contributions support global efforts toward sustainable energy transitions by enhancing system efficiency, resilience, and energy autonomy, and they open promising perspectives for future research on adaptive and hybrid intelligent control strategies for next-generation renewable energy systems.

Bibliography

[1] Pasqualetti, M.; Righter, R.; Gipe, P. History of Wind Energy. Encycl. Energy 2004, 6, 419–433.

[2] Szabó, L. The History of using solar energy. In Proceedings of the 7th International Conference on Modern Power Systems, Cluj-Napoca, Romania, 6–9 June 2017.

[3] Roberts, P. HSC Ancient History; Pascal Press: Glebe, UK, 2003.

[4] Bremmer, J.N.; Erskine, A. Gods of Ancient Greece: Identities and Transformations: Identities and Transformations; Edinburgh University Press: Edinburgh, UK, 2010.

[5] Smil, V. Energy in World History; Westview Press: Boulder, CO, USA, 1994.

[6] Perlin, J. Let It Shine: The 6000-Year Story of Solar Energy; New World Library: San Francisco, CA, USA, 2013.

[7] Plommer, H. Vitruvius and Later Roman Building Manuals; Cambridge University Press: London, UK, 1973.

[8] Ngô, C.; Natowitz, J. Our Energy Future: Resources, Alternatives and the Environment; John Wiley & Sons: Hoboken, NJ, USA, 2016.

[9] Available online: https://www.solarpaces.org/csp-technologies/csp-potential solar-thermal-energy-by-member-nation/ (accessed on 16 May 2023).

[10] Lu, X.; McElroy, M.B.; Kiviluoma, J. Global potential for wind Generated electricity. Proc. Natl. Acad. Sci. USA 2009, 106, 10933–10938.

[11] Atawi, I.E.; Al-Shetwi, A.Q.; Magableh, A.M.; Albalawi, O.H. Recent advances in hybrid energy storage system integrated renewable power generation: Configuration, control, applications, and future directions. Batteries 2023, 9, 29.

[12] IEA International Energy Agency. Renewable Energy Market Update May 2022. Available online: https://www.iea.org/ reports/renewable-energy-market-update-may-2022 (accessed on 16 May 2023).

[13] Tomas, W. FY22 Budget Outlook: DOE Applied Energy RD&D. Am. Inst. Phys. Available online: https://www.aip.org/fyi/2023/fy22-budget-outlook-doe-applied-energy-rdd (accessed on 16 May 2023).

[14] Andreas, A.; Stoffel, T. NREL Solar Radiation Research Laboratory (SRRL): Baseline Measurement System (BMS); NREL Report No. Tech. Rep. DA-5500-56488; U.S. Department of Energy: Washington, DC, USA, 1981.

[15] Badwawi, R.A.; Abusara, M.; Mallick, T. A review of hybrid solar pv and wind energy system. Smart Sci. 2015, 3, 127–138.

[16] Roy, P.; He, J.; Zhao, T.; Singh, Y.V. Recent advances of wind-solar hybrid renewable energy systems for power generation: A review. IEEE Open J. Ind. Electron. Soc. 2022, 3, 81–104.

[17] Alnejaili, T.; Chrifi-Alaoui, L.; Mehdi, D.; Alibi, A.; Drid, S. An advanced energy management system with an economical optimization for a multi-sources stand-alone Home. In Proceedings of the 7th International Conference on Systems and Control (ICSC), Valencia, Spain, 24–26 October 2018; pp. 154–159.

[18] Rathod, A.A.; Subramanian, B. Scrutiny of hybrid renewable energy systems for control, power management, optimization and sizing: Challenges and future possibilities. Sustainability 2022, 14, 16814.

[19] Chen, C.; Liu, H.; Xiao, Y.; Zhu, F.; Ding, L.; Yang, F. Power generation scheduling for a hydro-wind-solar hybrid system: A systematic survey and prospect. Energies 2022, 15, 8747.

[20] Trabish, H.K. Solar Wind Storage Developers 'Gearing Up' as Hybrid Projects Edge to Market. Utility Dive, July 2019. Available online: https://www.utilitydive.com/news/solar-wind-storage-developers-gearing-up-as-hybrid-projects-edge-to-m/556480/ (accessed on 16 May 2023).

[21] Bellini, E. Danish Fjord to Host 400 MW of Solar. PV Mag. Int. March 2020. Available online: https://www.pv-magazine.com (accessed on 16 May 2023).

[22] Walton, R. NextEra Inks 700 MW Wind Solar Battery Project, Largest in the US. Utility Dive, July 2019. Available online: https://www.utilitydive.com/news/nextera-inks-700-mw-wind-solar-battery-project-largest-in-the-us/559693/ (accessed on 16 May 2023).

[23] Chrifi-Alaoui, L.; Drid, S.; Ouriagli, M.; Mehdi, D. Overview of Photovoltaic and Wind Electrical Power Hybrid Systems. Energies 2023, 16, 4778. https://www.mdpi.com/1996-1073/16/12/4778

[24] L.M. Miller, N.A. Brunsell, D.B. Mechem, F. Gans, A.J. Monaghan, R. Vautard, A. Kleidon, Two methods for estimating limits to large-scale wind power generation, Proc. Natl. Acad. Sci. USA 112 (36) (2015) 11169–11174.

[25] Douifi Nadia, "Contribution to the Performance Improvement of Renewable Energy Systems Using Modern Control and Optimization Techniques", UNIVERSITY YAHIA FARES OF MEDEA, 2025.

[26] A. S. Al-Ezzi and M. N. M. Ansari, "Photovoltaic solar cells: a review," *Appl. Syst. Innov.*, vol. 5, no. 4, p. 67, 2022.

[27] Ö. Ü. A. ÜZÜM, "DESIGN AND SIMULATION OF SINGLE, DOUBLE AND MULTI-LAYER ANTIREFLECTION COATING FOR CRYSTALLINE SILICON SOLAR CELL," 2018.

[28] M. J. Abbass, R. Lis, and F. Saleem, "The maximum power point tracking (MPPT) of a partially shaded PV array for optimization using the antlion algorithm," *Energies*, vol. 16, no. 5, p. 2380, 2023.

[29] U. A. Ma'allin, "Design a photovoltaic system based on maximum power point tracking under partial shading," Universiti Tun Hussein Onn Malaysia, 2019.

[30] N. K. Ntiakoh, "Roach Infestation Optimization MPPT Algorithm of PV Systems for Adaptive to Fast-Changing Irradiation and Partial Shading Conditions," UiT Norges arktiske universitet, 2021.

[31] F. Belhachat and C. Larbes, "PV array reconfiguration techniques for maximum power optimization under partial shading conditions: A review," *Sol. Energy*, vol. 230, pp. 558–582, 2021.

[32] S. Guo, R. Abbassi, H. Jerbi, A. Rezvani, and K. Suzuki, "Efficient maximum power point tracking for a photovoltaic using hybrid shuffled frog-leaping and pattern search algorithm under changing environmental conditions," *J. Clean. Prod.*, vol. 297, p.126573, 2021.

[33] H.J. Wagner, J. Mathur, Introduction to Hydro Energy Systems: Basics, Technology and Operation, Springer Science & Business Media, 2011.

[34] S.J. Zarrouk, H. Moon, Efficiency of geothermal power plants: a worldwide review, Geothermics 51 (2014) 142–153.

[38] M. Y. Javed *et al.*, "A comprehensive review on a PV based system to harvest maximum power," *Electronics*, vol. 8, no. 12, p. 1480, 2019.

[39] S. M. Ferdous, M. A. Mohammad, F. Nasrullah, A. M. Saleque, and A. Z. M. S. Muttalib,"Design and simulation of an open voltage algorithm based maximum power point tracker for battery charging PV system," in *2012 7th International Conference on Electrical and Computer Engineering*, IEEE, 2012, pp. 908–911.

[40] J.J. Feria-Díaz, F. Correa-Mahecha, M.C. L´opez-M´endez, J.P. Rodríguez-Miranda, J. Barrera-Rojas, Recent desalination technologies by hybridization and integration with reverse osmosis: a review, Water 13 (10) (2021) 1369.

[41] Qusay Hassan, Sameer Algburi, Aws Zuhair Sameen, Hayder M. Salman, Marek Jaszczur. A review of hybrid renewable energy systems: Solar and wind-powered solutions: Challenges, opportunities, and policy implications. Results in Engineering 20 (2023) 101621 https://doi.org/10.1016/j.rineng.2023.101621

[42] Fahim, S.R.; Hasanien, H.M.; Turky, R.A.; Aleem, S.H.E.A.; C´ alasan, M.A. Comprehensive review of photovoltaic modules models and algorithms used in parameter extraction. Energies 2022, 15, 8941.

[43] Masuko, K.; Shigematsu, M.; Hashiguchi, T.; Fujishima, D.; Kai, M.; Yoshimura, N.; Yamaguchi, T.; Ichihashi, Y.; Mishima, T.; Matsubara, N. Achievement of more than 25% conversion efficiency with crystalline silicon heterojunction solar cell. IEEE J. Photovolt. 2014, 4, 1433–1435.

[44] Tihane, A.; Boulaid, M.; Elfanaoui, A.; Nya, M.; Ihlal, A. Performance analysis of mono and polycrystalline silicon photovoltaic modules under agadir climatic conditions in morocco. Mater. Today Proc. 2020, 24, 85–90.

[45] Cao, Y.; Zhu, X.Y.; Chen, H.B.; Zhang, X.T.; Zhouc, J.; Hu, Z.; Pang, J. Towards high efficiency inverted sb2se3 thin film solar cells. Sol. Energy Mater. Sol. Cells 2019, 200, 109945.

[46] Romero, J.M.; Almonacid, F.; Theristis, M.; Casa, J.; Georghiou, G.E.; Fernández, E.F. Comparative analysis of parameter extraction techniques for the electrical characterization of multi-junction CPV and m-si technologies. Sol. Energy 2018, 160,275–288.

[47] C´ alasan, M.; Al-Dhaifallah, M.; Ali, Z.M.; Aleem, S.H.E.A. Comparative analysis of different iterative methods for solving current–voltage

characteristics of double and triple diode models of solar cells. Mathematics 2022, 10, 3082.

[48] X. Li, D. Gui, Z. Zhao, X. Li, X. Wu, Y. Hua, H. Zhong, Operation optimization of electrical-heating integrated energy system based on concentrating solar power plant hybridized with combined heat and power plant, J. Clean. Prod. 289 (2021), 125712.

[49] Y. Ma, B. Li, Hybridized intelligent home renewable energy management system for smart grids, Sustainability 12 (5) (2020) 2117.

[50] A. Acakpovi, P. Adjei, N. Nwulu, N.Y. Asabere, Optimal hybrid renewable energy system: a comparative study of wind/hydrogen/fuel-cell and wind/battery storage, J. Electr. Comput. Eng. 2020 (2020) 1–15.

[51] Anaya-Lara, O. Wind Energy Generation: Modelling and Control; John Wiley & Sons: New York, NY, USA, 2009.

[52] 41. Wu, B.; Lang, Y.; Zargari, N.; Kouro, S. Wind Energy Conversion Systems; John Wiley & Sons: New York, NY, USA, 2011.

[53] Moriarty, P.J.; Butterfield, S.B. Wind turbine modelling overview for control engineers. In Proceedings of the American Control Conference, St. Louis, MO, USA, 10–12 June 2009; pp. 2090–2095.

[54] D. Bogdanov, M. Ram, A. Aghahosseini, A. Gulagi, A.S. Oyewo, M. Child, C. Breyer, Low-cost renewable electricity as the key driver of the global energy transition towards sustainability, Energy 227 (2021), 120467.

[55] Soriano, L.A.; Yu, W.; Rubio, J.D.J. Modeling and control of wind turbine. Math. Probl. Eng. 2013, 2013, 982597.

[56] Bolik, S.M. Modelling and Analysis of Variable Speed Wind Turbines with Induction Generator during Grid Fault. Ph.D. Thesis, Alborg University, Aalborg, Denmark, 2004.

[57] Moriarty, P.J.; Butterfield, S.B. Wind turbine modelling overview for control engineers. In Proceedings of the American Control Conference, St. Louis, MO, USA, 10–12 June 2009; pp. 2090–2095.

[58] Anaya-Lara, O. Wind Energy Generation: Modelling and Control; John Wiley & Sons: New York, NY, USA, 2009.

[59] Wu, B.; Lang, Y.; Zargari, N.; Kouro, S. Wind Energy Conversion Systems; John Wiley & Sons: New York, NY, USA, 2011.

[60] Q. Hassan, Evaluation and optimization of off-grid and on-grid photovoltaic power system for typical household electrification, Renew. Energy 164 (2021) 375–390.

[61] M. Jaszczur, Q. Hassan, P. Palej, J. Abdulateef, Multi-Objective optimisation of a micro-grid hybrid power system for household application, Energy 202 (2020), 117738.

[62] S. Chandak, P.K. Rout, The implementation framework of a microgrid: a review, Int. J. Energy Res. 45 (3) (2021) 3523–3547.

[63] Q. Hassan, M. Jaszczur, J. Abdulateef, Optimization of PV/wind/diesel hybrid power system in homer for rural electrification, in: Journal of Physics: Conference Series, IOP Publishing, 2016, September, 032006. Vol. 745, No. 3.

[64] Q. Hassan, Optimisation of solar-hydrogen power system for household applications, Int. J. Hydrogen Energy 45 (58) (2020) 33111–33127.

[65] B. Ceran, Q. Hassan, M. Jaszczur, K. Sroka, An analysis of hybrid power generation systems for a residential load, in: E3S Web of Conferences, vol. 14, EDP Sciences, 2017, 01020.

[66] Q. Hassan, M. Jaszczur, E. Przenzak, Mathematical model for the power generation from arbitrarily oriented photovoltaic panel, in: E3S Web of Conferences, vol. 14, EDP Sciences, 2017, 01028.

[67] M. Chennaif, M. Maaouane, H. Zahboune, M. Elhafyani, S. Zouggar, Tri-objective techno-economic sizing optimization of Off-grid and On-grid renewable energy systems using Electric system Cascade Extended analysis and system Advisor Model, Appl. Energy 305 (2022), 117844.

[68] B. Ceran, A. Mielcarek, Q. Hassan, J. Teneta, M. Jaszczur, Aging effects on modelling and operation of a photovoltaic system with hydrogen storage, Appl. Energy 297 (2021), 117161.

[69] M. Ali, A.S.J. Wardhana, E.S. Damarwan, W.S. Bagas, Design and implementation of trainer kit for hybrid on-grid solar power generation system,

in: Journal of Physics: Conference Series, IOP Publishing, 2021, 012002. Vol. 1737, No. 1.

[70] Q. Hassan, M.K. Abbas, A.M. Abdulateef, J. Abdulateef, A. Mohamad, Assessment the potential solar energy with the models for optimum tilt angles of maximum solar irradiance for Iraq, Case Stud. Chem. Environ. Eng. 4 (2021), 100140.

[71] J. Jurasz, M. Guezgouz, P.E. Campana, A. Kies, On the impact of load profile data on the optimization results of off-grid energy systems, Renew. Sustain. Energy Rev. 159 (2022), 112199.

[72] X. Qi, J. Wang, G. Kr´olczyk, P. Gardoni, Z. Li, Sustainability analysis of a hybrid renewable power system with battery storage for islands application, J. Energy Storage 50 (2022), 104682.

[73] J. Arkhangelski, P. Roncero-S´anchez, M. Abdou-Tankari, J. V´azquez, G. Lefebvre, Control and restrictions of a hybrid renewable energy system connected to the grid: a battery and supercapacitor storage case, Energies 12 (14) (2019) 2776.

[74] Rekioua, D. Energy Storage Systems for Photovoltaic and Wind Systems: A Review. Energies 2023, 16, 3893

[75] Aktas, A.; Kircicek, Y. Solar Hybrid Systems: Design and Application, Solar Hybrid Systems: Design and Application; Academic Press: Cambridge, MA, USA, 2021; pp. 1–356.

[76] Chen, J.; Li, J.; Zhang, Y.; Bao, G.; Ge, X.; Li, P. A hierarchical optimal operation strategy of hybrid energy storage system in distribution networks with high photovoltaic penetration. Energies 2018, 11, 389.

[77] Cruz, M.R.M.; Fitiwi, D.Z.; Santos, S.F.; Catalão, J.P.S. A comprehensive survey of flexibility options for supporting the low-carbon energy future. Renew. Sustain. Energy Rev. 2018, 97, 338–353.

[78] Tsakiris, A. Analysis of hydrogen fuel cell and battery efficiency. In Proceedings of the World Sustainable Energy Days 2019 Young Energy Researchers Conference, Wels, Austria, 27 February–1 March 2019.

[79] Yi, T.F.; Sari, H.M.K.; Li, X.;Wang, F.; Zhu, Y.R.; Hu, J.; Zhang, J.; Li, X. A review of niobium oxides-based nanocomposites for lithium-ion batteries, sodium-ion batteries and supercapacitors. Nano Energy 2021, 85, 105955.

[80] Revankar, S.T. Chemical Energy Storage. In Storage and Hybridization of Nuclear Energy: Techno-Economic Integration of Renewable and Nuclear Energy; Academic Press: Cambridge, MA, USA, 2019; pp. 177–227.

[81] Luo, X.; Wang, J.; Dooner, M.; Clarke, J. Overview of current development in electrical energy storage technologies and the application potential in power system operation. Appl. Energy 2015, 137, 511–536.

[82] Wang, Y.X.; Lai, W.H.; Chou, S.L.; Liu, H.K.; Dou, S.X. Remedies for polysulfide dissolution in room-temperature sodium–sulfur batteries. Adv. Mater. 2020, 32, 1903952.

[83] Zhang, Z.; Wang, X.; Li, X.; Zhao, J.; Liu, G.; Yu, W.; Dong, X.; Wang, J. Review on composite solid electrolytes for solid-state lithium-ion batteries Materials Today. Sustainability 2023, 21, 100316.

[84] Q. Hassan, B. Pawela, A. Hasan, M. Jaszczur, Optimization of large-scale battery storage capacity in conjunction with photovoltaic systems for maximum self-sustainability, Energies 15 (10) (2022) 3845.

[85] Q. Hassan, M. Jaszczur, A.K. Al-Jiboory, A. Hasan, A. Mohamad, Optimizing of hybrid renewable photovoltaic/wind turbine/super capacitor for improving self-sustainability, Energy Harvest. Syst. 9 (2) (2022) 151–164.

[86] Sebastian Günther, Astrid Bensmann ∗, Richard Hanke-Rauschenbach, Representative energy management strategies for hybrid energy storage systems derived from a meta-review. Renewable and Sustainable Energy Reviews 216 (2025) 115610

[87] Albasheri MA, Bouchhida O, Soufi Y, Cherifi A (2024) Enhanced supervisor energy management technique of DC microgrid-based PV/wind/battery/SC. Electr Eng.

[88] A. K. Podder, N. K. Roy, and H. R. Pota, “MPPT methods for solar PV systems: a critical review based on tracking nature,” *IET Renew. Power Gener.*, vol. 13, no. 10, pp. 1615–1632, 2019.

[89] [64] T. Ramki and L. N. Tripathy, "Comparison of different DC-DC converter for MPPT application of photovoltaic system," in *International Conference on Electrical, Electronics, Signals, Communication and Optimization (EESCO)*, 2015, pp. 1–6.

[90] [65] A. Belkaid, I. Colak, K. Kayisli, and R. Bayindir, "Design and implementation of a cuk converter controlled by a direct duty cycle INC-MPPT in PV battery system," *Int. J. Smart Grid-ij Smart Grid*, vol. 3, no. 1, pp. 19–25, 2019.

[91] [66] S. Sivakumar, M. J. Sathik, P. S. Manoj, and G. Sundararajan, "An assessment on performance of DC–DC converters for renewable energy applications," *Renew. Sustain. Energy Rev.*, vol. 58, pp. 1475–1485, 2016.

[92] S. N. Singh, "Selection of non-isolated DC-DC converters for solar photovoltaic system," *Renew. Sustain. Energy Rev.*, vol. 76, pp. 1230–1247, 2017.

[93] L. Jotham Jeremy, C. A. Ooi, and J. Teh, "Non-isolated conventional DC-DC converter comparison for a photovoltaic system: A review," *J. Renew. Sustain. Energy*, vol. 12, no. 1, 2020.

[94] K. V. G. Raghavendra *et al.*, "A comprehensive review of DC–DC converter topologies and modulation strategies with recent advances in solar photovoltaic systems, *"electronics*, vol. 9, no. 1, p. 31, 2019.

[95] F. Mumtaz, N. Z. Yahaya, S. T. Meraj, B. Singh, R. Kannan, and O. Ibrahim, "Review on non-isolated DC-DC converters and their control techniques for renewable energy applications," *Ain Shams Eng. J.*, vol. 12, no. 4, pp. 3747–3763, 2021.

[96] V. C. Kotak and P. Tyagi, "DC to DC Converter in maximum power point tracker," *Int. J. Adv. Res. Electr. Electron. Instrum. Eng.*, vol. 2, no. 12, pp. 6115–6125, 2013.

[97] P. P. Surya, D. Irawan, and M. Zuhri, "Review and comparison of DC-DC converters for maximum power point tracking system in standalone photovoltaic (PV) module," in *2017 International Conference on Advanced Mechatronics, Intelligent Manufacture, and Industrial Automation (ICAMIMIA)*, IEEE, 2017, pp. 242–247.

[98] J. L. Seguel, S. I. Seleme Jr, and L. M. F. Morais, "Comparative study of Buck-Boost, SEPIC, Cuk and Zeta DC-DC converters using different MPPT methods for photovoltaic applications," *Energies*, vol. 15, no. 21, p. 7936, 2022.

[99] R. B. Bollipo, S. Mikkili, and P. K. Bonthagorla, "Critical review on PV MPPT 156 techniques: classical, intelligent and optimisation," *IET Renew. Power Gener.*, vol. 14, no. 9, pp. 1433–1452, 2020.

[100] Ö. F. Tozlu and H. Çalık, "A review and classification of most used MPPT algorithms for photovoltaic systems," *Hittite J. Sci. Eng.*, vol. 8, no. 3, pp. 207–220, 2021.

[101] A. O. Baba, G. Liu, and X. Chen, "Classification and evaluation review of maximum power point tracking methods," *Sustain. Futur.*, vol. 2, p. 100020, 2020.

[102] A. K. Sharma *et al.*, "Role of metaheuristic approaches for implementation of integrated MPPT-PV systems: a comprehensive study," *Mathematics*, vol. 11, no. 2, p. 269, 2023.

[103] H. Islam *et al.*, "Performance evaluation of maximum power point tracking approaches and photovoltaic systems," *Energies*, vol. 11, no. 2, p. 365, 2018.

[104] M. Seyedmahmoudian *et al.*, "State of the art artificial intelligence-based MPPT techniques for mitigating partial shading effects on PV systems–A review," *Renew. Sustain. Energy Rev.*, vol. 64, pp. 435–455, 2016.

[105] C. B. Nzoundja Fapi *et al.*, "Fuzzy Logic-Based Maximum Power Point Tracking Control for Photovoltaic Systems: A Review and Experimental Applications," *Arch. Comput. Methods Eng.*, pp. 1–24, 2025.

[106] M. L. Katche, A. B. Makokha, S. O. Zachary, and M. S. Adaramola, "A comprehensive review of maximum power point tracking (mppt) techniques used in solar pv systems," *Energies*, vol. 16, no. 5, p. 2206, 2023.

[107] A. M. Eltamaly, "An improved cuckoo search algorithm for maximum power point tracking of photovoltaic systems under partial shading conditions," *Energies*, vol. 14, no. 4, p. 953, 2021.

[108] A. Bouguerra, S. Mekheilef, and A. Chouder, "Comparative Study of Perturb and Observe Incremental Conductance and Particle Swarm Optimisation for

Maximum Power Point Tracking Under Changing Irradiance," in *2023 2nd International Conference on Electronics, Energy and Measurement (IC2EM)*, IEEE, 2023, pp. 1–7.

[109] M. S. Endiz, G. Gökkuş, A. E. Coşgun, and H. Demir, "A Review of Traditional and Advanced MPPT Approaches for PV Systems Under Uniformly Insolation and Partially Shaded Conditions," *Appl. Sci.*, vol. 15, no. 3, p. 1031, 2025.

[110] K. Hu, S. Cao, W. Li, and F. Zhu, "An improved particle swarm optimization algorithm suitable for photovoltaic power tracking under partial shading conditions," *IEEE Access*, vol. 7, pp. 143217–143232, 2019.

[111] A. M. Eltamaly, H. M. H. Farh, and M. S. Al-Saud, "Grade point average assessment for metaheuristic GMPP techniques of partial shaded PV systems," *IET Renew. Power Gener.*, vol. 13, no. 8, pp. 1215–1231, 2019.

[112] M. S. Wasim, M. Amjad, S. Habib, M. A. Abbasi, A. R. Bhatti, and S. M. Muyeen, "A critical review and performance comparisons of swarm-based optimization algorithms in maximum power point tracking of photovoltaic systems under partial shading conditions," *Energy Reports*, vol. 8, pp. 4871–4898, 2022.

[113] K. Guo, L. Cui, M. Mao, L. Zhou, and Q. Zhang, "An improved gray wolf optimizer MPPT algorithm for PV system with BFBIC converter under partial shading," *IEEE Access*, vol. 8, pp. 103476–103490, 2020. 157

[114] X. Ma, D. Jiandong, W. Xiao, S. Tuo, W. Yanhang, and S. Ting, "Research of photovoltaic systems MPPT based on improved grey wolf algorithm under partial shading conditions," in *2018 2nd IEEE Conference on Energy Internet and Energy System Integration (EI2)*, IEEE, 2018, pp. 1–6.

[115] S. Natarajan and A. K. Loganathan, "Analysis of energy management controller in grid connected PV wind power system coupled with battery using whale optimization algorithm," *Iran. J. Sci. Technol. Trans. Electr. Eng.*, vol. 46, no. 1, pp. 77–90, 2022

[116] M. H. Nadimi-Shahraki, H. Zamani, Z. Asghari Varzaneh, and S. Mirjalili, "A systematic review of the whale optimization algorithm: theoretical foundation,

improvements, and hybridizations," *Arch. Comput. Methods Eng.*, vol. 30, no. 7, pp. 4113–4159, 2023.

[117] L. L. Jiang, D. L. Maskell, and J. C. Patra, "A novel ant colony optimization-based maximum power point tracking for photovoltaic systems under partially shaded conditions," *Energy Build.*, vol. 58, pp. 227–236, 2013.

[118] S. Titri, C. Larbes, K. Y. Toumi, and K. Benatchba, "A new MPPT controller based on the Ant colony optimization algorithm for Photovoltaic systems under partial shading conditions," *Appl. Soft Comput.*, vol. 58, pp. 465–479, 2017.

[119] P. Qi, H. Xia, X. Cai, M. Yu, N. Jiang, and Y. Dai, "Novel global MPPT technique based on hybrid cuckoo search and artificial bee colony under partial-shading conditions," *Electronics*, vol. 13, no. 7, p. 1337, 2024.

[120] M. I. Mosaad, M. O. abed el-Raouf, M. A. Al-Ahmar, and F. A. Banakher, "Maximum power point tracking of PV system based cuckoo search algorithm; review and comparison," *Energy procedia*, vol. 162, pp. 117–126, 2019.

[121] Xiang Tao1, Jianbo Xin1, Shuai Zhang2, *, Zaide Xu1, Zhonghai Ye3, Kai Wang3, Bo Chen1 and Ning Zhou1A Novel Harris-Hawk-Optimization-Based Maximum-Power-Point-Tracking Control Strategy for a Grid-Connected PV Power-Generation System. Energies 2024, 17, 76. https://doi.org/10.3390/en17010076

[122] Sarwar, S.; Hafeez, M.A.; Javed, M.Y.; Asghar, A.B.; Ejsmont, K.A Horse Herd Optimization Algorithm (HOA)-Based MPPT Technique under Partial and Complex Partial Shading Conditions. Energies 2022, 15, 1880. https://doi.org/10.3390/en15051880

[123] [96] P. Joshi and S. Arora, "Maximum power point tracking methodologies for solar PV systems–A review," *Renew. Sustain. Energy Rev.*, vol. 70, pp. 1154–1177, 2017.

[124] F. Aashoor, "Maximum power point tracking techniques for photovoltaic water pumping system," University of Bath, 2015

[125] X.-S. Yang, X.-S. He, and Q.-W. Fan, "Mathematical framework for algorithm analysis, "in *Nature-inspired computation and swarm intelligence*, Elsevier, 2020, pp. 89–108.

[126] C. Pradhan, M. K. Senapati, N. K. Ntiakoh, and R. K. Calay, "Roach infestation optimization MPPT algorithm for solar photovoltaic system," *Electronics*, vol. 11, no. 6, p. 927, 2022.

[127] H. Deboucha, S. Mekhilef, S. Belaid, and A. Guichi, “Modified deterministic Jaya (DMJaya)-based MPPT algorithm under partially shaded conditions for PV system,” *IET Power Electron.*, vol. 13, no. 19, pp. 4625–4632, 2020.

[128] Yazid Sadok Bouziane, Noureddine Henini, Abdelhalim Tlemçani, Energy Management of a Hybrid Generation System Based on Wind Turbine Coupled with a Battery/Supercapacitor. Journal Européen des Systèmes Automatisés Vol. 55, No. 5, October, 2022, pp. 623-6631, https://doi.org/10.18280/jesa.550507